FACULDADE DE ENGENHARIA DA UNIVERSIDADE DO PORTO


FEUP

# GPS-Independent Localization for Road Vehicles using Cooperation and Magnetic Anomalies

**Susana Pereira Bulas Cruz**

Doctoral Programme in Electrical and Computer Engineering

Supervisors: Prof. Ana Cristina Costa Aguiar
and Prof. João Francisco Cordeiro de Oliveira Barros

June 2019

# GPS-Independent Localization for Road Vehicles using Cooperation and Magnetic Anomalies

**Susana Pereira Bulas Cruz**

Doctoral Programme in Electrical and Computer Engineering

June 2019

# Resumo

O objectivo deste trabalho é propor uma abordagem de baixo custo e independente do GPS para localização em redes veiculares. A localização de veículos é um aspecto de extrema importância em sistemas de transporte inteligentes, que por sua vez desempenham um papel fundamental no futuro da mobilidade. O GPS é a solução mais amplamente conhecida e usada para veículos rodoviários em ambientes exteriores. No entanto, esta opção apresenta algumas limitações, nomeadamente erros elevados em ambientes com propagação multi-percurso e situações de falta de visibilidade para os satélites, como acontece por exemplo em túneis, centros urbanos com grande densidade de prédios altos e parques de estacionamento subterrâneos. Embora diversas fontes de informação possam ser combinadas com vista a aumentar o desempenho do sistema, a maioria dos métodos propostos são, contudo, significativamente dependentes do GPS. As alterativas geralmente requerem equipamentos ou infra-estruturas de custos elevados, ou ainda um elevado esforço de mapeamento de grandes áreas. Neste trabalho, propomos uma abordagem ao problema tanto numa perspectiva cooperativa como numa perspectiva individual.

Considerando um cenário colaborativo, aproveitamos as comunicações entre veículos, permitindo a estes últimos estimar ou melhorar a sua posição usando como âncoras de posicionamento os vizinhos mais próximos, que poderão ser eles próprios veículos com uma incerteza de localização associada. Assumindo que os veículos estão equipados com o protocolo 802.11p e sensores inerciais de baixo custo, aplicamos um filtro de Bayes com duas etapas para localizar o veículo ao longo do tempo: 1) um filtro de Kalman não linear para estimar o sentido do deslocamento e 2) um filtro de partículas que faz a fusão de diversas fontes de informação, nomeadamente indicação da potência do sinal recebido das comunicações entre veículos, usando-os como âncoras de posicionamento móveis e com posições incertas, velocidade, posição GPS e informação dos mapas. A nossa abordagem cooperativa conduz a um robusto sistema de posicionamento ao longo do tempo, capaz de fornecer informações úteis de localização mesmo na ausência de dados de GPS no veículo. O desempenho do algoritmo é avaliado com dados reais, recolhidos em quatro veículos capazes de comunicar entre si durante uma viagem em ambiente urbano com condições normais de tráfego. São consideradas diferentes combinações das fontes de informação e é incluída uma análise de condições adequadas para a utilização das âncoras de posicionamento. Estas experiências servem como uma prova de conceito à abordagem proposta.

Relativamente à localização individual de veículos, a informação magnética é frequentemente utilizada para efeitos de orientação em sistemas de navegação rodoviários. No entanto, fortes campos magnéticos locais causados por infra-estruturas presentes nas estradas são adicionados ao campo magnético terrestre, criando anomalias. Propomos neste trabalho: 1) um algoritmo de detecção que faz uso de janelas espaciais para processar séries temporais e aplica um conjunto de métodos de aprendizagem para classificação binária de anomalias em cada janela; e 2) um método de correspondência entre as anomalias recolhidas e as de referência, através da aplicação de um algoritmo baseado no centróide mais próximo (*one nearest centroid*) usando *dynamic time warping* para alinhamento e comparação entre séries temporais, e incluindo ainda diretrizes para

recolha e armazenamento das anomalias de referência. Ambos os passos são testados com dados reais recolhidos por *smartphones* comuns e usando equipamentos heterogéneos, demonstrando desta forma a viabilidade do conceito em cenários especialmente desafiantes, chegando a atingir uma detecção ao nível da faixa de rodagem. O conceito de posicionamento baseado em pontos de referência magnéticos que propomos, pode ser usado para evitar a propagação do erro em sistemas de navegação estimada (*dead-reckoning*), aumentando desta forma o seu desempenho. Sistemas de posicionamento baseados em satélites podem ainda expandir a sua área de cobertura e providenciar melhores resultados em áreas com conhecidas limitações.

As nossas contribuições podem ser usadas de forma independente: a primeira focando-se na cooperação entre os nós da rede independentemente da forma como cada um destes obteve a sua informação de posicionamento, e a segunda aplicada localmente a cada veículo. As abordagens propostas poderão ainda ser combinadas entre si, explorando sinergias para providenciar aos veículos localização cooperativa e independente do GPS. [1]

[1] Nota: Este texto é escrito ao abrigo do antigo acordo ortográfico.

# Abstract

Vehicle localization is an aspect of utmost relevance in intelligent transportation systems, which in turn play a key role in the future of mobility. GPS is the most widespread and commonly used solution for road vehicles in outdoor scenarios. However, it presents limitations, namely exhibiting large position errors in multipath environments and non-line-of-sight satellite conditions, e.g. tunnels, urban canyons, multilevel roads, and underground parking. Although several information sources can be combined for improved performance, most proposed methods are nonetheless heavily dependent on GPS. Alternatives usually require costly equipment, deploying infrastructure or a heavy mapping phase. The aim of this thesis is to propose a low-cost and GPS-independent localization approach for vehicular networks. We consider this problem from both cooperative and individual perspectives.

Regarding our cooperative scenario, we leverage vehicle communications by allowing vehicles to estimate or improve their position using one-hop neighbors with uncertain locations as anchors. Assuming vehicles are equipped with 802.11p wireless interfaces and low-cost inertial sensors, we employ a two-stage Bayesian filter to track their position: 1) an unscented Kalman filter for heading estimation, and 2) a particle filter that fuses vehicle-to-vehicle signal strength measurements received from mobile anchors, with velocity, GPS position, and map information. Our cooperative approach leads to a robust tracking system that is able to provide useful location information even in the absence of GPS data in the ego vehicle. We evaluate its performance using real-world measurements collected from four communicating vehicles in regular urban traffic conditions, considering different combinations of information sources, and providing an analysis of suitable anchor conditions. These experiments serve as a proof-of-concept for our approach.

Considering individual vehicle localization, magnetic information is frequently used for orientation purposes in navigation systems. However, strong local magnetic fields caused by road infrastructure add to the geomagnetic field, creating anomalies. We show that these present signatures for specific paths that can be leveraged for localization purposes, as magnetic landmarks. We propose: 1) a detection algorithm that uses a space-based window to process the time series and applies an ensemble method for anomaly binary classification of each window; and 2) a matching method that employs one nearest centroid algorithm with dynamic time warping, and includes guidelines for collecting and storing references. Both steps are evaluated with real-world data collected with off-the-shelf smartphones in challenging scenarios, showing the feasibility of the concept with diverse equipment, even for lane detection. Magnetic landmarks may be used to correct dead reckoning cumulative errors, increasing accuracy and reliability, or be combined with satellite-based systems, improving their localization performance in areas with known limitations.

The proposed approaches can be used independently since the first one focuses on cooperation among nodes, regardless of how each one obtains its location information, whereas the second is concerned with the individual location of a single vehicle. Our contributions may also be combined, exploring synergies to provide cooperative and GPS-independent localization for road vehicles.

# Acknowledgments

I would like to start by thanking my all my advisors during this work. They changed over the years but (in one person or another) never failed to provide the necessary support and guidance, including funding, insightful discussions and a principle to always demand high quality work. I always felt they believed in me, giving me freedom and encouragement to follow my own research path. I thank Prof. João Barros for creating such an international, talented and heterogeneous group here in Porto, for inviting me to join it when I had no idea what doing research really involved, and for choosing great professionals to guide me in his absence. I will always admire his enthusiasm and commitment to turn his vision into reality. I would like to express my gratitude to Dr. Traian Abrudan, who supervised the first part of my PhD work both while he was part of our group in Porto and while he was in Oxford. As a post-doc in our group, Traian has been a hard-working example of great research work. He taught me a lot on so many different topics, gave me friendly advice, and even from afar, has always been available and most helpful. I also thank him for welcoming me to Oxford, inviting me to his home to have lunch with his lovely family. His invitation to visit the Sensor Networks Group from the Department of Computer Science in the Oxford University was a greatly appreciated opportunity, whose outcome was my first journal paper. I extend my gratitude to Prof. Ana Aguiar for joining me on this journey until the end and for her unwearying dedication to our research group, giving it a new chapter. She has agreed to supervised me even though she was already so busy with all her responsibilities, offered key support and encouragement even when she was not my official advisor, and always gave her best during both good and bad moments. I highly appreciate her genuine and honest personality, her sense of ethics and her critical spirit.

I would also like to express my sincere thanks to Prof. Niki Trigoni for the opportunity of visiting her group in Oxford University and for her extremely valuable inputs during our brain-storming discussions; and to Zhuoling Xiao for his help implementing the motion model with the smartphone sensors. I also thank João Rodrigues for his support with his SenseMyCity app to collect smartphone data.

I thank University of Porto for providing such a welcoming environment for learning and sharing knowledge, and specially FEUP for being a second home during all these years. I feel very proud to have witnessed the great evolution this institution has suffered in its constant pursuit to do more and better. I extend my gratitude to Instituto de Telecomunicações (IT) for being a great host institution, providing all the resources necessary for my work, including infrastructure, work conditions, and opportunities, along with a friendly environment to do research. The work developed was not possible without the support provided by FCT – Fundação para a Ciência e a Tecnologia (Portuguese Foundation for Science and Technology) under individual grant SFRH/BD/70748/2010, and by the project S2MovingCity (CMUP-ERI/TIC/0010/2014).

A word of appreciation is also due to: my professors at FEUP, in particular Prof. Maria do Rosário Pinho, Prof. Pedro Guedes de Oliveira, Prof. Aníbal Matos and Prof. Jaime Cardoso for always being available when I knocked at their office door with a question; to the IT Porto

senior researchers and leaders for always organizing such good team building activities, events and meals, creating opportunities for us all to be together and have fun; to Prof. José Soeiro for his confidence in me by accepting my request to teach Operations Reserch when I was a junior PhD student; to Prof. Jaime Cardoso (again) for his generous distribution of Statistics and Probability tests correction tasks while I was writing this thesis; to the FEUP staff, namely José António, who kindly helped me with administrative matters in the department; Maria do Rosário Macedo and Isidro Ribeiro for their crucial help in organizing the 1st PhD Students Conference; to the IT staff, who changed over the years but whose help was a constant to aid PhD students deal with administrative matters; to the whole Veniam team for their welcoming attitude when I visited them; and to all the communities from FEUP and IT for providing such a pleasant environment to work and grow.

Thank you to my colleagues in IT Porto and FEUP, in particular all IT Shannon Lab researchers, who have been a source of friendship as well as good advice and collaboration. They are too many to name so I leave only a special greeting to (former and current) PhD students who shared a large part of this journey with me: Gerhad Maierbacher, João Paulo Vilela, Paulo Oliveira, Rui Costa, João Almeida, Diogo Ferreira, Mari Nistor, Hana Khamfroush, Alexandre Ligo, Luís Pinto, Saurabh Shintre, Rui Meireles, Pedro Santos, João Rodrigues, Damião Rodrigues, Orangel Contreras, Emanuel Lima, and Carla Silva, with an extra word of gratitude to the ones who helped me with the experiments for the cooperative approach, including the first ones in INESC park. To the Walking Shannons in the Skype group a gigantic thank you for all the shared meals, coffees, (inside) jokes (*I could but I can't*), and daily moments where we discussed complex research topic as well as everyday life trivialities. Your good humor, moral support, insightful discussions, and friendship are valuable to me.

There are numerous people who have crossed paths with me during this journey and who directly or indirectly helped me. Although I couldn't possibly name them all, I am grateful to each one of them. I conclude with some words of heartfelt gratitude in Portuguese to my most close friends and family.

Agradeço à minha família, original e adquirida, por ser um exemplo de convívio saudável, espírito trabalhador e me proporcionar diariamente um espaço onde crescer. Gostaria de dedicar uma palavra especial de gratidão à minha mãe, pela dedicação e apoio incondicionais em todos os momentos e aspectos da minha vida; ao meu pai, por ter respondido com prontidão, entusiasmo e boa vontade sempre que lhe pedi ajuda, sem excepção, e pelos conselhos que eu nem sempre segui mas sempre apreciei; aos meus irmãos Ana e João por me inspirarem a pensar em grande; aos meus amigos André, Alice e Rui pela presença nos bons e maus momentos; à Inês, colega feupinha, e à Daniela, cuja compreensão excede as palavras, pela amizade que nasceu no infantário e cresceu connosco ao logo dos anos e havia de incluir no seu percurso esta ideia ambiciosa que todas partilhamos de fazer um doutoramento; à minha prima que infelizmente não está cá para partilhar comigo esta etapa, mas cuja amizade acompanha e influecia diariamente a minha vida; e finalmente ao Pedro e à Líria por tudo aquilo que nunca caberia numa folha de papel. Obrigada por constituírem sempre um lugar caloroso e acolhedor para onde regressar.

Susana Pereira Bulas Cruz

# Contents

xiii

**1 Introduction** **1**
1.1 Problem Formulation . . . 2
1.1.1 Cooperative Approach . . . 3
1.1.2 Magnetic-Based Individual Localization . . . 5
1.2 Main Contributions . . . 6
1.3 Thesis Outline . . . 7

**2 Localization for Road Vehicles** **9**
2.1 Information Sources . . . 9
2.1.1 Satellite-Based Information: GNSS . . . 10
2.1.2 Kinematics Information: Motion-Based Sensors . . . 14
2.1.3 Wireless Signal-Based Information: Communication and Ranging Devices 14
2.1.4 Visual-Based Information: Cameras . . . 19
2.1.5 Map Information: Digital Road Maps . . . 20
2.1.6 Conclusions . . . 20
2.2 Information Fusion . . . 21
2.3 Performance Evaluation . . . 23
2.4 Cooperative Localization . . . 23
2.4.1 Context-Based Cooperative Localization . . . 24
2.4.2 GNSS-Based Cooperative Localization . . . 25
2.4.3 Range-Based Cooperative Localization . . . 26
2.4.4 Summary . . . 29
2.5 GPS-Independent Localization . . . 30
2.5.1 Magnetic-Based Localization . . . 33
2.6 Related Work Summary . . . 35

**3 Cooperative Localization in Vehicular Networks** **37**
3.1 Problem Formulation . . . 37
3.2 Model Assumptions . . . 38
3.2.1 Path-loss Channel Model . . . 38
3.2.2 Map Information . . . 42
3.3 Inference Algorithm . . . 42
3.3.1 Bayesian Approach . . . 42
3.3.2 Proposed Filter . . . 43
3.4 Experiments with Real Data . . . 46
3.5 Concluding Remarks . . . 53

**4 MagLand: Magnetic Landmarks for Road Vehicle Localization** **57**
4.1 Fundamental Insights . . . 58
4.2 MagLand Overview . . . 60
4.3 Sensor Data and Pre-Processing . . . 64
4.3.1 Sensor Data . . . 64
4.3.2 Data Pre-Processing . . . 65
4.4 Magnetic Anomaly Detection . . . 69
4.4.1 Anomaly Detection in Time Series . . . 70
4.4.2 Dataset Description . . . 71
4.4.3 Data Processing . . . 72
4.4.4 Classification Model . . . 75
4.4.5 Analysis per Block Anomaly . . . 79
4.5 Magnetic Anomaly Matching . . . 80
4.5.1 Dataset Description . . . 83
4.5.2 Classification Model . . . 84
4.5.3 Reference Signatures . . . 89
4.5.4 Performance Analysis . . . 90
4.6 Concluding Remarks . . . 92

**5 Discussion and Future Directions** **95**

**6 Conclusion** **99**

**References** **101**

# List of Figures


1.1 System scenario: a set of road vehicles with 802.11p communication capabilities and on-board sensors. . . . 3

2.1 GDOP examples . . . 11
2.2 Lateration examples . . . 15
2.3 Angulation examples . . . 16

3.1 System scenario: a set of road vehicles with 802.11p communication capabilities and onboard sensors, optional road side units and GPS availability. . . . 38
3.2 Pairs of GPS estimated distance and RSSI used to determine channel parameters along with the estimated model. . . . 39
3.3 Normalized histogram of the residual RSSI error for all pairs of GPS estimated distance and RSSI, using the estimated channel model, along with the corresponding Gaussian curve fit. . . . 40
3.4 3D view of the likelihood function of $V_0$'s position (top), and the corresponding heat map (bottom). . . . 41
3.5 Urban trajectory of approximately 7 km in Porto, Portugal. . . . 46
3.6 Setup for data collection in the four vehicles: NEC LinkBird MX and GPS receiver on top of the vehicles, and two smartphones (Nexus 4 and Nexus 5) inside each vehicle. . . . 47
3.7 Various metrics for the whole trip displayed per second. . . . 49
3.8 CDF of location error in meters. . . . 50
3.9 Video frames from the last vehicle, anchor $A_3$, for illustrative purposes of vehicle geometry during the trip. . . . 51
3.10 Geometry of anchors and $V_0$ during the trip: longitudinal distances (measured along the road) $D_{ij} \geq 0$ between the vehicles' antennas vary in time and represent the distribution of vehicles in space. The leading vehicle is $V_0$ and $A_1$, $A_2$ and $A_3$ follow in that order (their colors correspond to the ones used to represent them in Fig. 3.7), either in one lane or in two lanes when possible. Except for very close distances, both geometries have a similar impact. For large distances the configuration on the right can be approximated by the one on the left, so the geometry is mostly in line following the VOI. . . . 52
3.11 Likelihood from V2V for in line geometry of the anchors . . . 53

4.1 Examples of roads where magnetic anomalies are detected. . . . 57
4.2 Heading data from several information sources, with highlighted magnetic anomalies. . . . 58
4.3 Heading estimated in each of the four vehicles for the same subset of the trip. . . . 59

4.4 Seven locations with detected anomalies in all four vehicles in Porto's downtown area. . . . 60
4.5 Magnetic data in the three local axis of the smartphone collected in a highway crossing (length 64m) with different speeds from 30 km/h to 60 km/h, in both directions of the road. . . . 61
4.6 Data from the same highway crossing, collected on different dates, using distinct vehicles and smartphones, and with different speed patterns. The plots show the speed in m/s (top), and four magnetometer vector magnitude curves for each direction, in time (middle) and space (bottom), with offsets in *y* axis for clarity. . . 62
4.7 System model describing the different steps of the proposed approach. . . . 63
4.8 Vehicle setup for data collection in one of the trips, using three smartphones (two Nexus 4 and one Nexus 5) fixed on the windshield. Each of the smartphones includes a representation of its three local axes for illustration purposes. . . . 64
4.9 Illustrative examples of bias present in magnetometer data (trip ID 3 and trip ID 4 from Table 4.1) on the horizontal plane of the local vehicle frame (see Fig. 4.10b). The origin-centered circles (green) show the expected horizontal intensity of the geomagnetic field for the broad location (25.1$\mu$T), and the other circles (blue) fit the data. . . . 66
4.10 Reference frames for inertial data. . . . 69
4.11 Calibrated magnetic data (microtesla) projected on the horizontal plane with highlighted anomalies. . . . 72
4.12 Magnetic vertical data (microtesla) with highlighted anomalies. . . . 73
4.13 Boxplot for comparison of 10 classifiers using ROC, sensitivity, and specificity. . . 77
4.14 Training random forest parameters. . . . 78
4.15 Anomaly detection per block. . . . 80
4.16 Illustrative example of a DTW alignment. . . . 81
4.17 Roads where magnetic anomalies were collected: highway crossing 2.5, tunnel 2.2, road above underground station 2.1, and railway crossing 1.2. from Fig. 4.18 83
4.18 Datasets A, B and C maps and descriptions. . . . 84
4.19 Regions of anomaly obtained from Google Maps street view and Google Earth. . 85
4.20 DTW normalized distance histogram for CTS classifier, using dataset *A*. . . . 88
4.21 Classification errors for feature selection. . . . 89
4.22 Example of heading feature averaging for highway crossing 1.1 signature in South direction, in meters. It includes three of the 24 instances collected for reference, and the resultant reference using DBA technique. . . . 90
4.23 DTW normalized distance histogram for CTS classifier. . . . 93

# List of Tables


2.1 Classification of cooperative approaches for VANETs, including examples of each category. . . . . 29

3.1 Location errors for full trajectory (meters) . . . . . 48
3.2 Location errors for intervals with good conditions of the anchors (meters) . . . . 51

4.1 Characteristics of the anomaly detection dataset . . . . . 71
4.2 Time domain and frequency domain functions applied per window to each parameter: 1) minimum, 2) maximum, 3) mean, 4) mean absolute value, 5) absolute magnitude, 6) root mean square, 7) mean absolute difference, 8) mean absolute deviation, 9) standard deviation, 10) skewness, 11) kurtosis, 12) autocorrelation, 13) total spectral power, 14) mean spectral power, 15) peak spectral power, 16) peak frequency, 17) median frequency, 18) mean frequency, 19) first moment in the frequency, 20) spectral entropy. . . . . 74
4.3 Test results for window-based anomaly detection. . . . . 78
4.4 Alternative configurations for DTW classifiers . . . . . 82
4.5 Classification results for CTS classifier (road and lane matching). . . . . 91
4.6 Classification results for PTS 50% classifier (road matching). . . . . 91
4.7 Classification results for PTS 50% classifier (lane matching). . . . . 92

# Abbreviations

| | |
|---|---|
| 1NC | one nearest centroid |
| 1NN | one nearest neighbor |
| 2D | two dimensions |
| 3D | three dimensions |
| aNN | model averaged neural network |
| AOA | angle of arrival |
| AUC | area under the ROC curve |
| BLR | boosted logistic regression |
| C5 | boosting C5.0 |
| CDMA | code division multiple access |
| CFS | correlation-based feature selection |
| CRLB | Cramér-Rao Lower Bound |
| CTS | complete time series |
| DBA | DTW barycenter averaging |
| DGPS | differential GPS |
| DSRC | dedicated short-range communications |
| DT | decision tree |
| DTW | dynamic time warping |
| EKF | extended Kalman filter |
| ENU | East, North, Up |
| FN | false negative |
| FP | false positive |
| GBAS | ground based augmentation system |
| GBM | gradient boosting machine / stochastic gradient boosting |
| GDOP | geometric dilution of precision |
| GNSS | global navigation satellite system |
| GPS | global positioning system |
| IMU | inertial measurement unit |
| INS | inertial navigation system |
| KF | Kalman filter |
| kNN | k-nearest neighbors |
| LiDAR | light detection and ranging |
| LOS | line-of-sight |
| LS | least squares |
| MAE | mean absolute error |
| MAP | maximum *a posteriori* |
| MAP | maximum a posteriori |
| ML | maximum likelihood |

| | |
|---|---|
| NB | naive Bayes |
| NLOS | non-line-of-sight |
| NN | neural network |
| OBD | on-board diagnostics |
| OOB | out-of-bag |
| PF | particle filter |
| PPP | precise point positioning |
| PPS | precise positioning service |
| PTS | partial time series |
| RADAR | radio detection and ranging |
| RF | radio frequency |
| RF | random forest |
| RMSE | root-mean-square error |
| ROC | receiver operating characteristic |
| RSSI | received signal strength indicator |
| RSU | road side unit |
| RTK | real time kinematic |
| RTOA | round-trip time of arrival |
| SBAS | satellite based augmentation system |
| SD | standard deviation |
| SLAM | simultaneous localization and mapping |
| SPS | standard positioning service |
| SVM | support vector machine |
| TDOA | time difference of arrival |
| TN | true negative |
| TOA | time of arrival |
| TOF | time-of-flight |
| TP | true positive |
| TTFF | time-to-first-fix |
| UKF | unscented Kalman filter |
| V2I | vehicle-to-infrastructure |
| V2V | vehicle-to-vehicle |
| VANET | vehicular ad hoc network |
| VOI | vehicle of interest |
| WSN | wireless sensor network |

# Chapter 1

# Introduction

Mobility plays a key role in today's world, yet its limitations bring very significant problems for society such as traffic congestion, pollution, and road accidents that may result in injuries or fatalities. Vehicles are equipped with various sensors as well as good computation capabilities, with the purpose of providing a comfortable and safe driving experience [1]. While they allow the driver to be aware of the current vehicle status and offer several protection mechanisms, those benefits are individual for each vehicle and so have limitations. Intelligent transportation systems are taking a groundbreaking step towards a solution, using recent developments in technologies such as mobile computing, wireless communications, and remote sensing. Vehicles able to collect information about themselves and the surrounding environment take it to the next level by sharing that information with their neighbors, creating large cooperative networks. Communications will most likely become commonplace or even mandatory in future vehicles (e.g. in Europe [2, 3]). Vehicular ad hoc networks (VANETs) are a promising technology to provide reliable solutions for many of the current problems in traffic and enable interesting new user applications [4]. Networks of vehicles exchanging information with each other and the infrastructure are already a reality for citizens in their everyday lives. For example, in the city of Porto, Portugal, more than 600 vehicles including buses, taxis and municipal service vehicles are connected, providing free WiFi access for bus passengers and gathering urban data for smart city applications [5]. Internet access, multimedia sharing, dissemination of road information, autonomous vehicles, enhanced driver assistance, cooperative driving, cooperative cruise control, and vehicle collision warning are some interesting examples of possible applications enabled or enhanced by this VANET scenario [6, 7]. They all ultimately belong to one or more of the three following categories: transportation safety, transportation efficiency, and user services [1].

Most of the aforementioned applications require or benefit from knowing the location of the vehicles [8, 9]. Localization of vehicles is a broad topic. In many cases, such as geographic information dissemination, traffic control, or automatic positioning of accidents, global position information is crucial, while in other situations, such as security distance warning, it is the relative position between vehicles that is needed [10]. Also, different applications have distinct requirements in terms of accuracy [6, 11]. However, it is important to note that the performance

of a localization system is not exclusively about reached accuracy, but also concerns provided integrity, continuity of service, and availability [12]. While accuracy refers to the closeness of the estimation to the real values, integrity gives a measure of how trustworthy the information is. Continuity of service is the system's probability of continuously providing the intended service during the planned working period, and availability provides the percentage of the coverage area in which the system works.

The most widely used localization solution for road vehicles nowadays is given by Global Navigation Satellite Systems (GNSS) [9], mainly USA's Global Positioning System (GPS). In this thesis, we mention only GPS for simplicity, without loss of generality, since it is both the most used satellite system and a commonly applied non-technical term to designate a global position obtained by general satellite systems (for details on satellite based location please refer to Section 2.1.1). GPS provides 3D global position (latitude, longitude and altitude), speed and heading estimations with good availability in outdoor environments. However, this type of solution also has some limitations. The accuracy varies with the number of visible satellites, with their geometry, and with the presence of obstacles disturbing or blocking the signals, including buildings and trees. Consequently, it exhibits large position errors and sometimes ceases to work in multipath environments and non-line-of-sight satellite conditions, e.g. dense urban environments (frequently designated as urban canyons), tunnels, bridges, and indoor or underground areas like vehicle parks [8]. It does not guarantee enough robustness for many critical applications [6, 9]. For these reasons, it is not adequate to be solely used as a localization solution [13]. In addition, information redundancy is beneficial for integrity and security reasons [8]. Therefore, alternative sources of information are required and should be explored in order to provide better performance for localization systems [13].

**Thesis Statement**

It is possible to improve the performance of outdoor localization systems for road vehicles and provide an alternative to GPS in geographic contexts where it presents limitations, by leveraging communication in vehicular networks, available sensors from ubiquitous equipment (e.g. smartphones) and existing road infrastructure.

## 1.1 Problem Formulation

In this work, we consider the following real-world scenario that involves a set of road vehicles and optional road side units (RSUs), deployed in the area of interest, as illustrated in Fig. 1.1. We assume all vehicles are equipped with 802.11p connectivity and on-board sensors, including an accelerometer, a gyroscope and a magnetometer. The 802.11p connectivity allows wireless access in vehicular environments, enabling the vehicles to communicate with each other (V2V) and with the RSUs (V2I). The sensors can be low-cost, for example from the driver's smartphone. We also assume that each vehicle has access to its own speed information, estimated from the on-board sensors or from a different source, such as an OBD (on-board diagnostics) device or GPS receiver.

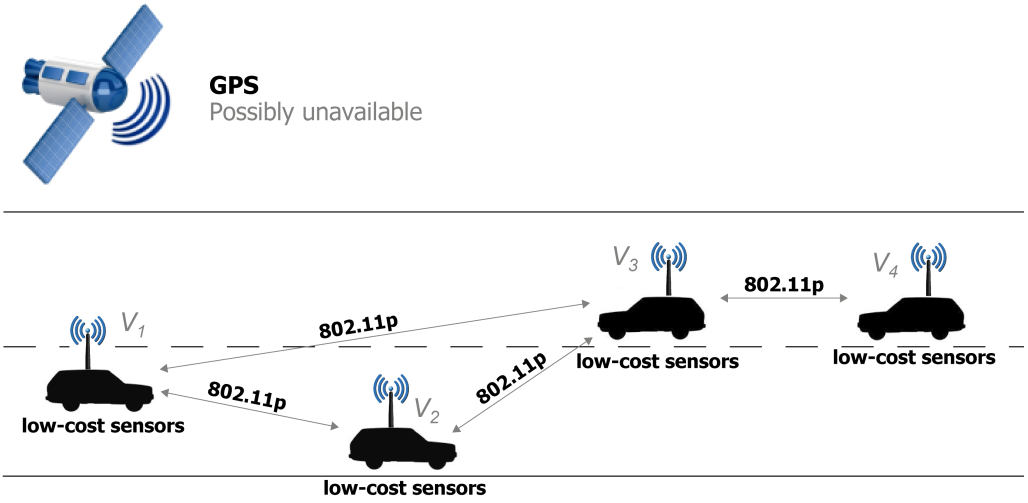


Figure 1.1: System scenario: a set of road vehicles with 802.11p communication capabilities and on-board sensors.

The ultimate goal of the localization problem in a vehicular network is for all vehicles to know and track their own location. We are not interested in overly expensive solutions that, while technically possible, are not feasible or practical to employ on a large scale. Therefore, it is very important to leverage easily accessible or existing equipment and infrastructure. It is also relevant for our solution to provide reliable localization in cases of GPS loss and GPS denied environments. We assume GPS and maps might be available and are integrated in our model making it more robust. However, they are not required for the solution to work.

Our main goal is to devise a GPS-independent localization system for road vehicles, without requiring specific infrastructure or high cost equipment. This system should be compatible with existing ones so that combined approaches result in improved performance. The work developed to achieve this goal explores communications in vehicular networks and low-cost smartphone sensors. These two aspects set the stage for the two pillars of our work: cooperation and individual localization. We address each of them separately.

### 1.1.1 Cooperative Approach

In the first part of our work, we focus on a cooperative approach for localization in VANETs. We define cooperation in our context of vehicle localization, highlight both its great potential and the associated challenges.

Typical localization techniques based on the concept of anchors, consider these as nodes that know their exact location and share this information with others to help them estimate their own positions. By exchanging information with anchors, but not among themselves, regular nodes are able to learn their relative positions with respect to the anchors, and consequently their own locations. The major limitation of this approach is that in order to be applied with full coverage, allowing all nodes in an area to rely on anchors for localization, either high density of anchors

or long-range anchor transmission is required [14]. In vehicular networks, RSUs, also designated as base stations, are used as anchors and the communication range of 802.11p is up to 1000 meters [1]. Obstructions between vehicles and anchors, including other vehicles traveling on the road [15], create non-line-of-sight conditions reducing this range in real scenarios. Therefore, urban environments typically present a communication range of few hundreds of meters [16], depending on the conditions. In this context, deploying a whole network in which any node has enough anchors at reach at all times is highly costly. On the other hand, lower anchor density does not provide enough accuracy or coverage. Cooperative localization arises as an alternative approach to overcome this limitation [17].

The principle of cooperation is that all nodes can contribute to global improvement by sharing useful information with each other. In localization, even without a node's full knowledge of its global position, data such as the estimate of a node's location with the respective uncertainty, its neighbors (nodes at its reach) and its relative position to them, adds new information to the system, leading to superior positioning performance without the need for all regular nodes to be within communication range of fixed anchors [18]. VANETs can highly benefit from these collaborative approaches since vehicles typically have a much higher density on roads than RSUs, making it easier for any vehicle to have several nodes at a short distance. However, using cooperation among connected vehicles presents several challenges, e.g. in terms of scalability, propagation and mobility conditions [19], privacy and security [7].

In real traffic systems, there are thousands of vehicles in the same area creating a very large and highly mobile network of nodes with heterogeneous and imperfect information, imposing significant opportunities and challenges. A relevant element concerns the architecture of the solution. While offering easier algorithm design and usually better estimation accuracy [20], centralized approaches present scalability problems. In networks with high number of nodes, a centralized setting with a single fusion center is inefficient for the task due to limited computational and communication capacities [21]. A distributed scheme enables a more flexible and scalable solution for dealing with dynamic vehicle networks, by handling information locally and processing it in the vehicle itself, spreading the computational burden among the vehicles. Nonetheless, distributed algorithms exhibit different issues, such as how to perform efficient message dissemination under bandwidth limitations. Vehicles also have to deal with the lack of perfect information, data association uncertainties, coordinate transformations, scalability, and avoid the over convergence problem that may arise from error propagation from multiple iterations due to inter-estimate correlation [21, 22]. Another factor to take into account in this context is the time it takes to reach a stable value, since the process cannot take longer than what is acceptable in these types of dynamic networks with high mobility patterns [20]. Several approaches address distributed cooperative localization, proposing novel paths towards a solution, but the complex and large nature of the challenges makes this an active topic in the research community.

### 1.1.2 Magnetic-Based Individual Localization

Cooperative localization has great potential but depends on the quality of the information each node has to share with its neighbors. In outdoor vehicle localization, individual information is usually based on GPS. Frequent availability with line of sight to the satellites, considering temporary exceptions due to multiplath or shadowing [12], is usually assumed. Methods often combine satellite-based information with augmentation systems and/or other sources of information, such as inertial sensors and road maps, to improve the performance, especially in those critical areas, making the estimation more accurate and robust. While these assumptions are reasonable for typical conditions, the solutions based on them are not suitable for special scenarios with permanent absence of GPS or frequent and prolonged periods with imperfect conditions. Our work on individual localization is particularly focused on these challenging scenarios, being nonetheless useful for regular conditions.

Road vehicle localization solutions independent from GPS often require costly infrastructure installations or expensive equipment for the mobile node, preventing an efficient large scale implementation. Although indoor localization consists in a different scenario with distinct requirements and context, as a GPS denied environment it can be a good source of inspiration to develop strategies for this purpose [23, 24]. Yet, it is important to note that, since buildings are a well limited area, it is easier and more acceptable in such scenarios to propose solutions that require a very detailed mapping or installing infrastructure. Magnetic information is frequently used jointly with inertial sensors for orientation estimation in numerous scenarios, including indoor pedestrian tracking and outdoors road navigation. Inside buildings, however, existing metallic structures distort the magnetic field, making it difficult to accurately estimate orientation. Magnetic fingerprinting leverages those distortions. A detailed magnetic map of the whole building is recorded, taking advantage of existing structures that distort the magnetic field in particular ways in different locations, stable in time, allowing their identification and the consequent tracking of a person or object by continuously measuring the magnetic field through their path.

Magnetic data in road vehicle localization is extensively used for orientation purposes, despite the occasional strong local magnetic fields caused by road infrastructures that add to the Earth's magnetic field, creating anomalies. These anomalies are significantly less frequent than in indoor environments. There are a few methods proposing embedded magnetic markers on roads, but deploying infrastructure is quite expensive. Moreover, mapping in detail a large area, e.g. a whole city implies a very high effort. Both would seem unnecessary, especially when GPS already provides near global coverage. The concept of opportunistic magnetic fingerprinting was therefore rarely applied outdoors. We explore how to leverage these anomalies caused by local magnetic fields as magnetic landmarks, taking advantage of easily available magnetic data from low-cost sensors to provide useful location information in road vehicular scenarios. We don't require infrastructure deployment and significantly reduce the mapping effort by focusing on opportunistic locations where distortions are very high. This additional source of information can be very useful to improve reliability and accuracy of localization systems, for example reset dead reckoning

cumulative errors or provide an alternative in environments where satellite-based solutions have limitations, increasing availability and continuity of service.

## 1.2 Main Contributions

The key research question addressed in this work is how to leverage vehicle communications, low-cost equipment and existing road infrastructure in order to improve localization performance in vehicular networks and provide an alternative in GPS limited or denied environments. In the first part of our work, we focus on the cooperation among vehicles and propose a location tracking approach, allowing vehicles to estimate or improve their position using information shared by one-hop neighbors with uncertain locations. This work, presented in Chapter 3, has been peer-reviewed and published at IEEE Transactions on Intelligent Transportation Systems [25]. The second part of our work focuses on providing individual vehicle localization independent from GPS by using ubiquitous sensors (e.g. smartphones). We take advantage of easily available magnetic data, detecting anomalies created by road infrastructure and using them as signatures to provide useful location information. This work, presented in Chapter 4, is under review for IEEE Transactions on Vehicular Technology with the title *MagLand: Magnetic Landmarks for Road Vehicle Localization* and on the process of submitting a request for protection of intellectual property.

Our main contributions can be summarized as follows:

1. a new neighbor-aided localization and tracking approach using moving vehicles with uncertain positions as anchors and proposing suitable V2V anchor conditions;

2. a distributed inference algorithm adequate for large-scale vehicular networks, fusing in a particle filter V2V signal strength measurements, GPS positions, inertial data from a smartphone, and map information;

3. evaluation of proposed approach using real-world data in a challenging urban scenario with quality assessment for flexible combinations of the location information sources, including the lack of GPS information in the ego vehicle;

4. a proposal for individual localization in outdoor scenarios using magnetic landmarks by exploring strong local magnetic fields created by road infrastructure that are regarded as anomalies from an orientation perspective and can act as signatures for a particular path;

5. a method for detecting magnetic anomalies, including data pre-processing, feature engineering and a binary classifier;

6. a method for matching magnetic anomalies, including feature engineering and a classifier, complemented with a process to collect and save instances for reference;

7. evaluation of classification performance for both steps with sensor data collected in field trials including challenging real scenarios.

## 1.3 Thesis Outline

The rest of the document is organized as follows.

**Chapter 2**

In this chapter, we offer an overview of wireless positioning techniques with a particular focus on road vehicular scenarios, comprising different sources of information used for location estimation, methods for information fusion, and performance evaluation. This is followed by a section with a critical state of the art on cooperative approaches for localization in vehicular networks, relative to the work presented in Chapter 3. The last section addresses GPS independent localization methods, giving special attention to the ones based on magnetic information, providing related work concerning the approach described in Chapter 4.

**Chapter 3**

Our proposed cooperative approach is explained in this chapter. We begin by detailing the path-loss model used to extract range information from the strength of the received signal, and then derive fundamental statistical limits on the location error characteristics. We describe our proposed Bayesian inference algorithm and the corresponding state space model for vehicle tracking. As a proof-of-concept, we conduct experiments with collected data on a real scenario, providing an analysis for its performance.

**Chapter 4**

This chapter concerns the individual localization approach based on magnetic landmarks: MagLand. We propose a classification method for the first step, the detection, and the second step, the identification of the magnetic anomalies, using matching and including also a procedure to collect and save anomalies for reference. We evaluate the performance of both steps with real data on challenging scenarios.

**Chapter 5**

We offer an integrated discussion about all the presented work, including strengths, limitations, and future directions.

**Chapter 6**

This last chapter concludes the thesis, giving a personal interpretation of the work and its scope, as well as an analysis of its alignment with the thesis statement and goals.

# Chapter 2

# Localization for Road Vehicles

In this chapter, the broad topic of road vehicle localization is considered. This overview takes into account both network and individual perspectives, since each vehicle can be regarded independently or as a node in a vehicular network.

We start by addressing different sources of data, information fusion methods, and how the performance evaluation of proposed models is achieved in the literature. Some of these techniques are widely applied to different objects and contexts, e.g. satellite-based localization and filters for information fusion. They are, therefore, presented in a more general perspective. Others are more specific to road vehicle scenarios, e.g. several on-board motion sensors and map matching, and so we consider this particular application in more detail.

In the last two sections, we present a more specific and detailed state of the art in the topics of our proposed approaches. In Section 2.4, we focus on cooperative localization in the vehicular network perspective, reviewing and categorizing existing approaches, in relation to the work presented in Chapter 3. We provide an overview of GPS independent solutions in Section 2.5, highlighting magnetic-based strategies. The reader may prefer to initially skip this section and read it only after finishing Chapter 3, as a literature review directly related to the work presented in Chapter 4.

We provide a critical literature review covering all these subjects, considering the depth of the analysis in the light of their relevance to the problem at hand.

## 2.1 Information Sources

We begin by providing a list of the most common information sources and respective techniques to locate nodes, in this case vehicles, individually or as part of wireless networks. Satellite-based solutions are addressed in Section 2.1.1, covering the topic of global navigation satellite systems (GNSS), with a focus on GPS due to its privileged role of currently most used service for

localization. Several types of on-board sensors can be used to gather information useful for localization. These may be divided into three categories: motion (Section 2.1.2), wireless signal[1] (Section 2.1.3), and visual (Section 2.1.4). Triangulation, presented in Section 2.1.3.1 as one of several radio frequency-based positioning techniques, comprises examples of network oriented approaches, widely applied with fixed anchor nodes to wireless sensor networks. In Section 2.1.5, we consider the use of road maps and respective map matching techniques for localization.

### 2.1.1 Satellite-Based Information: GNSS

Satellite-based location information comes from at least one Global Navigation Satellite System (GNSS), which consists in a constellation of satellites transmitting signals from space. These signals allow to obtain global 3D positioning (longitude, latitude, and altitude) and time data. GNSSs use time of flight measurements between receiver and satellite, applying the time difference of arrival technique (see details in Section 2.1.3), to estimate the distance to each of the visible satellites, called pseudorange. To obtain this information at least four satellites need to be available to the receiver, i.e. visible in the sky from its perspective at that moment. The Doppler frequency shift of the signals from the satellites can be measured to provide velocity information for the located node with higher accuracy than the one obtained from differencing consecutive positions.

There are currently four GNSS in either full operational capability or nearing full operational capability status: GPS, GLONASS, Galileo, and BeiDou. There are other positioning systems that do not provide global coverage and function on a regional basis, namely Indian NavIC and Japanese QZSS. The most well-know and used worldwide GNSS is the USA's Global Positioning System (GPS) [26]. GPS operates on two levels: precise positioning service, reserved for authorities, controlled users and USA military, and standard positioning service, globally available for free to anyone with a capable receiver. Restricted access governmental services, such as GPS precise positioning service, are out of scope in this work. Russian GLONASS (***Glo****balnaya* ***Na****vigatsionnaya* ***S****putnikovaya* ***S****istema*, which means Global Navigation Satellite System) is also fully operational [27]. Compared to the GPS, GLONASS market penetration is lower [28]. Europe's Galileo [29], named after the Italian astronomer Galileo Galilei, and China's BeiDou [30] are currently under development and expected to reach full operating capacity with their latest technology by 2020 [28]. In total there are already more than a hundred GNSS satellites in orbit. GPS and GLONASS are employing modernization efforts in order to achieve better performance and higher interoperability. Technical differences between the mentioned GNSS are also out of scope. All of them apply similar principles of positioning. It is worth mentioning that GLONASS uses frequency division multiple access (FDMA) technique, i.e. transmitting satellites are distinguished by the frequency, unlike the other systems, which apply code division multiple access (CDMA), meaning transmitting satellites are distinguished by the code. However, the new generation of GLONASS satellites already implement CDMA strategy in order to improve the

[1] GNSS are also based on wireless signals but due to their specificity and relevance to localization, we opted to address them in a separate section.

compatibility with the remaining GNSSs. The trend in new receivers is the support for multiple constellations and multiple frequencies, which is becoming increasingly widespread in mass market devices [28].

GPS, as an example, is composed of a minimum of 24 (up to 32) operational satellites in medium Earth orbit at an altitude of approximately 20,200 km. The way in which they are distributed guarantees the minimum of four available satellites at any time from virtually anywhere in the globe. The extra satellites improve the precision of the results due to the redundant measurements. The accuracy however does not only depend on the number of visible satellites, but also highly varies with their geometry. Geometric Dilution of Precision (GDOP) measures how errors in the pseudoranges affect the positional estimation precision. The concept of GDOP is illustrated in 2D in Fig. 2.1. While we experience the same error in the estimated distance from each satellite in both cases, the resultant uncertainty of the node location is much higher in Fig. 2.1b because the satellites are placed in a similar direction relative to the node. If, on the other hand, they are well distributed over the whole sky, as illustrated by Fig. 2.1a, the determined position has higher precision.


(a) Good geometrical alignment of satellites (b) Bad geometrical alignment of satellites

Figure 2.1: GDOP examples

Error sources in GNSS can be divided in two types: common or global errors, which are highly correlated among receivers in a wide area (several tens of kilometers), and non-common or local errors, which depend on the precise location and technical construction of the receiver [12]. The main causes of global errors are the atmospheric effects, shifts in the satellite orbits, and clock drifts. Atmospheric effects are related to the reduced velocity of propagation of the GNSS signals in the troposphere and ionosphere due to the fluctuations of the atmospheric conditions, compared to the speed of light of the radio signals in the outer space. Signals from satellites close to the horizon are more affected than signals from satellites directly overhead, since they take a longer route through the atmosphere and are therefore exposed to larger interference. The ionosphere effects

are more severe and introduce higher inaccuracies than the troposphere effects. However, ionosphere effects are frequency dependent and can thus be calculated and mostly corrected with dual frequency transmissions, while troposphere effects cannot be eliminated by combinations of dual frequency measurements. In spite of having very precise orbits, satellites can slightly deviate from them due to gravitation forces. This data is controlled and corrected regularly, being compiled and sent in the package of ephemeris data to the receivers. By processing ephemeris information, these can compensate for some orbital errors. Fine correction is usually available offline, and measurements can be post-processed to improve the location estimation. The atomic clocks on satellites are extremely accurate. Nevertheless, they suffer from noise and clock drift errors. Those errors can be estimated and fairly reduced when that information is available. Concerning non-common errors, we can mention multipath and measurement noise. The multipath effect, also mentioned in Section 2.1.3.1 for affecting time based techniques in general, is caused by reflection of signals on obstacles. For GNSS signals it mainly occurs around large buildings or elevations.

GNSS receivers perform measurements on the pseudoranges to obtain observables of different two types: code and carrier phase. Code phase-based solutions are robust but exhibit limited accuracy. Carrier phase-based solutions can potentially offer very high accuracy, yet have lower robustness and require an estimation of the ambiguities. Single point positioning (SPP), either with single frequency or dual frequency, is based on the code phase observables and is the default method. Single frequency receivers are still the most wide-spread [28]. Dual frequency receivers, limited to professional or governmental users until recently due to their high price, are now available for mass market and becoming increasingly more common. Dual frequency receivers enable the estimation of ionospheric delays, providing not only better accuracy, but also some protection in terms of improved resistance to jamming. There are professional grade receivers that already support triple frequency, allowing integer ambiguity resolution in less time.

It is possible to enhance GPS [2] results with augmentation systems and services, which act as a complement to GPS to improve its performance. These comprise DGPS, RTK, and PPP. Assisted GPS (A-GPS) may also be included. The time required to obtain the signal from the satellites and acquire an initial position estimate, designated as time-to-first-fix (TTFF), can be up to 15 minutes if the receiver was completely turned off (cold start) [31]. To overcome this limitation A-GPS, is frequently employed. This technique provides information useful for positioning to the receiver via a separate communication link. It is widely used, for example in smartphones, to acquire the satellite almanac information using the cellular network. This improves TTFF and also power efficiency.

Differential GPS (DGPS) is a technique that aims to reduce atmospheric and other common errors by using a base station at a known location, or a network of them, serving as a reference receiver that generates pseudorange corrections calculating the offset on the range towards each satellite [32]. This is based on the principle that most errors affecting the measurements are

[2] These techniques are general and apply to any GNSS. However, for consistency with the rest of the document and due to the terms DGPS and AGPS being well known and more commonly applied than AGNSS and DGNSS, we use the term GPS instead of GNSS.

spatially and temporally correlated, so by differencing simultaneous observations made by close receivers they cancel each other out [31]. The designation DGPS relates to code observations. In case the observations are relative to the carrier phase, the technique is called Real Time Kinematic (RTK). The communication link used to transmit these pseudorange corrections to the receivers so that they can improve their estimated location defines the two main types of augmentation systems: satellite based augmentation systems (SBAS) and ground based augmentation systems (GBAS). SBAS rely on a network of reference ground stations deployed across a vast area (covering entire continents) to transmit differential corrections and integrity messages for navigation satellites [33]. Different systems are available in distinct areas of the Earth, although all are compatible and interoperable, as they comply to a common global standard. Examples are EGNOS (European Geostationary Navigation Overlay Service) in Europe and WAAS (Wide Area Augmentation System) in North America. Measurements from the reference stations are sent to geostationary satellites primarily dedicated to the provision of integrity information and wide area corrections. These broadcast the correction messages to that area so that enabled GPS receivers can correct most of the global errors. GBAS support local augmentation through the use of terrestrial radio messages, e.g. dedicated radio communication link or a cellular communication system. Ground stations that accurately know their location take GPS measurements and broadcast real-time corrections to close nodes. In these techniques, the nearer the receiver is to the base station providing the corrections, the more correlated are the errors and so the better is the improvement [32]. Their coverage varies relatively to the baseline, i.e. distance to the base station: SBAS has continent-wide coverage, i.e. can be used up to thousands of km, DGPS (GBAS) can be used up to hundreds of km, and RTK up to tens of km [28].

Precise Point Positioning (PPP) is an alternative to differential methods that consists in estimating all individual error components. While DGPS and RTK depend on the existence of a base station and on baseline length, PPP is based on very precise orbits and clock estimates expressed in a global reference frame, instead of the broadcast satellite orbit and clock information. The solution is global, without a requirement for base stations, and can be either shared with the nodes in real time or used in a post-processed manner. It is characterized by long convergence times and earlier solutions can be used at the cost of accuracy. This limitation may be reduced by the availability of multi constellation, multi-frequency, and RTK information.

A typical GPS receiver performing SPP has an average horizontal accuracy that ranges from a few meters to above 20 m [11]. DGPS increases horizontal accuracy to around 1 m while RTK and PPP enable centimeter-level horizontal accuracy [28]. These techniques[3] focus on common error sources, and require LOS to the satellites to compute a position that may then be enhanced. This means that, despite multi constellation, multi-frequency and augmentation systems significantly improving standalone GPS performance, it still suffers from lack of availability or large errors in NLOS to the satellites and strong multipath scenarios, e.g. dense urban environments, as we have mentioned in Chapter 1.

[3] With the exception of AGPS, a designation that may also be applied in a wider sense and include using information extracted from cellular of Wifi networks to provide location when GPS fails.

### 2.1.2 Kinematics Information: Motion-Based Sensors

There are several on-board motion sensors that can be used for positioning in vehicles. Some examples are odometer, velocity encoder, steering encoder, accelerometer, gyroscope, and magnetometer. These extract information relative to the vehicle kinematics, such as traveled distance, heading, speed, and acceleration. Inertial navigation systems (INS) are autonomous systems that provide dynamic information of the vehicle on which they are mounted through direct measurements, applying dead reckoning techniques [34]. A typical inertial measurement unit (IMU) is composed of three orthogonal accelerometers, three orthogonal rate gyroscopes, and occasionally magnetometers. Although they are widely used in all areas of navigation, INS present position errors that grow with time and distance. Gyroscope and accelerometer data must be integrated to provide absolute measurements of orientation, position and velocity. Consequently, even small errors in the measured data cause an unbounded growth in the error of integrated measurements. To provide useful position information for road vehicles the INS must periodically reset inertial sensors to eliminate their cumulative errors. This can be done by combining INS with other absolute location sources, such as GPS. In fact, combining GPS with dead reckoning is a very common solution for localization of road vehicles, because the first provides global positions but might have frequent short periods of unavailability, and the second has good performance during short periods of time after resetting its cumulative errors [6]. In [35], the authors cover the general topic of inertial motion tracking, identifying aspects with room for improvement in the current state of the art on motion tracking techniques.

### 2.1.3 Wireless Signal-Based Information: Communication and Ranging Devices

Wireless signals are used for localization employing different types of techniques. We first explain triangulation, an anchor-based approach that allows the estimation of relative positions between pairs of nodes in a network with communication signals. Different communication technologies may be used for this purpose, e.g. from cellular networks, vehicular networks, WiFi networks (see Table II from [13] for details on several communication technologies). We also describe relative positioning with exteroceptive sensors specifically used for ranging in current vehicles, such as RADAR or LiDAR. Finally, we address fingerprinting techniques with wireless signals. It is worth mentioning that range-rate measurements may be done using the Doppler frequency shift, provided there is a minimum relative motion between nodes, but we do not provide details about this technique. For details, please refer to Alam et al. [36].

#### 2.1.3.1 Triangulation

Communications in a wireless network may be used to estimate the location of the network nodes [37]. There are several parameters that can be extracted from the measurements, in order to estimate the relative orientation or the distance between pairs of nodes, which allows us to calculate the nodes relative positions [38]. The principle relies on anchor nodes, which are nodes that know and share their location [39]. The most common method to locate nodes through

radio frequency (RF) signals is triangulation. It can be applied using lateration and angulation techniques, which measure, respectively, ranges and angles between a node and the anchors in its reach. In a 2D scenario without errors, in order to determine the possible position of the node by lateration, we would need measurements from at least three non-collinear anchors (see Fig. 2.2a), whereas at least two anchors would be required in the case of angulation (see Fig. 2.3a).

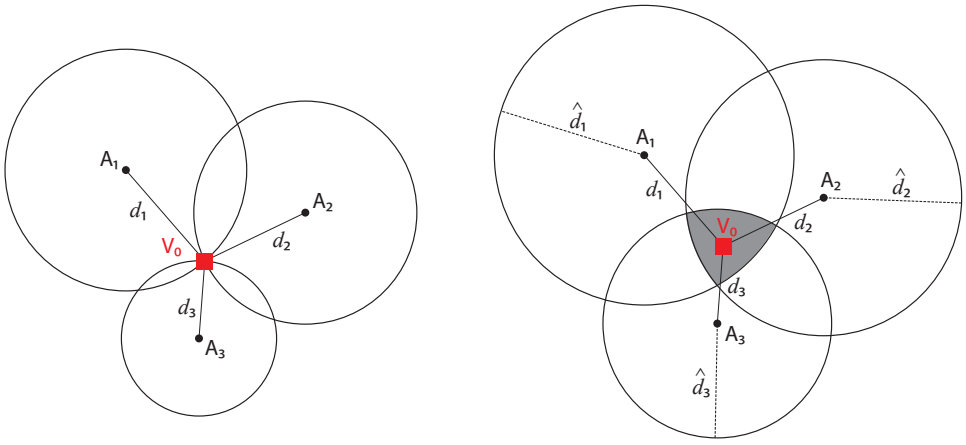


(a) Trilateration with perfect measurements (b) Trilateration with over estimated ranges

Figure 2.2: Lateration examples

However, in a real scenario, the physical medium introduces errors in these range and angle measurements. The errors are usually both time-varying errors (e.g. due to additive noise and interference) and environment-dependent errors resultant of the physical arrangement of objects (e.g. buildings, trees, and obstacles) [37]. Due to the errors in the measurements, the ranges do not intersect perfectly in a single point but rather indicate an area where the position of the node is more likely to be. The chosen point within that area will depend on the applied estimator to calculate the position, for example least squares estimator or maximum likelihood estimator [40]. In Fig. 2.2b lateration with overestimated distances is presented. Fig. 2.3b shows angulation applied to measurements with errors from three anchors.

Different techniques have different sources of error, costs, accuracy, and associated complexity. Therefore, which one is most suitable has to be analyzed for each specific application with its resources, requirements, and goals.

### Lateration

The distance between the nodes may be estimated through a variety of metrics. The two most widely used ranging techniques are based on the received signal strength and the propagation time of the wireless signals [20]. The first one applies calibrated channel models to exploit the relation between power loss and the distance separating sender and receiver, using the RSSI that is

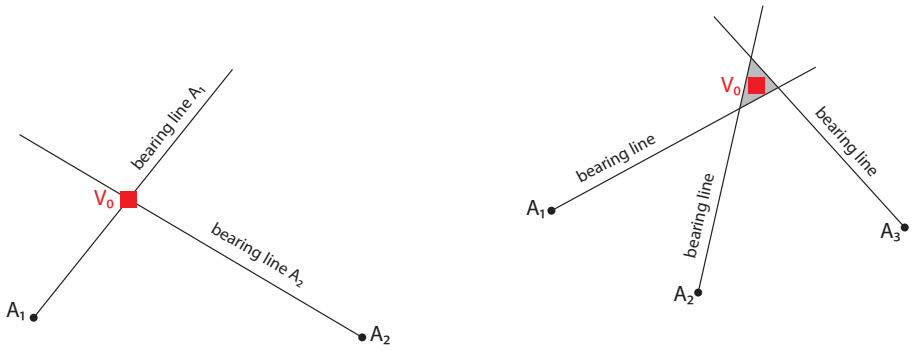


(a) Two anchors with perfect measurements (b) Three anchors with measurement errors

Figure 2.3: Angulation examples

a standard feature found in most wireless devices. Time-based systems include different methods, namely time of arrival (TOA) that uses one-way propagation time measurements, round-trip time of arrival (RTOA) that uses round-trip propagation time measurements, and time difference of arrival (TDOA) that uses time differences measurements.

**RSSI:** In free space, the power of a signal decays proportionally to $d^2$, being $d$ the distance between the transmitter and the receiver. This effect is described in Equation (2.1), known as Friis equation, where $P_r$ and $P_t$ are respectively the received and transmitted power, $G_r$ and $G_t$ are antenna gains (not in dB) of the receiver and the transmitter, and $\lambda$ is the wavelength of the transmitted signal in same units as $d$ (usually meters) [20]. The inverse of the squared factor in parentheses is called free-space path loss, as it shows the loss in signal strength of an electromagnetic wave in free space, i.e. in a line-of-sight path with absolutely no obstacles affecting the signal.

$$P_r(d) = P_t G_t G_r \left(\frac{\lambda}{4\pi d}\right)^2 \tag{2.1}$$

In real-world channels, however, the propagation of a signal is affected by various phenomena such as reflection, refraction, diffraction, and scattering. It is nonetheless accepted on the basis of empirical evidence that it is reasonable to model the received signal strength at the receiver as a random and log-normally distributed variable with a distance-dependent mean value [20]. Since the aforementioned effects are environment dependent, the models have to be calibrated for the intended scenario.

The two major sources of error in this technique are multipath and shadowing [37]. Multipath consists in multiple signals with different amplitudes and phases arriving at the receiver, which makes it difficult to detect the direct path between the nodes to determine their distance. Shadowing arises from the attenuation that the signal suffers due to obstructions, such as walls,

buildings, and trees, which force the signal to pass through the obstacle or diffract around it in its direct path to the receiver. These effects can make the RSSI measurements quite unpredictable, hence the sources of error must be well understood so that the localization is efficient. The significant advantage of RSSI method is that it requires no additional hardware, and thus no additional costs. It is possible to measure the received signal strength of RF signals during normal data communication among nodes. It is also fairly inexpensive in terms of local power consumption and bandwidth [20].

**Time-of-flight:** The distance $d$ between a pair of nodes can also be calculated through time-of-flight (TOF) measurements $t$ and the travel speed of electromagnetic waves $c$.

The first technique, TOA, consists in measuring the one-way propagation time. The transmitter sends a packet containing the instant of transmission $t_1$. Under ideal conditions, i.e. if both clocks are perfectly synchronized to a common time reference, when the packet arrives at the receiver at $t_2$, it is possible to obtain $t = t_2 - t_1$, the propagation time of the wireless signal, from which the distance can be estimated. Therefore, to use TOA in a real scenario the local times at the transmitter and the receiver must be accurately synchronized, since a synchronization error significantly affects ranging error. This requires highly accurate clocks and sophisticated synchronization mechanisms, which increase both the cost and the complexity of the network nodes [20].

To avoid the need for a common time reference, RTOA may be used [41]. In this case, the transmitter sends the packet with a timestamp $t_1$ and receives it back at $t_2$, estimating the distance from the two-way ranging. Because the same clock was used to compute the round-trip propagation time, synchronization is not a problem. The major error is from the response delay $\tau$ required for handling the signal in the other node. This internal delay is either estimated via a priori calibration or measured in the receiver and sent to the original transmitter to be subtracted $t = (t_2 - t_1 - \tau)/2$ [20]. However, even a small relative clock offset will correspond to a large error in estimation of $t$ due to error accumulation over $\tau$, which can be of some microseconds, while the propagation within a few meters is typically in the order of nanoseconds [42]. RTOA is the most practical time-based technique in a distributed architecture, since a common time reference between nodes is not necessary [14].

Differential time of arrival technique differs from the TOA approach by eliminating the need to know when the signal was transmitted, i.e. it does not require the node whose location is estimated to be synchronized with the anchors, but it does require all the anchors to be precisely synchronized among themselves. The signal is received by these nodes that know their position and have a common time reference, and TDOA uses the difference in arrival times at a specific time instant to estimate the location of the transmitter. This is done using a hyperbolic technique, since the measurement from each pair of anchors defines a hyperbole in which the node is located (assuming perfect measurements) [20].

The key of time-based techniques is the node's ability to accurately estimate the arrival time of the line-of-sight (LOS) signal [37]. Therefore, non-line-of-sight (NLOS) conditions caused by obstructions in the direct path between nodes often lead to overestimated ranges [42]. Other sources of error in TOF techniques are multipath effects, additive noise, and the aforementioned

clock drifts. The first can make the detection of the direct path component, if it exists, very difficult, leading to large errors in the distance estimate.

#### Angulation

Angle of arrival (AOA) measurements provide localization information by estimating the direction to neighboring nodes (see Fig. 2.3), rather than the distance. The angle of arrival of a signal can be estimated using antenna arrays and AOA estimation techniques. These are based either on amplitude and/or phase response of the receiver antenna array [20]. The first one takes the received signal strength ratio between distinct directions and the second makes use of phase differences of arrival measured on the different antenna elements. Both approaches require multiple antenna elements, so AOA techniques are usually costly due to the specific hardware and can also imply devices with higher size [37]. Another disadvantage is the need of direct LOS path from the transmitter to the receiver for reliable results. Measurements corrupted by NLOS effects may lead to very large errors. AOA sources of error include additive noise, shadowing and multipath. The accuracy of the measurements is also limited by the directivity of the antennas [20].

### 2.1.3.2 Exteroceptive Ranging Sensors

RADAR (Radio Detection and Ranging) and LiDAR (Light Detection and Ranging) are on-board sensors that detect obstacles surrounding the vehicle, including other vehicles. They do this by emitting periodic signals, which bounce back from the obstacles, and allow the application of TOF measurements to estimate the distance between the sensor and the obstacle. While radar uses radio waves for this purpose, lidar uses laser signals. They are frequently applied to estimate ranges in current vehicles, for example in forward collision warning, lane change assistance and adaptive cruise control [32] and are relevant technologies for future autonomous vehicles [11].

**RADAR:** Radar sensors present low power consumption [11], provide relative speed, and are consistent in different weather and illumination conditions [43]. There are two main radar technologies in ITS, namely impulse radar and frequency-modulated continuous wave radar [32]. Automotive radars usually operate at 24 and 77 GHz [44]. Typically, radars are categorized as short-range or long-range. The first are suitable for urban scenarios with low speeds, providing a limited range of less than 50 m, have wider field of view (up to $\pm 30^{o}$) and higher spatial resolution (0.1 m). The latter are suitable for high speed applications, have perception ranges up to 250 m, usually have smaller field of view (around $\pm 10^{o}$) and lower spacial resolution (0.5 m) [44]. The narrow field of view has a negative impact in across track accuracy. The 79 GHz frequency band has been recently made available for long-term operation of radar sensors by the European Commission, which has several advantages: decreased dimension and weight, increased Doppler sensitivity, better performance in accuracy and object discrimination, and possibility of developing common technology for short-range and long-range radars [32].

**LiDAR:** LiDAR devices use 2D or 3D laser scanners to provide high-resolution maps with dense point clouds and are increasingly used in advanced automotive applications [44]. They usually work with wavelengths beyond the visual light spectrum (near infrared) and so their transmit power is limited to complying with eye-safety regulations, imposing practical limits on the measuring range [32]. They typically provide good range accuracy (between 0.02 m and 0.5 m), ranges up to 200 m, and there are laser scanners that have 360$^{o}$ field of view [32]. Lidar devices are not able to measure relative speed, so this information is obtained by differentiating the range of successive scans. Their main disadvantages are the high price and power requirements compared to radars, and the negative impact on performance in some adverse environmental conditions such as incident sunlight, fog, rain, snow, dust, and dirt [11].

#### 2.1.3.3 WiFi Fingerprinting

Another important signal-based technique for localization is WiFi fingerprinting [45]. It consists in an initial phase during which a map of the signal pattern is constructed, e.g. signal strength or the multipath characteristics, and then a second phase in which the node estimates its position by matching observed signals with the values of the reference data. This is a pattern recognition method, whose accuracy greatly depends on the quality of the radio map, i.e. the number of nearby access points and how exhaustive is the training phase. WiFi fingerprint method is mainly used indoors due to the absence of GPS providing a global location, but it is also well-known in outdoor scenarios for road vehicles, mainly in urban areas where the availability of access points is usually higher. In these scenarios, the most common technique to create a signal map is known as war driving [46].

### 2.1.4 Visual-Based Information: Cameras

Visual-based localization consists in estimating the location of the camera that captured a given image. Due to the lack of standard designation and its wide scope, different terms are used relative to this area of study, including camera-based localization, visual geo-localization, image-based pose estimation and similar. Piasco et al. [47] provide a survey on this topic focusing on urban scenarios and categorize the methods into two distinct categories: indirect and direct localization systems. While indirect methods (e.g. [48]) address this problem as an image retrieval task, providing coarse location information by matching reference images, direct methods (e.g. [49]) retrieve the absolute pose of the camera, including position and orientation, according to a known representation, which might be obtained using a mapping modules like SfM (structure from motion) or SLAM (simultaneous localization and mapping).

Robustness to environment appearance changes over time, and data representation, which may be local (point features and geometric features), global (hand-crafted features and learned features) or hybrid (patch features and combined features), are important aspects in this context. These methods are sensitive to severe weather and illumination conditions, as well as observation angle [11]. Reaching high precision pose estimation within a large area coverage is a challenge

for visual localization systems, so their typical trade-off concerns the balance between scale and precision.

### 2.1.5 Map Information: Digital Road Maps

Road vehicles, such as cars, trucks, buses, etc, as the name indicates usually travel on the roads. This is an important piece of information that, if we have access to digital road maps, can be used to reduce the set of possible positions and thus improve the accuracy of estimated location. This technique is known as map matching and consists in correcting vehicles' positions and trajectories to the roads. Some examples of map matching algorithms are available in [50–54]. A survey on this topic is provided by Quddus et al. [55], considering generic and real-time map matching algorithms.

The authors classify the approaches to map matching in four categories: geometric analysis, topological analysis, probabilistic algorithms, and advanced techniques. The first one considers only the geometric shape of the spacial road links and matches the position to the closest point of the road segment. This can be done with point-to-point matching, point-to-curve matching, or curve-to-curve matching. This geometric analysis ignores links connections to each other. Topological map-matching algorithms, on the other hand, use the geometry of the links as well as their connectivity and proximity. Probabilistic approach requires a confidence interval around the estimated position defining an error region. This region is derived from the variance of the sensors used to estimate the location. If only one road segment intersects the region, the vehicle is assumed to be traveling on that road. If more are available, the best match is found employing heading, connectivity, and closeness criteria. Advanced map-matching algorithms involve more complex processes including the applications of probability theory, fuzzy logic theory, and belief theory.

As we mentioned in the previous sections, all sensors that collect data for localization have associated errors. Digital maps also contain errors. Those errors can be geometric, for example displacement and rotation of map features, or topological, such as missing road features [56]. Even if both raw positioning data and map quality are good, map-matching cannot always determine the correct road segment. Several constraints and limitations of existing map-matching algorithms have been identified in [55]. These are related to vehicle position initial determination, the issues of correcting locations in complex road layouts such as Y-junctions, roundabouts and fly-overs, the evaluation of performance particularly in dense urban areas, and the development of confidence indicators.

### 2.1.6 Conclusions

Having addressed each of the main sources of information in road vehicle localization, we can conclude that none can successfully work in every situation [13]. They all present particular requirements, costs, and weaknesses, as well as different strengths. The most effective solution

for localization is to fuse complementary sources that allow better performance and robustness in diverse conditions.

## 2.2 Information Fusion

We described several sources of information and techniques that allow to determine and improve the location of vehicles. The next challenge is how to fuse different types of data in a single estimator for the position.

Considering lateration and angulation techniques, described in Section 2.1.3.1, we can apply either a non-parametric or a parametric approach. Deterministic methods do not make assumptions about the probability density function of the uncertainties and solve the problem by optimizing certain criteria [14]. An example of a non-parametric estimator would be the least squares (LS) estimator, which minimizes the error in a least squares sense. Parametric approaches instead, take into account the statistics of the error in the estimation. Based on the assumption that the errors corresponding to different sensors are statistically independent, a joint likelihood of all available information can be calculated. The greater the amount of data taken into account, the smaller the variance of the likelihood function, i.e. less uncertainty in the estimation. Maximum likelihood (ML) estimator is a parametric estimation method that maximizes the likelihood function [57,58].

Both LS and ML estimators are non-Bayesian, since they do not include any prior knowledge in the estimation process [14]. Bayesian inference methods, which involve prior information and not only the likelihood, can be applied to fuse data from different sources. The posterior distribution is based on both a likelihood of the incoming measurement, and a prior distribution, and these are used to update the posterior dynamically. Therefore, the approach includes an underlying motion model. For a description and comparison of several motion models, please refer to Schubert et al. [59]. The most popular Bayesian estimators are the minimum mean squared error (MMSE) and the maximum *a posteriori* (MAP), which calculate respectively the mean and the mode of the posterior distribution [14].

Typically, when estimating time-varying parameters (a process designated as tracking), filtering algorithms are used. The filters operate in a sequential manner, i.e. they take into account all the past measurements, update the current posterior with each new measurement. They are also able to incorporate a prediction model for the dynamics of the parameters. The idea is to find the best possible estimate for the true state of the system given some noisy observations of that system, predicting next values before the new measurements are received. It is a two-steps process: prediction and update. The choice of a filter is based on a trade-off between accuracy and complexity. The model seeks to provide an appropriate description of the system while being simple enough to present feasible real time computation complexity [12]. This depends on a number of factors including the dimension of the state vector being estimated, the sparseness of the covariance matrix, the data rate of the measurements, the desired accuracy of the state vector, the degree of nonlinearity, and the shape of the probability densities [60]. Next, we describe the most common filters in this context.

**Kalman Filter:** The Kalman Filter (KF) was widely used for navigation for its simplicity of implementation, tractability and robustness. While it is optimal when the measurement and the state transition models are both linear and all errors are Gaussian distributed, information observations and vehicle dynamics in road navigation are nonlinear processes. Therefore, the traditional KF is not adequate for such scenario and the focus of this section are nonlinear filtering methods suitable for vehicle navigation.

**Extended Kalman Filter:** The Extended Kalman Filter (EKF) linearizes the nonlinear functions with first-order Taylor series around the current estimate, in this case the navigation and observation equations, so that the linear KF can be applied. The main issue is that this approach may cause the system to diverge, since approximating the system by a linear one and solving it optimally, is not the same as approximating the solution of the actual system. Nevertheless, it is frequently used in proposed solutions for vehicle navigation, e.g. see Section 2.4. The computational complexity is in the order of $j^3$ for the estimation of a dimension $j$ state vector [60].

**Unscented Kalman Filter:** The Unscented Kalman Filter (UKF) [61], also called Sigma-Point Filter, appears as an alternative to the EKF, specially for highly nonlinear systems for which the latter gives particularly poor performance. The UKF consists in propagating a minimal set of deterministically chosen weighted sample points, called sigma points, that parameterize the mean and covariance of the prior through nonlinear transformations, known as the unscented transformation. The sigma points, by undergoing the nonlinearity transformations, capture the posterior mean and covariance more accurately, while UKF computation complexity is approximately the same as the EKF.

**Particle Filter:** Particle Filter (PF), also known as Sequential Monte Carlo method, uses a set of samples, called particles, to represent the distributions. Each particle is a state with an associated nonnegative weight, the importance factor. All weights sum up to one and the principle is that the higher the weights in one area of the function, the higher the density of particles in that area should be to adequately describe the shape of the distribution. Recursively updating these particles at each time step, leads to a degeneracy problem where only a few of the particles have significant weights, while all the other particles are negligible, giving a poor representation of the posterior density. One way to mitigate this problem is to use a resampling method. Different resampling techniques may be used (see [58]), the most common being importance sampling. This consists in replacing some of the too small weight particles by copies of the most significant ones. Although importance sampling attenuates the degeneracy problem, it also reduces the diversity of the particles, so we have to be careful to avoid severe sample impoverishment, i.e. in an extreme case all particles would occupy the same point in the state space. Usually, choosing a sufficient number of particles prevents this situation, but at a higher computational cost. In fact, the main problem of this filtering method is the large computational complexity compared to the other filters, specially when applied to high-dimensional systems. This is known as the curse of dimensionality [62]. More details on the comparison of nonlinear filters can be found in [60]. The great advantage of PFs is that they make no restrictive assumption about the dynamics of the state-space or the density function.

## 2.3 Performance Evaluation

A very relevant aspect concerning proposed solutions in the literature is how their performance is evaluated. Tests in real environments are complex and expensive, so usually simulations are used for this analysis. These simulations might be based on artificial data, on real data collected in a controlled environment, or on real data collected in a realistic setting. All these options present an increasing trade-off between simplicity that represents low costs, ease of implementation and more quick results, and complexity that while more expensive and time consuming is also more representative of realistic scenarios and consequently provides more reliable insights and stronger conclusions. Other relevant aspects are the size and diversity of the dataset. These depend on the tested approach, but might include number of nodes, vehicles, trips, duration, runs, and how heterogeneous are the analyzed scenarios and used equipment. When using real data, particularly in large datasets, how to obtain localization ground truth is also a very important aspect for performance evaluation.

## 2.4 Cooperative Localization

In Chapter 1, we have explained the concept of cooperative localization and why we believe it is beneficial. We now present a state of the art on the topic, focusing on solutions developed specifically for VANETs.

There is a lot of research in cooperative localization for general wireless sensor networks (WSN) and also in the area of robotics. While parts of those works may be related to our problem and interesting in a vehicular environment, some assumptions and applications make them quite different scenarios. WSN solutions frequently focus on energy and computation constraints, not so significant in VANETs, and are based on static or moderate mobility assumptions, while VANETs are highly dynamic [63]. Despite those differences, there are very relevant works for cooperative localization in wireless networks, e.g. [14, 37].

The area of robotics also addresses the problem of cooperative localization. However, motion and control models for robots differ from the ones for road vehicles. Moreover, robots forming an ad-hoc network typically work together within a limited group that shares a common goal. This also makes it much easier for nodes to have homogeneous and expensive sensors. Nonetheless, there is much to learn from mobile robots localization algorithms, such as the cooperative and distributed approaches presented in [64, 65].

VANETs are a very special type of ad-hoc networks, with particular constraints on vehicle movement, high mobility causing rapid changes in topology, and limited bandwidth [66]. These fundamental differences call for specially tailored solutions. Many authors address the localization problem in VANETs, pointing out that GPS is insufficient, mainly in urban areas. Fusing data from a variety of sources has a positive impact not only on the accuracy, but also on the reliability and other performance metrics, namely coverage and continuity of service. As described in Section 2.1 each information source and technique has different advantages and disadvantages. This makes

certain solutions more suitable for a given scenario than others. Being complementary concerning their limitations is a very important aspect when combining these sources. Information from independent sources can also be useful for integrity monitoring. We believe that exploiting inter-vehicle communications for localization shows great potential. It is the least explored approach in this area so far, compared to satellite-based information, vehicle kinematics, and road maps. First approaches using cooperation among vehicles for localization purposes were presented during the decade of the 2000s and in the last twelve years numerous new ones were proposed. In this section we do our best to make a comprehensive overview. We classify cooperative approaches for vehicular network localization into three categories related to the type of cooperation employed: 1) context-based, 2) GNSS-based, and 3) range-based. In some cases, we consider only one work from each research group.

### 2.4.1 Context-Based Cooperative Localization

Context-based approaches rely either on the road configuration (usually applying digital road maps) or on a mapping of the scene (using exteroceptive sensors like radar, lidar or camera) to perform cooperative localization.

#### Group Map Matching

The first ones are based on the assumption that all vehicles in the network, being geographically close to each other, suffer a common GNSS bias in their local estimated positions that dominates the position error, usually considering non-common error as negligible. The map matching can be performed jointly using constraints from all vehicles to cooperatively match them to the roads, thus improving their location estimates by compensating for the common bias. Lee et al. [67] present such an approach as a cooperative position fix scheme, Mattern et al. [68] include a group map matching as part of their CoVeL positioning system fusing GNSS, odometry and maps, and Rohani et al. [69] and Shen et al. [70] propose approaches that perform cooperative map matching on shared raw GPS data. Dao et al. [71] do not directly use road maps, but share GPS data among vehicles to find lane positions on a highway scenario with a Markov-based approach. They test it with two cars equipped with low-cost GPS receivers. Lee et al. [67] test their map matching approach (not localization) with a large GPS dataset from taxis with no ground truth. The other three approaches use particle filters for cooperative map matching, assuming digital maps with lane information, as part of a location tracking algorithm. Rohani et al. [69] test it with Monte Carlo simulations. Shen et al. [70] perform simulation and real data experiments considering only a static scenario. COVEL project [68] uses a fleet of six vehicles although only four end up being used for tests. One of them is equipped with a high accuracy and high availability GPS+INS reference system to be used as a ground truth for comparison. In [72], Shen et al. present a theoretical study evaluating the impact of road constraints on cooperative map matching.

#### Indirect Cooperative Localization

Context-based indirect cooperative approaches consist in measuring environment range information using exteroceptive sensors to estimate inter-vehicle distances implicitly. This information is combined with absolute position from each vehicle, usually from GPS. Li and Nashashibi [73] perform SLAM with GPS, odometer and laser scanner in each vehicle, merging local maps to indirectly estimate relative pose between vehicles. They use EKF for self-localization and test their approach with real data from an experiment with 2 vehicles in a trajectory of approximately 200 meters inside a campus, using an RTK-GPS for ground truth and degrading it to simulate low-accuracy GPS. In Gulati et al. [22], an infrastructure radar sensor maps the vehicles' topology and provides inter-vehicle distances, used as constraints in factor graphs that contain absolute location information from vehicles on-board sensors. Soatti et al. [74] propose using non-cooperative physical features (e.g. people, traffic lights, inactive cars) sensed by each vehicle (e.g. radar, lidar, camera) as common noisy reference points to jointly refine their location estimates (GNSS). Fröhle et al. [75] track in each vehicle its own state (GNSS) and features in the surrounding environment (radar), sending these to RSU (V2I) to centrally apply nonparametric belief propagation and enabling accurate vehicle states estimation through cooperative feature tracking. The last three approaches use factor graphs and are tested through simulations.

### 2.4.2 GNSS-Based Cooperative Localization

In GNSS-based cooperative localization the distances between vehicles are obtained from raw GNSS observables. These approaches usually require good GNSS coverage with pseudorange information from at least four satellites. This information, as explained in Section 2.1.1, might be based on code or carrier phase measurements. While code delay measurements are robust and unambiguous but noisy, carrier phase measurements can offer high precision but suffer from cycle slipping phenomenon and require solving the integer ambiguity problem [9]. This makes cooperative approaches for vehicular networks based on code measurements much more common than those based on carrier measurements. Although we can mention the works by Bento et al. [76, 77] and Müller et al. [78] as examples of cooperative approaches sharing carrier-phase measurements, we do not consider these further our related work.

#### Cooperative DGPS

The concept of DGPS (see Section 2.1.1) has been extended from the fixed base station aiding mobile nodes to a setup comprised only of mobile nodes where none has the role of base station, i.e. no nodes needs to be static and have an accurately known position. Richter et al. [79] introduced the idea of exchanging GNSS code pseudorange data for inter-vehicle estimation and cooperative relative localization. Their work presents the theoretical formulation but is only based on simulations, without real-world measurements. Pseudorange double differentiation is tested in field experiments for cooperative vehicle localization with fixed positions by Yang et al. [80] (3 and 8

meters baseline) and Liu et al. [81], using a weighted least squares method. Alam et al. [82] are the first to test their DGPS-based relative positioning approach, using tight integration, with real data from moving vehicles. Rohani et al. [83] present their approach as a decentralized dynamic base DGPS method. Several research groups use pseudoranges double difference with a multisensor fusion approach performing dead reckoning, e.g. Müller et al. [84] and Lassoued et al. [85]. All these contributions are based on the assumption that GNSS code pseudoranges are mainly affected by common error sources. Uncorrelated error sources such as thermal noise of the receiver, multipath and other residual errors are viewed as negligible and not taken into account. Tahir et al. [9], considering that this is not a realistic assumption, especially when in densely populated urban environments, study four different ways in which GNSS code observables can be used: 1) absolute positions of the vehicles provided by GNSS receivers, 2) raw code pseudoranges; 3) single difference of the raw code pseudoranges, and 4) double difference of the raw code pseudoranges. They conclude that double difference method is only superior in open sky environments. This technique increases uncorrelated errors and receiver noise while reducing correlated errors, so in dynamic environments with strong multipath, ranging using raw pseudorange is more effective.

Concerning performance, four works are evaluated using real data experiments collected from two moving vehicles: Alam et al. [82] analyze 12 minutes along different roads near the University of New South Wales in Sydney with different speeds and good satellite coverage using single-band GPS receivers and comparing to RTK GPS for ground truth, Müller et al. [84] analyze 30 minutes from a two lane highway scenario and 220 seconds snapshot from a urban scenario in the city of Munich using an automotive laser scanner for ground truth, Lassoued et al. [85] analyze 4 minutes, and Tahir et al. [9] analyze two dynamic scenarios (highway and dense urban).

### 2.4.3 Range-Based Cooperative Localization

Range-based cooperative localization comprises approaches focused on improving vehicles estimated location by using the relative distances between pairs of vehicles. Inter-vehicle distance may be directly measured using advanced on-board range measurement devices (Section 2.1.3.2) or estimated from communication devices using triangulation (Section 2.1.3.1). The first provides higher accuracy [13] and allows to estimate relative bearing between vehicles while the latter only estimates distances. On the other hand, vehicle identification and data association between received information and range measurements are more difficult when using range measurement devices. These are also more susceptible to the requirement of direct visibility: they require direct line-of-sight between objects for detection, while communication devices only need line-of-sight between antennas, which can result in better detection performance in crowded urban areas where vehicles can communicate but block each others visibility [86]. Some exteroceptive sensors (e.g. lidar) have their performance significantly degraded by harsh environment conditions such as heavy rain, snow, fog or darkness [11]. Although in theory we know some of these weather conditions may also affect communications, we did not find conclusive studies considering their impact on ranging estimation using communication devices. These are the main differences between the two methods. We give examples of research works applying each one.

### Range-Based Cooperative Localization using Exteroceptive Sensors

Fujii et al. [87] assume some vehicles are equipped with a ranging sensor such as a millimeter wave radar and measure relative angles and distances to other vehicles in immediate sight until 100 m range, with the goal of estimating the positions of equipped vehicles more accurately than GPS and those of non-equipped vehicles. Li and Nashashibi [21] and Bounini et al. [88] assume each vehicle is able to estimate the relative pose of neighboring vehicles, i.e. relative position and orientation, using exteroceptive sensors such as radar or laser scanners, focusing on the algorithm for information fusion to overcome the over-convergence problem. Sakr and Bansal [89] propose a multi-sensor multi-target track association to perform a track-to-track association for the data coming from two independent sources, which are a ranging sensor that measures the relative pose of different objects in its surroundings (e.g. camera, radar, or lidar) and a DSRC transceiver for V2V communications with vehicles state information. Shen et al. [90] propose a minimal but scalable sensor configuration for a fleet of vehicles localizing on the urban road, although related work and problem description are framed in terms of robots instead of vehicles, assuming a range sensor such as lidar or camera to track relative distance and bearing angle from surrounding robots/vehicles. Jeong et al. [91] formulates the state association problem with a framework of spatiotemporal local-remote sensor fusion, considering the absolute state received from neighbor vehicles and the relative state measured at the on-board radar, presenting a comprehensive model that reflects the detailed limitations of automotive radars.

Information fusion and tracking filters vary considerably in aforementioned approaches: likelihood, Kalman filter and its extended version, and covariance intersection are considered. They are evaluated with simulations except in Shen et al. [90], where three vehicles in a urban scenario (average speed of 3 m/s) perform ranging with 2D lidar sensors (the trajectory does not have a reported length, but from the provided material we estimate it as being around 270 meters).

### Range-Based Cooperative Localization using Triangulation

Considering triangulation methods for inter-vehicle distance estimation, there are some authors that assume the use of these techniques without specifying any in particular. Drawil and Basir [92] propose an approach in which every vehicle is equipped with a GPS receiver, an INS and a VANET transceiver. The inter-vehicle communication system extracts information pertinent to the location estimates of vehicles in its vicinity: the distance between the vehicle and its neighbors, the location estimates of the neighbors, and the level of uncertainty in their location estimates. Vehicles with the smallest uncertainty in their location estimate are used as anchors. The work includes a multipath detection unit, which is trained using a neural network, and vehicles with detected multipath are not used as anchors. Ahammed et al. [93] present VLOCI2 algorithm. The goal is to improve GPS position accuracy with ranging techniques (RSSI or TOA), using a weight function so that closer vehicles have higher impact since inaccuracies increase with the distance. The position estimation is updated in various iterations and afterwards rounded to the center of the nearest lane. Yao et al. [94] examine the impact of range information exchange overhead. They state

that the frequent exchange of large amounts of data required in cooperative positioning can cause significant packet collisions, mainly in dense traffic conditions, affecting both the effectiveness of the algorithms for positioning and the performance of the applications that use this information. Some mechanisms for optimizing cooperative positioning in dense vehicular networks, in terms of improving positioning accuracy and reducing the packet collision rates, are proposed: piggybacking, compressing the range information, tuning the broadcast frequency, and combining multiple packets using network coding. Rohani et al. [86] propose a pre-filtering of GPS positioning measurement using inter-vehicle distances and other vehicles GPS measurements obtained from V2V communications, before applying the tracking algorithm. Ekambaram et al. [95] provide a practical distributed localization algorithm using an analytical graphical model framework, considering a multipath-rich environment with low percentage (less than 35%) of LOS signals. Gulati et al. [96] formulate range information from vehicle communications as a new DSRC range factor, in addition to the symmetric measurement equation factor, in a factor graph in order to perform cooperative localization. In all these approaches the algorithms vary, comprising graphic models, KF, EKF, PF, and combinations of those. All proposed models are evaluated using simulations.

There is also research focusing on a particular method for ranging estimation with wireless communication devices. Alam et al. [97] propose improving GPS estimates using inter-vehicle ranges based on the extracted Doppler shift from the carrier frequency offset of the received packets from neighbor vehicles traveling in the opposite direction. Golestan et al. [98] use both TOA and AOA measurements to estimate the distance and angle to one hop neighbors in order to improve vehicles location information. Fascista et al. [99] define a tracking algorithm with asynchronous updates triggered by beacon packet receptions, obtaining opportunistically angle of arrival estimates. Mohammadabadi and Valaee [100] introduce a new distance ranging method that uses time-difference-of-arrival in synchronous positive orthogonal codes. Elazab et al. [101] present a cooperative localization scheme that utilizes RTOA for inter-vehicle distance calculation. Yuan et al. [102] provide a factor graph representation of the joint localization and time synchronization problem based on TOA measurements, taking NLOS measurements into consideration. Li et al. [103] propose a two steps method for TOA estimation using the IEEE 802.11p short preamble. Hoang et al. [104] propose a cooperative localization approach that relies on V2V communications (802.11p) to share GPS position estimates and on impulse radio - ultra wideband V2V ranging measurements based on TOF to estimate distances between vehicles. Considering the use of signal strength measurements for range estimation, Parker and Valaee [105] published in 2007 one of the first, most important and the most cited paper concerning cooperative localization in vehicular networks. In [105], each vehicle shares its own velocity and distance to the neighbors, calculated through RSSI, among its cluster of vehicles. GPS, if available, is used only to define the initial position since the focus is on the vehicles relative positions. Accuracy is increased by using road constraints downloaded from the nearest RSU. Uncertainty along the road is set to be higher than uncertainty in the orthogonal direction. To the best of our knowledge no other work for cooperative localization of road vehicles focused specifically on RSSI for range measurement until very recently (see Section 3.5). Again, applied filters vary, being KF and its extensions,

| | | |
|---|---|---|
| Context-Based | Cooperative Map Matching | E.g.: Dao et al. [71], Mattern et al. [68], Rohani et al. [69] |
| | Indirect Cooperative Localization | E.g.: Li and Nashashibi [73], Gulati et al. [22], Soatti et al. [74] |
| GNSS-Based | Code Observables | E.g.: Richter et al. [79], Alam et al. [82], Liu et al. [81], Tahir et al. [9] |
| Range-Based | Exteroceptive Sensors | E.g.: Fujii et al. [87], Li and Nashashibi [21], Sakr and Bansal [89] |
| | Communication Devices | E.g.: Parker and Valaee [105], Drawil and Basir [92], Ekambaram et al. [95], Yuan et al. [102], Fascista et al. [99] |

Table 2.1: Classification of cooperative approaches for VANETs, including examples of each category.

mainly EKF the most common, followed by PF. The only approach not evaluated with simulated data is Hoang et al. [104]. Three vehicles in a highway scenario forming a platoon are tested using impulse radio ultra wideband for ranging measurements between vehicles. Selected 30s sections with consistent data are used for analysis. None of these ranging estimation methods with V2V 802.11p communication devices has been evaluated with real world data.

### 2.4.4 Summary

We summarize our classification of cooperative localization approaches for road vehicles in Table 2.1, providing examples of research works from each category. Cooperative map matching and GNSS-based approaches rely on GNSS measurements, assuming low local error. They suffer, therefore, the same problems of all satellite-based approaches in NLOS satellite conditions and multipath environments. Indirect cooperative localization and range-based approaches using exteroceptive sensors share the limitations associated with the use of these sensors. These include requirements for LOS between vehicles or vehicles and features, data association issues, as well as specific constraints of each type of sensor. Localization using communication devices for V2V triangulation is affected by the variability of the wireless medium, NLOS conditions between antennas, shadowing and multipath scenarios [36]. It is also limited by the particularities of each technique, as detailed in Section 2.1.3.1.

**Information Sources:** It is interesting to observe that all these approaches are based on the combination of several data sources. Not only, as cooperative approaches, information collected with a vehicle's on-board sensors about its state and surrounding environment is combined with information collected and shared by other vehicles, but also individual data frequently fuses measurements from more than one type of sensor. Absolute positioning is provided by GPS and is frequently combined with some form of odometry (e.g. wheels and yaw rate sensors [68], distance and yaw rate from odometer [73], INS [92], MEMS-INS and speed and steering wheel from OBD [103]) and/or digital road maps. Inter-vehicle distances are obtained from GPS (assuming

common bias and negligible non-common errors), range measurement devices, or triangulation from V2V communication signals.

**Information Fusion:** Considering the fusion of all these sources of information, different algorithms are used. Although in context-based approaches particle filters are the most common choice for cooperative map matching and factor graphs for indirect ranging localization, overall EKF is the most used filter for information fusion and location tracking (e.g. [73, 88, 92, 97, 99, 101, 105]). Some approaches use a combination of different filters, e.g. EKF and PF [98], UKF and PF [68], KF and UKF [84], and PF, Sage-Husa adaptive filtering and KF [103]. In [21], a Split Covariance Intersection Filter is proposed to overcome the over-convergence problem.

**Performance Evaluation:** Some of the aforementioned research papers provide a theoretical analysis by calculating the Cramér–Rao lower bound (CRLB), e.g. [82, 94, 95, 105]. The majority of the presented approaches perform simulations with artificial data for their performance evaluation. Some of these consider limited scenarios (e.g. a straight highway of few kilometers [92, 105]) that do not pose most of the challenges faced in real situations, especially in urban settings, such as alternative paths (bifurcations, intersections, roundabouts, etc), sinuous routes, multipath and shadowing effects from numerous obstacles (including moving ones) and non-line-of-sight communications. Only few cooperative localization approaches evaluate their proposed algorithms with post-processed data collected in real scenarios [68, 73, 82, 84, 104]. Context-based and GNSS-based approaches contain more evaluations with real data, possibly because GNSS data is easier to collect than V2V communications data.

Recent surveys address relative positioning of vehicles using ranging sensors and cooperative approaches [32], localization techniques and their potential for autonomous vehicle applications [11] including a section about cooperative localization, and connected vehicles landscape [7], exploring key enabling technologies, opportunities and challenges. VANETs are a very special type of ad-hoc networks, with particular constraints on vehicle movement, high mobility causing rapid topology changes, and limited bandwidth [66]. These fundamental differences ask for specific solutions. To be comprehensive, these should take into account the protocol to exchange data, the drawbacks of wireless communications in the real world, such as bandwidth limitations, packet drops, channel congestion, obstacles (including vehicles [15]), data security, and user privacy [106], and location integrity and reliability [107]. Cooperative localization focusing on vehicular scenarios is a relatively recent area (just over 10 years) that has experienced great contributions but still offers numerous research challenges.

## 2.5 GPS-Independent Localization

As aforementioned, a variety of information sources can be combined for better performance in road vehicle localization. It is common to focus on GPS as the base of the proposed solution, combining it with additional data and techniques to make it more accurate and robust. Most existing solutions for outdoor vehicle localization are heavily dependent on GPS due to its global positioning information that also provides velocity and time, broad availability outdoors and good

accuracy in open spaces with line-of-sight to numerous satellites with suitable geometry. Even when fusing diverse sources of information, most methods rely on GPS availability, either fully or partially, frequently with minimum performance requirements such as the minimum number of visible satellites, negligible multipath, maximum outage time, etc. Considering the types of approaches most dependent on GPS in vehicular networks, we can mention those that rely on GPS combined with augmentation systems, GPS combined with digital maps, GNSS-based cooperative approaches, and group map matching.

However, when the ideal conditions for GPS are not present, these approaches suffer from poor performance. Scenarios common for vehicles such as tunnels, urban canyons, underground or indoor facilities like car parks, multiple highway crossings at different heights, or any other situations where GPS fails, are not covered by these models. Their core assumption that there is recurrently an adequate global position from the GPS obtained with LOS to the satellites, which is then improved by additional sources, is not verified. We dedicate this section to review localization approaches that consider the absence of GPS, either permanent or temporary, giving particular attention to their requirements in terms of expensive equipment and infrastructure.

There are different types of approaches that rely only partially on GPS. These include the ones that are robust to GPS temporary outages, and those that are mainly based on relative position information, using GPS only for initial positions or assuming its availability solely in a subset of the network nodes. The first ones typically rely on on-board motion sensors to provide adequate positioning during GPS absence. However, due to the cumulative nature of the errors from these sensors (see Section 2.1.2), they are resilient only to a limited period without GPS signal or with high GPS errors, e.g. Najjar and Bonnifait [52] and Rezaei and Sengupta [108] test their proposed approaches with GPS outages of 2 km and 30 seconds, respectively. Cooperative approaches focused on range-based data, both from communication devices and range sensors, can extend aforementioned individual localization solutions to make them more robust to GPS failures, high errors and temporary or permanent absences.

There are different perspectives concerning how the dependence of each approach on absolute position information, usually obtained from an on-board GPS receiver in the vehicles, is presented. We consider the following assumptions: 1) full availability including ego vehicle, 2) availability for a subset of the network nodes, 3) availability only for initialization, and 4) not considered. The first one is the assumption of absolute position information in all network nodes. GPS availability is a reasonable assumption in many environments, so in these cooperative approaches GPS absence is not addressed. Since its impact is not evaluated, we regard those as dependent on GPS even if they may potentially be resilient to some nodes or some periods without GPS. The second perspective takes into account the absence of GPS in a percentage of the vehicles and evaluates that impact on the proposed model, e.g. Lee et al. [109] and Elazab et al. [110]. There are also some methods that include GPS as part of the proposed system, but do not consider it vital, since only an initial global position is required, e.g. Parker and Valaee [105] and Levinson et al. [111]. Communications among vehicles allow them to share both individual localization and inter-vehicle distance measurements. Some approaches focus on relative localization and make

no considerations about the availability of absolute position information in any of network nodes, e.g. Alotaibi et al. [112].

Finally, we consider the types of approaches that are not dependent on GPS, which comprise both those that do not include GPS and those that consider GPS as a non-vital part of the system, i.e. the system may have GPS but it can work even if it is completely absent. We identify two main categories of vehicle localization approaches, concerning the core strategy that enables absolute positioning: fingerprinting-based and infrastructure-based approaches. These are not mutually exclusive.

Fingerprinting-based approaches require an offline mapping phase and an online localization phase. Their main limitations are related to their opportunistic nature, which does not guarantee availability of distinguishing features to allow global positioning with enough accuracy for envisioned applications, and to the high mapping effort. Fingerprinting-based strategies for road vehicle localization include WiFi fingerprinting, visual fingerprinting, and localization using lidar maps.

Infrastructure-based approaches rely on infrastructure deployment with a certain density to enable global coverage. Applied techniques are based on either proximity or triangulation. Proximity-based approaches share the main principles of fingerprinting, but relying on installed rather than opportunistic infrastructure, e.g. RFID or embedded magnetic markers on the roads. Triangulation (see Section 2.1.3.1) uses base stations that broadcast their known and fixed location so that nodes in range can use it along with lateration or angulation techniques to locate themselves. It can be applied to different types of networks and required density depends on signal range and on accuracy requirements. In vehicular networks, infrastructure-based approaches using triangulation mainly consist of vehicles estimating their locations using V2I communications to RSUs. For example, Ou [113] uses TOA techniques, relying on a large infrastructure of RSUs deployed in both sides of the road so that a vehicle can be connected to at least one pair of RSUs at all times. More recently, Ma et al. [114] propose an IMU-assisted single RSU localization algorithm.

We can conclude that while most proposed vehicle localization approaches in the literature rely on the almost ubiquitous availability of GPS, there are several solutions that do not depend on it or are partially robust to its absence. Inertial sensors and maps are useful information sources but require some form of absolute positioning to provide an initial position and to recurrently reset dead reckoning cumulative errors. Cooperative approaches can significantly improve performance in the perspective of relative localization but require at least some of the vehicles to occasionally have access to an independent source with absolute location information to enable all network nodes to localize themselves with global positions. These global positions, if not available through GPS, can be provided with deployed infrastructure or opportunistic fingerprinting based on existing infrastructure. Infrastructure deployment implies high costs so we focus on opportunistic fingerprinting strategies. As mentioned in Section 2.1.3.2 lidar sensors are still expensive to be installed on vehicles in large scale. Camera-based approaches could be used in the online phase jointly with lidar maps to reduce costs [11] but both cameras and lidar sensors are affected by harsh environmental and light conditions and have LOS requirements. Also, as mentioned in Sec-

tion 2.1.4, vision-based approaches present a trade-off between scale and precision. WiFi-based fingerprinting (Section 2.1.3.3) has lower costs, but depends on already installed access points and it has low accuracy [11]. We dedicate the next section to a fingerprint strategy frequently used indoors but rarely explored outdoors: magnetic-based fingerprinting.

### 2.5.1 Magnetic-Based Localization

Inspired by many animals that rely on the Earth's magnetic field, also designated geomagnetic field, to locate themselves relatively to their destinations, the use of magnetic fields for positioning purposes has been applied for a long time in many different contexts. Some examples are road vehicle navigation, pedestrian dead reckoning, and mobile robot orientation. A survey on magnetic field based positioning systems is provided by Pasku et al. [115]. These can be divided in two main approaches: one uses the geomagnetic field, occasionally distorted by existing infrastructures; the other employs artificially generated magnetic fields and so requires magnetic based infrastructure deployment in the area of interest, e.g. Lopes et al. [116] and Abrudan et al. [117]. In this work, we focus on the first due to our requirements for a low-cost and infrastructure deployment free approach. In our scenario of interest, measuring the geomagnetic field is widely applied for orientation in dead reckoning techniques, as described in Section 2.1.2. In this section, we focus our attention on magnetic fingerprinting based approaches.

Proposed for indoor localization inside buildings, this concept assumes that the steel and other materials found in structures of buildings, which causes a distortion to the Earth's magnetic field, allows the utilization of the magnetic data to track the location inside a previously mapped area. Several authors explore this concept for indoor positioning with different approaches and scenarios. The first solutions are one-dimensional, proposed for mobile robots localization along the corridors inside a building and combined odometry with magnetic signatures, e.g. Suksakulchai et al. [118] and Haverinen and Kemppainen [119]. More recent methods, such as LocateMe by Subbu et al. [120], MaLoc by Xie et al. [121], and Magicol by Shu et al. [122], are developed for indoor pedestrian localization using smartphones. The work by Li et al. [123] studies the feasibility of using the magnetic field alone for indoor positing. The authors conclude that this approach has many advantages, namely no deployment of infrastructure is required, the magnetic field is everywhere and relatively stable, but also presents challenges such as the small number of elements that can be used to create the fingerprint database (maximum three, usually two in many applications), and the surveying of the area of interest. The change of magnetic field with location is quite significant, which is good for precise positioning, but demands efficient methods to create the database. Combining geomagnetic field positioning with other technologies e.g. WiFi fingerprint, is indicated as an interesting area for further research. IndoorAtlas [124] is a commercial system that enables cross-platform indoor positioning of smartphones by fusing different information sources, including geomagnetic fingerprint maps. On some devices, positioning is often infrastructure free, since accurate positioning can be achieved using fingerprints of existing Wi-Fi signals and magnetic fields. It is a cloud-based platform that requires a floor plan image and a preliminary mapping of the environment.

This concept seems to have rarely been applied to outdoor scenarios. We believe this is due to both the existence of GPS, ideally providing global coverage, and the lower density of disturbances from local magnetic fields in outdoor environment compared to indoors, making it easier to rely on the geomagnetic field for orientation and the effort of mapping the whole area too difficult and unnecessary. Experiments performed for a master thesis by Selçuk [125] describe the use of IndoorAtlas application and its approach in crowded, central and busy locations of Tallinn and Istanbul outdoor environments. It is tested both for pedestrians and vehicles, concluding that this is a helpful approach to develop a GPS-independent outdoor positioning system. A survey on fingerprinting based outdoor localization by Vo and De [46] categorizes approaches as visual, motion, and signal, also including some hybrid ones that combine different methods. Magnetometer data is used in some approaches for motion fingerprint based localization, e.g. Youssef et al. [126], although the section describing these is mainly focused on pedestrian dead reckoning, which is out of our scope since it differs from vehicle dead reckoning by using step information. Most reviewed systems use GPS, although briefly and infrequently, to reduce accumulated error from inertial sensors, as a trade-off between accuracy and energy consumption. As relevant hybrid techniques for our scenario, we can mention WheelLoc by Wang et al. [127] and Dejavu by Aly and Youssef [128], both including GSM antenna, accelerometer and magnetometer data for localization of road vehicles, as an energy versus accuracy trade-off perspective. WheelLoc seeks to capture the user mobility trace (traveled distance and turns) and match it to the maps using a Hidden Markov Model and Viterbi decoding, limiting the searching area by the cell towers observed, and obtaining point locations through interpolation or extrapolation. Magnetometer is used along with accelerometer for estimating mobility trace and transportation mode. Dejavu employs a dead-reckoning approach using low-energy profile inertial sensors from mobile devices, and leverages road landmarks (e.g. bumps, potholes, bridges, tunnels, and turns) that affect inertial and other sensors with unique signatures to reset the error accumulation in the dead-reckoning displacement. Magnetic data is specifically mentioned in the detection of tunnels along with weak GSM signal. It builds the database with crowd-sourcing using accelerometer, magnetometer, gyroscope, WiFi and cellular network information. SmartLoc by Bo et al. [129] uses the inertial sensors from smartphones as a complement to GPS in order to improve its performance in locations with poor signal. Along with dead reckoning, it also leverages particular driving patterns and road landmarks, such as braking and speeding in traffic lights or turning at intersections, as a calibration strategy. Wei et al. [130], propose a vehicle localization approach based on magnetic data by using odometry assisted with magnetic matching. This includes an offline phase to construct the magnetic map with magnetic field intensities and coordinates of reference points, uniformly distributed along the road. During the online phase, magnetic field intensities in a certain distance window are matched to the previously constructed magnetic map, providing a position estimation. These four approaches were tested with more than a hundred km of data in the cities of Beijing, Alexandria, Chicago, and Beijing, respectively.

## 2.6 Related Work Summary

Satellite-based systems, which are the current de facto solution for outdoor vehicle localization, present large errors in multipath environments and NLOS satellite conditions. Our work is specially focused on these challenging scenarios, although it is also useful in general. To improve or provide localization for road vehicles in a low-cost manner, we propose to leverage available anchors and landmarks.

**Cooperative Approach:** Our focus is on RSSI-based lateration since TOF-based measurements for ranging purposes require specific hardware, which is costly and not widely available. RSSI is available in standard equipment. Research papers on cooperative approaches for vehicular networks frequently assume knowledge of the inter-vehicle distances with a certain associated error, e.g. zero mean white noise [92], zero mean Gaussian noise [86], zero mean Gaussian noise with distance dependent standard deviation (distance percentage) [93], without considering a specific method to estimate the distances. The chosen method and associated models have a high impact on the errors of inter-vehicle distances estimated with real data. Parker and Valaee [105] propose to use RSSI for inter-vehicle range estimation in order to provide relative positioning. EKFs are usually applied to track the positions of vehicles, combining the location estimates (GPS) with inter-vehicle ranging data. The solution obtained with the linearization of non-linear functions and Guassian error assumptions in EKFs may not be a good approximation for real data and cause the system to diverge (see Section 2.2). All performance assessments from the proposed algorithms are done with simulations using artificial data and scenarios.

We develop our algorithm taking real data into account. We track the position of the ego vehicle applying Bayesian inference with a particle filter, enabling a flexible combination of information sources. PFs make no restrictive assumptions about the dynamics of the state space or the density function and are therefore more adequate to deal with the non-linearities of the real world than EKFs. To experiment with our developed algorithm, we implement a prototype using inertial data collected with an off-the-shelf smartphone, GPS, road maps, and RSSI measurements. We use RSSI measurements with path-loss model for ranging estimation to one-hop neighbors, which can be vehicles with uncertain positions, to estimate locations of nodes in a vehicular network.

**MagLand approach:** Continuous magnetic fingerprinting has been well explored to complement dead reckoning for location tracking in indoor environments, relying in frequent distortions created by the building structure. This scenario is very different from road vehicle localization outdoors because 1) distortions in outdoor environments are less frequent, 2) satellite-based systems have high availability outdoors unlike inside buildings, 3) road vehicle dynamics are different from indoor pedestrian and indoor robot dynamics, and 4) coverage area is not so easily limited (building versus roads), which impacts the mapping effort and the feasibility to determine the initial position. As a consequence of 1), most areas outdoors provide few distinctive patterns, which results in low matching accuracy, at higher costs in terms of mapping area and database size due to 4). Moreover, as a consequence of 1) continuous matching is not needed outdoors.

Wei et al. [130] recently proposed an odometry assisted magnetic matching for road vehicle

localization. It performs continuous matching with a normalization product correlation algorithm in a space-based window and requires a mapping of the whole coverage area (roads). A limited initial area is used in order to start tracking, since, according to the authors, matching in the whole map database is time consuming and inefficient. Performance evaluation for location tracking is done with data from experiments with a mini bus in Beijing, China.

Our proposed approach for outdoor scenarios, MagLand, is focused on leveraging opportunistic distortions to the geomagnetic field created by road infrastructure as magnetic landmarks. Magnetic matching to mapped data is performed only during detected anomalies, i.e. when there are significant distortions to the geomagnetic field. Unlike existing approaches, we do not focus on continuous matching because it offers a bad trade-off in terms of effort versus accuracy, when there are better alternatives. Areas without magnetic anomalies (where we do not perform matching) are most likely areas with few infrastructure, and so satellite-based systems have open sky conditions and can provide location. This way, MagLand allows to concentrate the mapping and matching efforts only in locations where the distortions are significant, presenting distinctive patterns and so enabling a good localization accuracy. Moreover, many of these locations coincide with areas of known limitations of satellite-based systems, e.g. tunnels, which makes MagLand very useful.

We perform a proof-of-concept with real data from Porto, Portugal, for the detection, matching and mapping steps. In the detection, we use a space-based window with a random forest binary anomaly classifier for each window. In the matching step, we apply a one nearest centroid classifier with dynamic time warping (DTW) to match time series irrespective of their pace, so accounting for different collection speeds. The mapping uses a DTW barycenter averaging algorithm to calculate the centroid for each class, making the signatures more robust at a reduced complexity. This approach enables initial position determination without any extra source of information in an efficient way even if the database is large [131].

In summary, we explore both cooperation between vehicles and information from the environment in new ways to improve localization performance, and the proposed approaches were developed taking real scenarios and real data into account.

# Chapter 3

# Cooperative Localization in Vehicular Networks

In the previous chapter, we presented a literature review, where we covered the most relevant topics related to localization of road vehicles in respect to this thesis. We addressed typical information sources, fusion techniques, performance evaluation methods, collaborative strategies, and GPS-independent vehicle localization. In this chapter, we present our cooperative approach in detail. We start by describing the problem in Section 3.1 and our assumptions in Section 3.2. Our proposed inference algorithm is explained in Section 3.3, followed by a proof-of-concept with real data in Section 3.4. We conclude with some final remarks in Section 3.5.

## 3.1 Problem Formulation

Our system is composed by a group of vehicles (and RSUs if available), all equipped with IEEE 802.11p vehicular connectivity. For simplicity, the state of a vehicle consists in its 2D position and velocity (heading and speed). Concerning sources of information, we assume that vehicles are heterogeneous and each may have access to different types of data. Examples of potential sources comprise GPS, on-board inertial sensors, road maps, and WiFi signals. In our implementation, we include the first three. The flexibility of our approach allows for our implementation to be easily extended to comprise extra information sources and a more complex state, including for example 3D position and acceleration.

We focus on the computations performed in a single vehicle as the center of the network, denoted as $V_0$, as illustrated in Fig. 3.1. This vehicle of interest[1] (VOI) aims to calculate its own state. Considering the whole network, our goal is to estimate the state of all vehicles, each performing the calculations by seeing itself as the VOI and its one-hop neighbors as mobile anchors.

As explained in Section 1.1.1, we opt for a distributed architecture since it is more scalable and flexible for dynamic vehicular networks than a centralized one. By handling information locally and processing it in the vehicle itself, the computational burden is spread among the vehicles. A

[1] Also frequently designated in the literature as ego vehicle

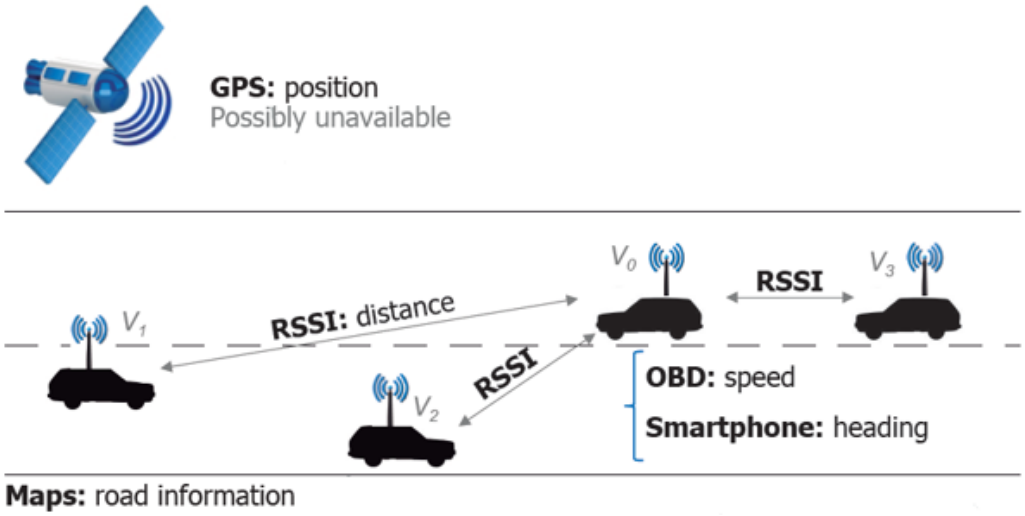


Figure 3.1: System scenario: a set of road vehicles with 802.11p communication capabilities and onboard sensors, optional road side units and GPS availability.

centralized architecture would imply a high use of resources and be less robust to failure [17] since it would require all measurements to be sent to a central processor that would then transmit the computed results to the vehicles. One limitation of distributed algorithms is the circular reasoning that can arise from inter-estimate dependency, which might lead to over convergence [21]. To avoid this issue, in our work the vehicles do not share any estimation made with external data, i.e. data collected and shared by other vehicles. Each vehicle sends a position estimate obtained only with data acquired from its own sensors, which we denote as individual position information. This location is shared along with a corresponding measure of uncertainty.

We are considering a collaborative approach with a distributed setting for large scale application. All the nodes within the network should have processing capabilities enabling the application of the selected techniques, so no expensive sensors or impractical devices to install in a vehicle should be chosen. Following the discussion from Section 2.1.3.1, we select RSSI measurements as the best option in our case for the simplicity and low costs of implementation compared to AOA and TOF techniques, which need specific hardware, namely antenna arrays and highly precise clocks, respectively. RSSI has the advantage of being in full compliance with future connect vehicles by using information already provided through beacon signals defined in the standards [13], namely BSM in DSRC (USA) and CAM in ITS-G5 (Europe) [3].

## 3.2 Model Assumptions

### 3.2.1 Path-loss Channel Model

In free space, the power of a radio-frequency signal decays proportionally to $d^2$, where $d$ is the distance between transmitter and receiver. In real-world channels, however, the propagation of a signal is affected by various phenomena such as reflection, refraction, diffraction, and scattering.

It is nonetheless accepted on the basis of empirical evidence that the received signal strength may be modeled as a log-normally distributed random variable with a distance-dependent location parameter [20]. Since the aforementioned effects are environment dependent, the models have to be calibrated for the intended scenario. Eq. (3.1) provides a path-loss channel model that describes the received signal strength $\rho$ measured in dBm (decibel milliwatt) given the transmitter-receiver distance $d$ (in meters), using three parameters: received signal strength $\rho_0$ [dBm] at a reference distance of 1 m, channel path-loss exponent $\alpha$, and the fading $v_\sigma$, modeled as a zero-mean Gaussian random variable with variance $\sigma^2$, i.e., $v_\sigma \sim \mathcal{N}(0, \sigma^2)$.

$$\rho(d) = \rho_0 - 10\alpha \log_{10}(d) + v_\sigma \tag{3.1}$$

Fig. 3.2 shows a set of real measurements along with the estimated path-loss model (using logarithmic scale for the distance, the model becomes linear). We collected the data in an urban scenario, using four vehicles communicating through 802.11p with 50Hz beacons, during a ten minutes' drive of approximately 5.5 km, in Porto, Portugal. The linear model in Fig. 3.2 was obtained from the measurement data of one of the vehicles using linear regression. The estimated values for the channel parameters are $\rho_0 = -34$ dBm, $\alpha = 2.1$, and $\sigma = 5.5$ dB.

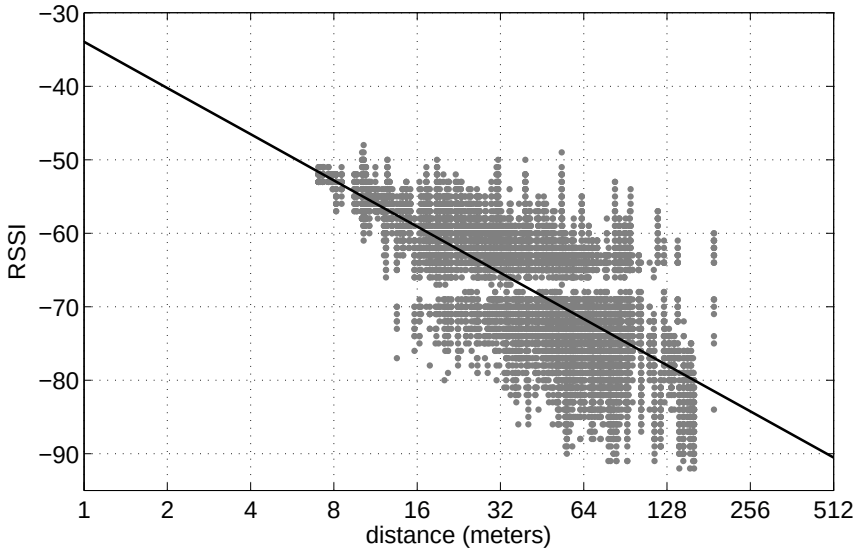


Figure 3.2: Pairs of GPS estimated distance and RSSI used to determine channel parameters along with the estimated model.

In Fig. 3.2, a horizontal band with fewer measurements can be observed around $-67$ dBm. We believe this to be an error specific to the hardware we used (for more details see Section 3.4), possibly in the component that maps the received signal strength to the reported RSSI value. Due to the unitary quantization made by the hardware, the measurements overlap along the vertical axis and the number of such overlapping points for a given RSSI value is not discernible in the plot. Therefore, the Gaussian nature of residual RSSI errors (difference between measured and model predicted RSSI values) is not clear in Fig. 3.2, so we provide in Fig. 3.3 the normalized histogram

of residual RSSI errors with the corresponding Gaussian fit (zero mean and $\sigma = 5.5$ dB). The estimated standard deviation for the fading includes all points and is generalized for all distances, despite the slight increase with distance that can be perceived in Fig. 3.2. It is also important to highlight that this is an aggregated model that includes both LOS and NLOS measurements, and therefore can be applied to both LOS and NLOS scenarios. While a reliable LOS and NLOS detection with separate models should improve the range estimation, such distinction is not considered in this work.

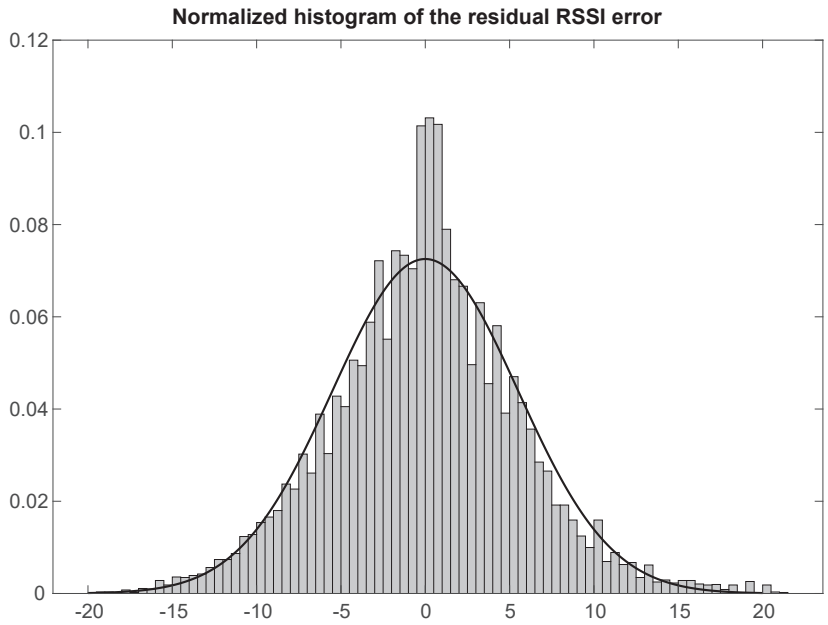


Figure 3.3: Normalized histogram of the residual RSSI error for all pairs of GPS estimated distance and RSSI, using the estimated channel model, along with the corresponding Gaussian curve fit.

Having calculated these channel parameters, we are able to apply the path-loss model to estimate the distances from the RSSI values of the neighbors. Different techniques can be used to estimate the position of the vehicle from the distance to its neighbors. We opted for a parametric approach as it takes into account the uncertainty of the measurements. In order to estimate the location of a vehicle, we calculate the likelihood function $l_\rho(d) = p(\rho|d)$ corresponding to the path-loss model in (3.1).

$$l_\rho(d) = \mathcal{N}(\rho_0 - 10\alpha \log_{10}(d), \sigma^2) \tag{3.2}$$

It is important to note that several parameters impact ranging precision, such as the true distance $d$, the fading variance $\sigma^2$, and the number of available measurements $M$. Below, we provide the Cramér-Rao Lower Bound (CRLB), a lower bound on the variance of any unbiased estimator $\hat{d}$ of $d$:

$$\text{CRLB}(\hat{d}) = \frac{1}{M}\left(\frac{\sigma d \ln 10}{10\alpha}\right)^2. \tag{3.3}$$

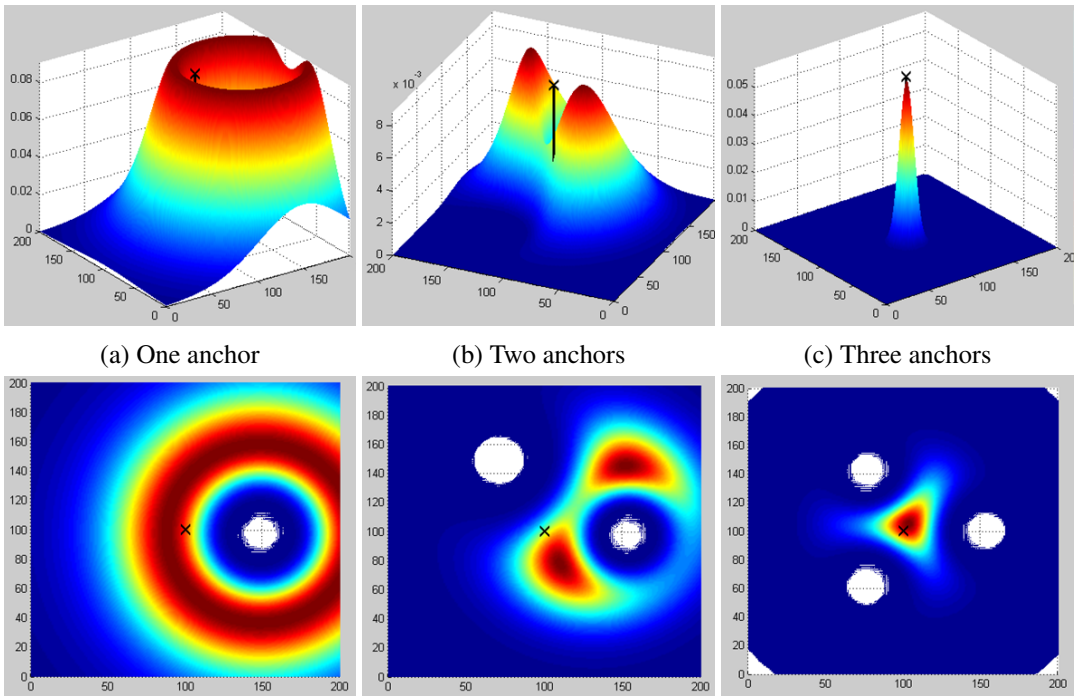

(a) One anchor (b) Two anchors (c) Three anchors

(d) One anchor (e) Two anchors (f) Three anchors

Figure 3.4: 3D view of the likelihood function of $V_0$'s position (top), and the corresponding heat map (bottom).

Eq. (3.3) highlights the importance of each parameter in the estimator variance. The CRLB increases quadratically with $d$ and $\sigma$ and is inversely proportional to $M$.

We substitute $d$ by the Euclidean distance between a vehicle position $\mathbf{x}_0 = [x_0, y_0]^\intercal$ and anchor position $\mathbf{x}_a = [x_a, y_a]^\intercal$ to obtain the likelihood of the location of the VOI $V_0$.

We assume that $n_A$ anchors are available, and that the channel model is the same for all anchors. Since the anchors are at different locations separated by a distance much higher than the wavelength, we also assume that the vehicles experience independent fading. Therefore, the joint likelihood function of the position factorizes as follows:

$$l_\rho(\mathbf{x}_0) = \prod_{a=1}^{n_A} \mathcal{N}(\rho_0 - 10\alpha \lg \|\mathbf{x}_a - \mathbf{x}_0\|, \sigma^2). \tag{3.4}$$

To illustrate the likelihood function given in Eq. 3.4, we show in Fig. 3.4 synthetic examples for one, two and three anchors with known positions.

The corresponding CRLB for the general scenario with $n_A$ anchors, each providing $M_a$ independent RSSI measurements, is given by (3.5). We observe that the number of anchors and their geometry relative to the VOI impact the lowest achievable variance. These results are consistent with the ones presented in [37] for a location estimation algorithm using RSSI, although we show ours from the perspective of a single vehicle, VOI, while in [37] they are calculated for the whole network. In [132], the authors present the CRLB for the scenario of network topology uncertainty.

Fundamental limits of wideband localization are presented in the literature, namely [133, 134].

$$\mathrm{CRLB}(\hat{\mathbf{x}}_0) = \left(\frac{\sigma \ln 10}{10\alpha}\right)^2 \left[\sum_{a=1}^{n_A} \frac{(\mathbf{x}_a - \mathbf{x}_0)(\mathbf{x}_a - \mathbf{x}_0)^\mathsf{T}}{M_a^{-1} \, \|\mathbf{x}_a - \mathbf{x}_0\|^4}\right]^{-1} \tag{3.5}$$

A higher number of anchors helps to build up the rank of the Fisher information matrix (FIM) by summing up rank-one matrices (outer products) in (3.5). The FIM rank is increased as long as the corresponding position vectors are linearly independent. For example, 2D position estimation requires a rank-two (invertible) FIM. When the anchors lie approximately on a line, the rank of the FIM tends to one, and therefore the positioning estimator exhibits very large variance along the direction orthogonal to the corresponding line (null space). This conclusion is also consistent with the concept of horizontal dilution of precision (HDOP), which quantifies the impact of range estimation errors on the positioning error given certain anchor configurations.

### 3.2.2 Map Information

If a road map is available, we distinguish between road and non-road areas. In our implementation we use basic map data from Open Street Map: each road segment is defined simply by two edge points. We consider this segment as the center of the road. The map does not include the width of the roads or their number of lanes. Since our focus is on urban environments, we attribute a default width of 10.5 m to all road segments, assuming a three-lane road (3.5 m each lane) as the largest possible scenario. Most streets in the city have either one or two lanes (same or opposite directions), so this value already gives us a safe margin by including potential roadsides or parking spaces. By choosing the highest value, we may keep non-road locations flanking narrower roads as valid but we also guarantee that we do not eliminate suitable position candidates. This assumption can be adapted depending on the scenario and the available map details.

## 3.3 Inference Algorithm

### 3.3.1 Bayesian Approach

Fusing different types of data with different degrees of reliability in a single position estimator can be achieved in many different ways. Parametric estimation approaches, such as Maximum Likelihood, rely on statistical models associated with erroneous measurements. Based on the assumption that the errors corresponding to different sensors are statically independent, a joint likelihood of all available information can be calculated [58]. Bayesian-filters are powerful statistical tools for state estimation that are able to combine information originating from multiple sources with different degrees of reliability [135]. In order to track the location over time, we employ a two-stage Bayesian filter. The main stage is a particle filter for location tracking. We have chosen this filter because it allows the representation of arbitrary probability density functions and makes it very easy to incorporate road restrictions. We are, however, mindful of their potential large complexity

and careful to keep the computational cost feasible. Once the posterior function has been calculated, in order to obtain the state estimate, we use a MAP estimate, which corresponds to the mode of the posterior density. As our state-space model is highly non-linear, we opt for a bootstrap particle filter that implements a sequential importance sampling with the transition prior probability distribution as importance function [58]. This main filtering stage includes a prediction phase based on the vehicle's dynamics, namely the velocity (speed and heading). A secondary filtering stage, which is a UKF, is employed and outputs the heading estimate required by the main stage. This UKF fuses inertial measurements collected from a smartphone (magnetometer, gyroscope and accelerometer data).

### 3.3.2 Proposed Filter

We first introduce the state-space model corresponding to the main stage of our Bayesian filter, i.e., the particle filter for position tracking. We define the current full state of the vehicle of interest $V_0$ at time $k$ in Cartesian coordinates as

$$X_0(k) = [x_0(k), y_0(k), s_0(k), h_0(k)]^\intercal, \tag{3.6}$$

where $x_0(k), y_0(k)$ are the vehicle position coordinates (in meters) at time $k$, $s_0(k)$ is the vehicle speed (in meters/second), and $h_0(k)$ denotes the vehicle's heading (measured in radians from the $x$-axis that coincides with the East direction, and positive angles are measured from East to North).

The state-space model of the second stage is given as:

$$x_0(k) = x_0(k-1) + T s_0(k-1)\cos(h_0(k-1)) \tag{3.7}$$

$$y_0(k) = y_0(k-1) + T s_0(k-1)\sin(h_0(k-1)) \tag{3.8}$$

$$s_0(k) = \hat{s_0}(k) + w_{s_k} \tag{3.9}$$

$$h_0(k) = h_0(k-1) + \Delta\hat{h} + w_{h_k} \tag{3.10}$$

where $T$ is the time interval between instances $k-1$ and $k$ (in seconds), whereas $\Delta\hat{h}$ is the estimated heading change rate during interval $T$, and $\hat{s_k}$ is the estimated average speed within that time interval. The process noise is defined for both heading and speed as Gaussian distributions, represented by $w_{h_k}$ and $w_{s_k}$, respectively. The corresponding normal distributions have zero mean and variances $T\sigma_h^2$ and $T\sigma_s^2$, respectively, where $\sigma_h$ and $\sigma_s$ are the reference standard deviations for an interval of one second.

We present the state and measurement equations as well as the map restrictions. We provide a description of the algorithm step by step, in Algorithm 1, including also an analysis of its computational cost.

#### 3.3.2.1 State Equations

The state prediction equation is a simple linear motion model along each coordinate $x$ and $y$, as shown in Eqs. (3.7) and (3.8), respectively. We assume the vehicle has access to heading and

speed estimates to be used in the motion model. These can be obtained from any source, without loss of generality. For example, the speed information can be collected by a low-cost on-board diagnostics (OBD) device connected to the vehicle. In our case, the heading is estimated using the inertial sensors available in an on-board smartphone, namely accelerometer, magnetometer and gyroscope. A UKF implementation based on [136] was used, corresponding to the secondary stage of the proposed Bayesian filter. Please refer to Section 5.2 of [136] for details about the algorithm for orientation estimation.

#### 3.3.2.2 Measurement Equations

We define $Z(k)$, a composite measurement vector at time $k$ which is comprised of individual GPS position estimates and RSSI measurements the VOI collects from available anchors. A different model is necessary for each sensor in composite vector $Z(k)$. For RSSI, the model is derived from Eq. (3.1), rewriting the distance $d$ in terms of coordinates of the VOI $\mathbf{x}_0(k)$ for all available anchors $\mathbf{x}_a(k)$. The RSSI measurement $\rho_a(k)$ corresponding to the packets sent from an anchor $a$ at time $k$ is related to the vehicle position $\mathbf{x}_0(k)$ as follows

$$\rho_a(k) = \rho_0 - 10\alpha \lg \|\mathbf{x}_a(k) - \mathbf{x}_0(k)\| + v_\sigma(k), \tag{3.11}$$

and the corresponding joint likelihood function for $n_A$ anchors is given in Eq. (3.4). In our model, moving vehicles that are in the range of $V_0$ act as mobile anchors. They know their positions with some degree of uncertainty and share their own estimated positions $\hat{\mathbf{x}}_a(k) = [\hat{x}_a, \hat{y}_a]^\intercal$ along with respective uncertainty, e.g. (a representation of) their location posterior density. In the implementation, we used GPS position estimates along with position reliability measure provided by the GPS receiver. Due to anchor position uncertainty, their realizations have been drawn from a Gaussian distribution with mean $\mathbf{x}_a$ as the measured GPS position, and standard deviation $\sigma_a$ derived from the corresponding position reliability measure. The likelihood corresponding to the anchor's GPS measurements is given by $\mathcal{N}(\hat{\mathbf{x}}_a(k), \sigma_a(k))$, where $\hat{\mathbf{x}}_a(k)$ and $\sigma_a$ are the estimated GPS position and its standard deviation at time $k$. In our algorithm (see Algorithm 1), in order to reduce the computational cost of calculating the joint likelihood function for $n_A$ anchors with uncertain positions online, we precompute it using 100 particles drawn from the aforementioned Gaussian function to represent each anchor and save the results in a lookup table.

If individual location estimates are available at the vehicles, for example from GPS, the corresponding likelihood functions are modeled according to the reliability of these estimates. The composite likelihood function $p(Z(k)|X(k))$ is given by

$$p(Z(k)|X(k)) = l_L(\mathbf{x}_0(k)) l_\rho(\mathbf{x}_0(k)) \tag{3.12}$$

where $l_L(\mathbf{x}_0(k))$ is the product of the probabilities of $\mathbf{x}_0(k)$ being the current position of V0, for each alternative source of individual information. The global positions coordinates have been converted to Cartesian ones using an equirectangular projection.

```
Data: State and weight of each particle
Result: Estimated location
get initial position and uncertainty from individual position data or mean of anchors positions;
initialize particles' states randomly (3σ area around initial position) and weights uniformly;
foreach time instance do
    get speed measurements;
    get heading change from UKF;
    foreach particle do
        sample speed error;
        sample heading error;
        calculate displacement;
        update state;
    end
    if using map restrictions then
        delete particles outside road;
        replicate current particles using weights;
    end
    if using individual position data then
        get individual position and respective uncertainty;
        foreach particle do
            calculate Gaussian probability of location;
            update weight;
        end
        normalize weights (sum to 1);
    end
    if using V2V ranging data then
        foreach anchor do
            get mean RSSI;
            get individual position and uncertainty;
        end
        foreach particle do
            foreach anchor do
                if σ_a <= 15 m then
                    calculate likelihood of particle position from RSSI, distance to the anchor and
                      anchor uncertainty (from a previously created lookup table);
                    update weight;
                end
            end
        end
        if sum(weight) < ZeroThreshold then
            restart filter;
        else
            normalize weights (sum to 1);
        end
    end
    if 1/sum(weight^2) < ResamplingThreshold then
        delete lowest weighted particles;
        copy highest weighted particles according to their weights maintaining the total number of
          particles;
        normalize weights (sum to 1);
    end
    get MAP estimate: the state (location and velocity) of highest weighted particle;
end
```

**Algorithm 1:** Vehicle tracking algorithm using particle filter

#### 3.3.2.3 Map Restrictions

For each particle, we check whether its position lies on a road or not. Particles outside the roads are deleted. To maintain the total number of particles, the ones on the roads are replicated according to their weights, so that particles with higher weights have higher probability of being replicated.

#### 3.3.2.4 Computational Cost

The computational complexity of our particle filter is $\mathcal{O}(n_A n_P)$ at each time instance $k$, where $n_A$ is the number of anchors and $n_P$ the number of particles. The number of anchors is usually much lower than the number of particles and anchors should be limited to the closest and more promising neighbors (the ones with higher confidence in their position). Therefore the computational cost is mostly driven by the number of particles used in the filter, a trade-off between the accuracy of the estimation and the required computational resources to achieve it in suitable time. For example, considering an update rate of few Hz, and one thousand particles, the computation could be easily carried out by most modern multi-core processors based smartphones.

## 3.4 Experiments with Real Data

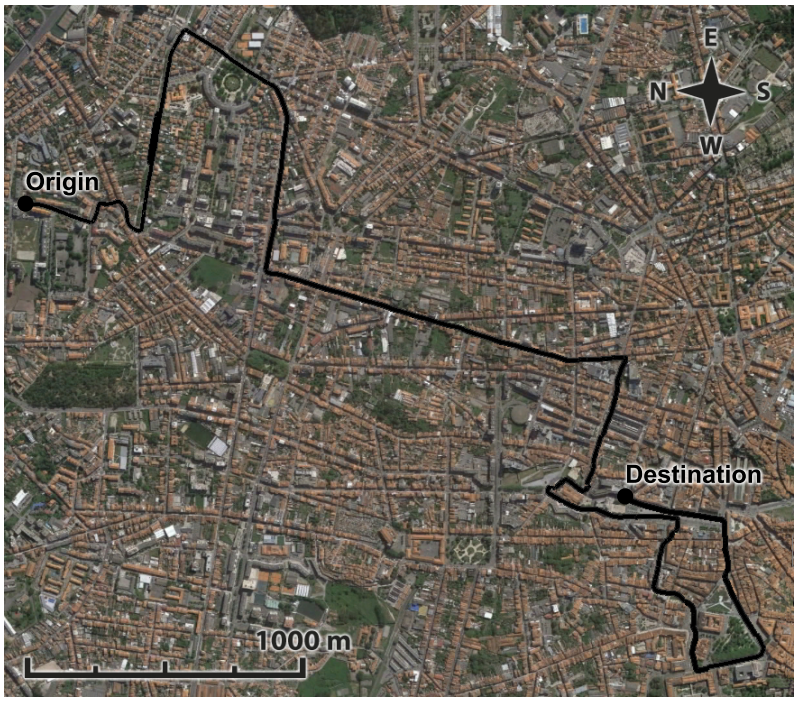


Figure 3.5: Urban trajectory of approximately 7 km in Porto, Portugal.

We show experiments as a proof-of-concept for our approach in a real world setting, providing an evaluation of quality among different combinations of information sources. Four cars were driven for 30 minutes in the city of Porto along the route shown in Fig. 3.5, facing everyday traffic conditions with regular driving behavior. No special environments or settings were chosen, other


Figure 3.6: Setup for data collection in the four vehicles: NEC LinkBird MX and GPS receiver on top of the vehicles, and two smartphones (Nexus 4 and Nexus 5) inside each vehicle.

than keeping the vehicles in communication reach of each other for as long as possible while being safe and compliant with road rules. Each vehicle was equipped with a purpose-built development platform for vehicle communication, NEC LinkBird MX (see Fig. 3.6), which implements 802.11p wireless standard (5.85–5.925 GHz) and has built-in beaconing functionality of 50 beacons per second. A GPS receiver was positioned on the rooftop of the vehicles, connected to the LinkBird. Inside, two Nexus 4 or 5 smartphones (near the windshield, see Fig. 3.6) collect inertial, Wi-Fi and GPS measurements with the maximum possible sampling rates. Video (1080p, 30 fps) was also captured in order to infer location ground truth. The path includes some zones with poor GPS coverage, mainly during the second half of the drive, in downtown area, due to narrow streets flanked by buildings. We chose the front vehicle, equipped with two cameras (front and rear) as

the vehicle of interest. Nevertheless, the approach applies to all vehicles, acting simultaneously as a vehicle of interest from their own perspective and as an anchor relative to their neighbors. The estimated mean GPS location error of the anchors is 7 m for a confidence interval of $1\sigma_a$. The mean GPS distance between $V_0$ and each of the anchors is 23.2 m, 48.3 m, and 55.8 m. These parameters are show in Fig. 3.7a and Fig. 3.7c, respectively, for each anchor throughout the trip. The mean RSSI values from 50 beacons per second are shown as well in Fig. 3.7b.

The following parameters were used in the experiments. The *ResamplingThreshold* was set to 10% of the total number of particles and the *ZeroThreshold* was set to $10^{-18}$. The particle filter used 1000 particles with resampling eliminating the lowest 10% weights and replicating the top 80%. It applied $T = 1$ s iterations with sub-iterations of 200 Hz for the motion model (UKF). The channel parameters were $\rho_0 = -34$ dBm, $\alpha = 2.1$, and $\sigma = 5.5$ dB, obtained as described in Section 3.2.1 from previous experiments in similar conditions[2]. The individual locations and respective uncertainty from the anchors were provided by their own GPS receivers from one the smartphones[3]. If available, GPS position estimates were drawn from a Gaussian distribution with position as mean and an estimated horizontal standard deviation provided by the GPS receiver (when unavailable we used $\sigma_{\text{GPS}} = 5$ m). The gyroscope and accelerometer from the smartphone collected data at 200 Hz sampling rate, and magnetometer at 50 Hz. The speed measurement was obtained from the GPS (even when GPS is not used in the update phase) since we did not have the OBD device available for these experiments. The standard deviations used in the motion model were set to $\sigma_h = 2^\circ$/s and $\sigma_s = 0.75$ m/s. Map information from Open Street Map was used as described in Section 3.2.2.

The ground truth of the position was marked manually using videos as the main source. Two different videos were obtained from cameras at the front and back of the vehicle of interest, as well as at the front of all three vehicles following it. In addition, we used the map and GPS from various devices to disambiguate some situations (when the videos did not provide clear landmarks). We choose the position of the smartphone attached to the mid-section of the windshield (containing the front camera and collecting GPS data) as the true position of the vehicle. Although the trajectory may be very close to the real one, some error introduced by the manual labeling is unfortunately inevitable at high speeds.

| Location sources | GPS | GPS + map | V2V | V2V + map | GPS + V2V | GPS + V2V + map |
|---|---|---|---|---|---|---|
| RMSE | 9.80 | 9.84 | 25.71 | 13.63 | 9.68 | 9.47 |
| MAE | 8.37 | 8.31 | 17.01 | 11.60 | 7.92 | 7.70 |
| SD [heading] | 2.68 | 2.51 | 4.70 | 3.03 | 2.26 | 2.10 |
| SD [⊥heading] | 2.90 | 2.62 | 5.51 | 3.25 | 2.39 | 2.19 |

Table 3.1: Location errors for full trajectory (meters)

[2]The same vehicles driving a different path in the same city were used.
[3]The smartphone GPS receiver was used instead of the one on the rooftop because the obtained results were better.

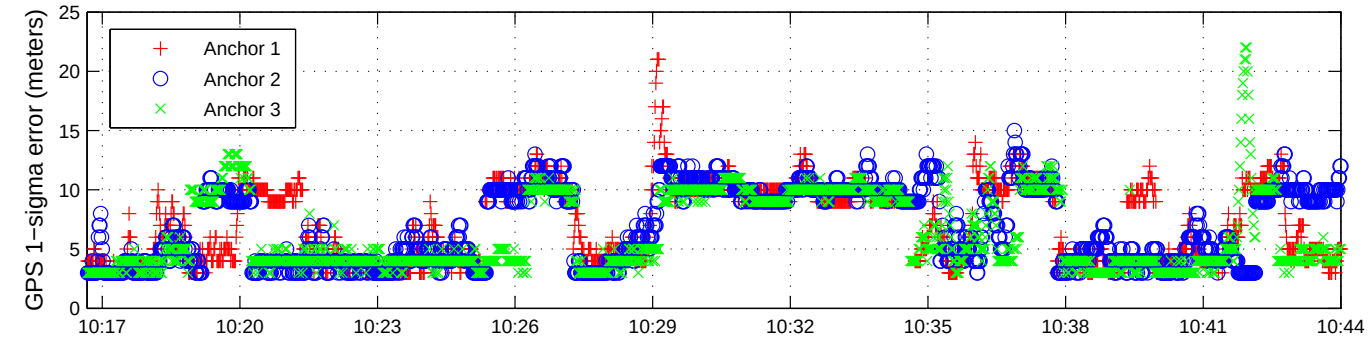


(a) Horizontal $1\sigma_a$ error from each anchor

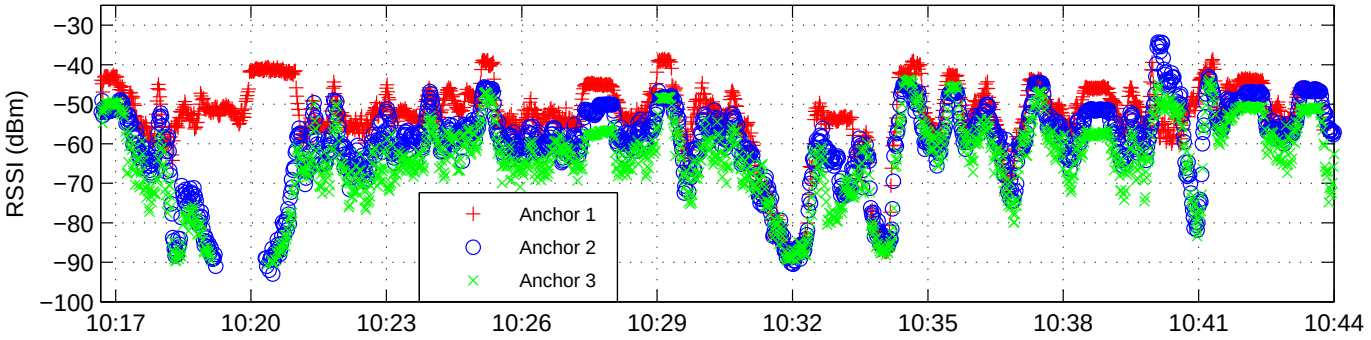


(b) Mean RSSI (using 50 beacons per second) from each anchor

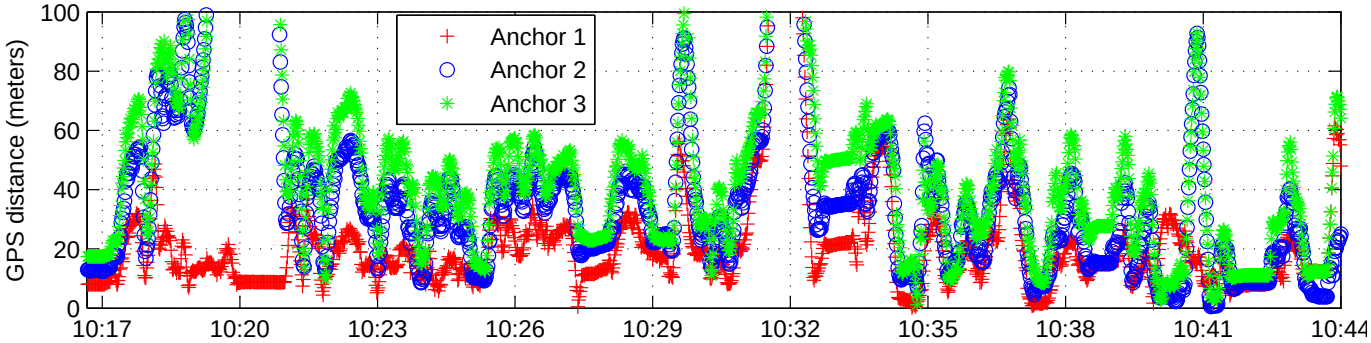


(c) GPS distance from VOI to each anchor

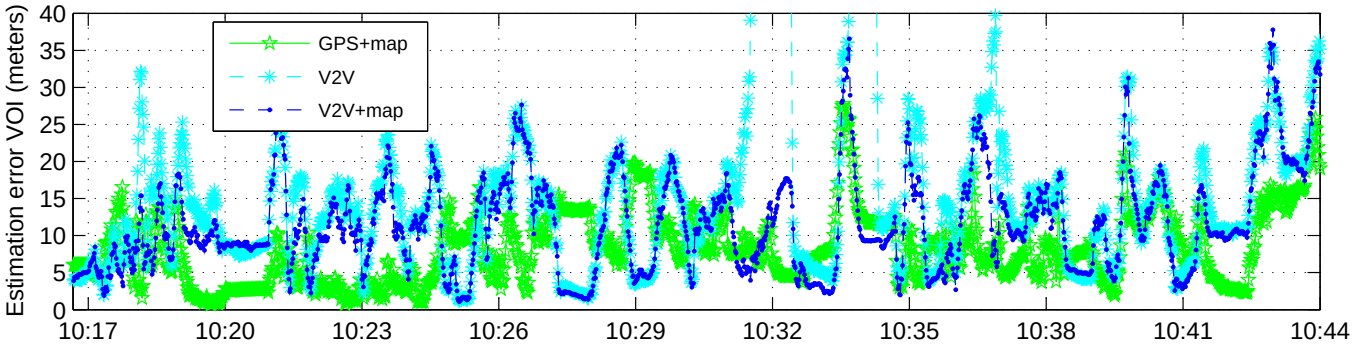


(d) Mean estimation error from 20 runs

Figure 3.7: Various metrics for the whole trip displayed per second.

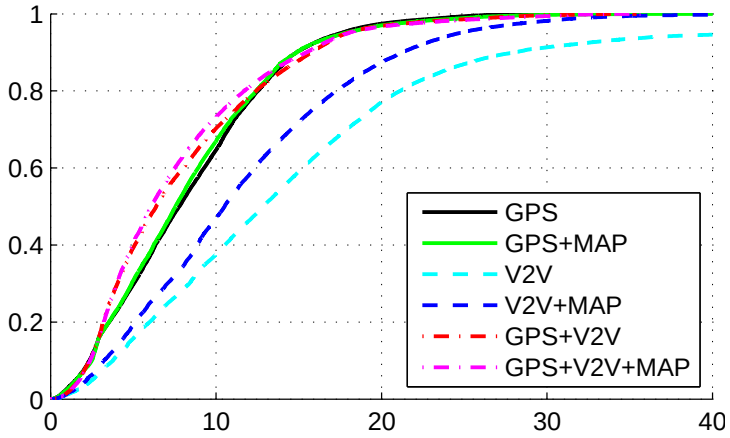


Figure 3.8: CDF of location error in meters.

The results for 20 runs of the algorithm are presented in Table 3.1 for six different combinations of the three location information sources: GPS, RSSI ranging information denominated V2V for simplicity, and map restrictions. We show the root-mean-square error (RMSE), the mean absolute error (MAE), which is the mean of location error, and the standard deviation (SD) of the posterior function, providing a measure of confidence in the estimated position, both in the direction of motion (heading), that will mostly coincide with the direction of the road, and in the perpendicular direction. In order to have a better picture of the errors we also present the cumulative distribution function (CDF) of the location error in meters in Fig. 3.8. We observe that, as expected, both maps and V2V improve GPS results when combined with it, and all three sources of information jointly provide the best configuration. The position accuracy achieved in this case is less than 6.1 m for 50% of the trip, and less than 11.7 m for 80%. It is important to note that not only the accuracy is better, but also the reliability of the results is improved in comparison to using only a subset of the available information sources. The V2V based model, with no GPS available in the vehicle of interest or fixed anchors with known exact positions, relying on the GPS estimates of its neighbors, often out-of-reach or in poorly covered GPS areas, is able to provide localization with a position accuracy of 12.8 m for 50% of the trip, even without the map. It's relevant to point out that this configuration shows a small percentage of very large errors (5% of the errors are higher than 40 m) from a specific situation where $V_0$ was separated from the rest of the vehicles, which got delayed by a traffic light (see in Fig. 3.7 the interval of 1 minute centered in 10:32), resulting not only in very large distances between the vehicle of interest and the anchors but also in a especially poor anchor geometry. In fact, very close to each other from a large distance of $V_0$, these 3 anchors behave as virtually only one and the likelihood takes an annular shape, not allowing the model to distinguish the correct road in a bifurcation. When combining map restrictions, we are able avoid these high errors and improve significantly the quality of the overall estimation. The error for the V2V configuration combined with map restrictions is less than 10.5 m in 50% of the cases and less than 17.3 m in 80%. We observe that the use of map restrictions, particularly when combined with V2V, improves both the accuracy and the reliability

of the estimation significantly.

| Location sources | GPS | GPS + map | V2V | V2V + map | GPS + V2V | GPS + V2V + map |
|---|---|---|---|---|---|---|
| RMSE | 9.62 | 9.23 | 9.60 | 8.70 | 7.30 | 6.93 |
| MAE | 8.64 | 8.28 | 8.05 | 7.32 | 6.18 | 5.90 |
| SD [heading] | 2.08 | 2.10 | 2.57 | 2.18 | 1.58 | 1.54 |
| SD [⊥heading] | 2.25 | 2.03 | 2.66 | 2.28 | 1.68 | 1.58 |

Table 3.2: Location errors for intervals with good conditions of the anchors (meters)

Figure 3.9: Video frames from the last vehicle, anchor $A_3$, for illustrative purposes of vehicle geometry during the trip.

In Fig. 3.7d, we show the values of the location error (MAE) throughout the trip, allowing the observation of its relation with the error of the anchors and the distance to $V_0$, for the configurations without GPS, and provide the GPS with maps as a benchmark. We confirm that the moments for which the V2V errors are larger, coincide with the situations where all three anchors were at large distances from the vehicle of interest. It is very important to stress that in these experiments we were limited to those three vehicles as anchors. They were often distant (sometimes even completely out of reach) and providing a poor anchor geometry. However, in a typical scenario of a densely populated urban area, a larger number of vehicles is expected to be within communication reach of $V_0$ and the ones providing the best geometry and lowest position errors might be chosen as anchors.

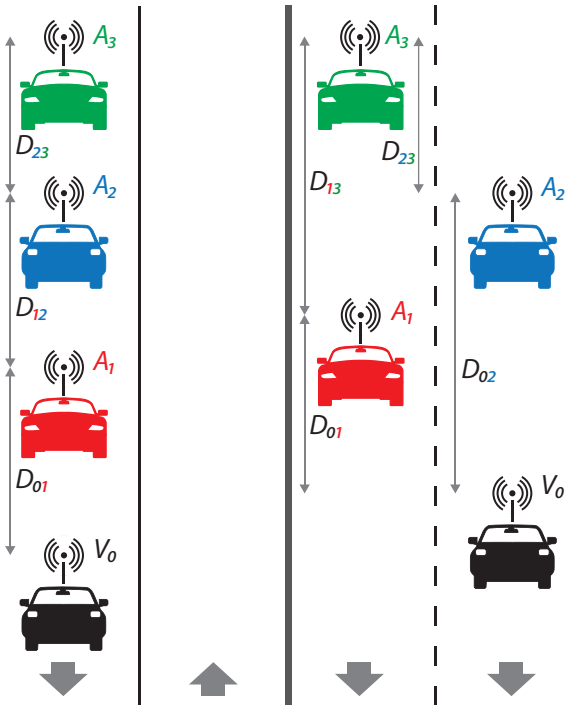


Figure 3.10: Geometry of anchors and $V_0$ during the trip: longitudinal distances (measured along the road) $D_{ij} \geq 0$ between the vehicles' antennas vary in time and represent the distribution of vehicles in space. The leading vehicle is $V_0$ and $A_1$, $A_2$ and $A_3$ follow in that order (their colors correspond to the ones used to represent them in Fig. 3.7), either in one lane or in two lanes when possible. Except for very close distances, both geometries have a similar impact. For large distances the configuration on the right can be approximated by the one on the left, so the geometry is mostly in line following the VOI.

We present in Table 3.2, the results only for moments that provide favorable conditions to apply V2V. In this case we define these as all three anchors close to the leading vehicle (less than 40m of GPS distance) and with good position accuracy (less than 8 m for $1\sigma_a$ confidence interval). In our experiment they correspond approximately to 23% of the trip, but we expect them to occur much more frequently in large vehicular networks. We observe that for these favorable conditions, the performance of our tracking algorithm even when $V_0$ has no access to GPS position is good. The location error of the V2V based configuration is 8 m and the estimation has a standard deviation of approximately 2.6 m, which is a performance equivalent to the GPS for the same context. The accuracy of the configuration V2V+map is 7.3 m, exceeding the accuracy of the GPS+map, which is 8.3 m. This shows the potential of our proposed approach. It is also interesting to note that, since the anchors follow the leading vehicle (see Fig. 3.9), the distribution of the vehicles in space is mostly in line or in two lanes in the same direction, as depicted in Fig. 3.10, which is a poor geometry. However, while this limits more the longitudinal error (along the direction of the road/movement), as illustrated in Fig. 3.11), using map restrictions bounds the lateral error (perpendicular to the previous direction), leading to a balanced combination of information sources. In our implementation the road restrictions assume a worse case road width, so the impact is mostly

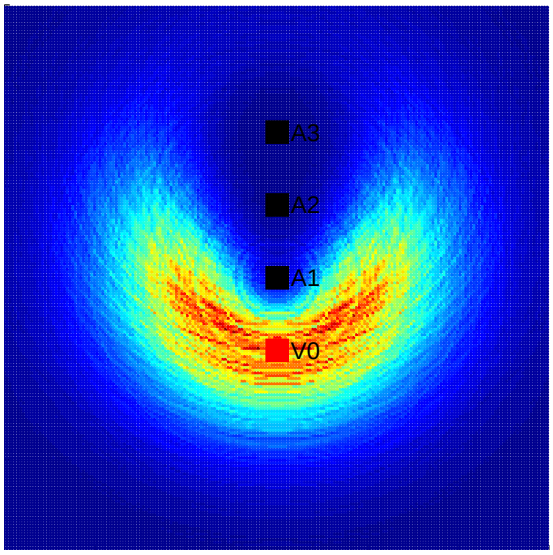


Figure 3.11: Likelihood from V2V for in line geometry of the anchors

noticeable in situations for which the errors are very high (e.g. very distant anchors). Nevertheless, using more tight road constraints, for example having access to the actual width of each road, would lead to an even higher impact on location performance.

## 3.5 Concluding Remarks

We propose a localization and tracking approach for vehicular networks, allowing vehicles to estimate or improve their position using widely available low-cost smartphone sensors and information shared by one-hop neighbors with uncertain locations. We provide a proof-of-concept using data from four communicating vehicles in a real urban scenario with 7 km, collecting their GPS, RSSI, and inertial data, and using available road maps.

It is worth pointing out that, to the best of our knowledge, this was the first approach to include RSSI for range estimation in cooperative localization of road vehicles after Parker and Valaee's seminal work in 2007 [105]. While they looked at this problem in a relative positioning perspective, not including any absolute source of position information except for initialization of relative node positions, and used an EKF to fuse different measurements, we focused on absolute position estimation and applied a PF for data fusion. We published it in IEEE Transactions on Intelligent Transportation Systems in 2017 [25] and since then Alami et al. [137] have proposed an approach that relies on exchanging GPS-acquired position data and RSSI measurements from neighboring vehicles and RSUs, citing our work and stating they improve on it by resetting the vehicle position when passing by RSUs.

We present results evaluating the quality of different combinations of information sources. By combining all of them (GPS, RSSI, inertial data, and road maps), we provide a mean location error of 7.7 m during the whole trip, including urban downtown areas with low GPS coverage, as well as relying on anchors with uncertain and often poor position estimates and geometry.

For intervals with good conditions of the anchors, we reduce this value to 5.9 m. We propose a maximum distance of 40 m as favorable condition for using V2V ranging, when in range of at least 3 neighbor vehicles with good position accuracy. In these V2V conditions, we show it is possible to provide a performance comparable to the one obtained from GPS even when the VOI lacks access to GPS, achieving a mean location error of approximately 8 m.

One limitation of our system is that the obtained accuracy in not sufficient for critical applications. This was expected as it is a direct consequence of our decision to use only off-the-shelf equipment and easily available information. As explained in Section 2.1 GPS augmentation systems, high-quality motion sensors, lidar ranging devices and high quality digital maps, for example, would improve the reached accuracy significantly compared to regular GPS, smartphone inertial sensors, V2V ranging with RSSI measurements and public available road maps from Open Street Map. Our aim was to propose and evaluate an approach feasible in a large scale for being low-cost. It can, nonetheless, be easily extended to incorporate extra, and possibility more accurate, sources of information. Actually, the cooperation approach is general and can be applied to any type of individual information, as long as the vehicle can abstract it into a position and a respective confidence measure ($1\sigma$ error) to share with its neighbors. The model makes no prior assumptions concerning the sources of this information. Vehicles might be heterogeneous and each may have access to different sources and types of data.

It is relevant to note that by leveraging independent sources of information not only the accuracy is improved, but the system is also more reliable and robust to failure. In the absence of GPS, the combination of ranging information from neighbor vehicles and map data is particularly interesting since while the map limits the lateral error, the V2V ranging helps to reduce the error along the road direction, where the closest anchors are distributed. This conclusion about the V2V location error being dominated by the cross-track component is expected and later confirmed by Severi et al. [13] with real data collected using three vehicles forming a platoon in a highway scenario.

It is important to highlight the contribution and associated effort of the presented experiments using real data from four communicating vehicles in a long urban trajectory. Considering our literature review in Section 2.4, we conclude few of the proposed cooperative approaches include experiments with real data to evaluate their performance. We observe it is more frequent to have real data results in context-based (e.g. [68, 73]) and GNSS-based approaches (e.g. [9, 84]) than in range-based approaches. We suppose this is due to GPS measurements being sufficient for the first two, while the latter usually require both GPS and range measurements from several vehicles, making data collection more challenging. Also, most of these approaches use only two vehicles for performance evaluation with real data (e.g. [9, 73, 82, 84, 85]), which would be insufficient to obtain a unique position using triangulation techniques, since each vehicle could only use a single anchor. Considering proposed range-based approaches with communication devices, Hoang et al. [104] test their TOA technique using impulse radio ultra wideband V2V ranging measurements in a highway scenario with three vehicles forming a platoon, in Helmond, Netherlands. To the best of our knowledge, ours was the first research work for ranging estimation with V2V 802.11p

communication devices in a vehicular scenario that has been evaluated with real world data. Since then, Severiet al. [13] also included RSSI for ranging estimation using real data from experiments performed in the same location and using the same vehicles as those mentioned in [104]. They tested RSSI V2V ranging in a highway scenario with three vehicles forming a platoon. This leaves our work as the sole evaluation performed in this context with data from a real urban scenario.

# Chapter 4

# MagLand: Magnetic Landmarks for Road Vehicle Localization

In this chapter, we focus on individual localization for road vehicles and propose **MagLand**, an approach that provides opportunistic magnetic landmarks by leveraging sensors from off-the-shelf mobile devices and existing road infrastructure. Magland's design is driven by a key observation: we can create location signatures from local magnetic fields that in the context of orientation estimation for motion tracking are perceived as anomalies in the expected geomagnetic field, also designated as magnetic disturbances [136] or magnetic interference [35]. In outdoor scenarios, these are typically caused by road infrastructure and detected in areas such as the ones from Fig. 4.1: tunnels, bridges, and roads above underground structures. Our goal is to design the system that is capable of exploiting this observation.


Figure 4.1: Examples of roads where magnetic anomalies are detected.

## 4.1 Fundamental Insights

Magnetometer data is frequently used for orientation estimation, e.g. in road vehicle navigation [25]. Anomalies caused by strong local magnetic fields are observable in magnetometer measurements collected with off-the-shelf devices, as shown in Fig. 4.2. This figure gives an example of heading estimation using inertial data collected with a Nexus 4 smartphone from the field experiments described in the previous chapter.

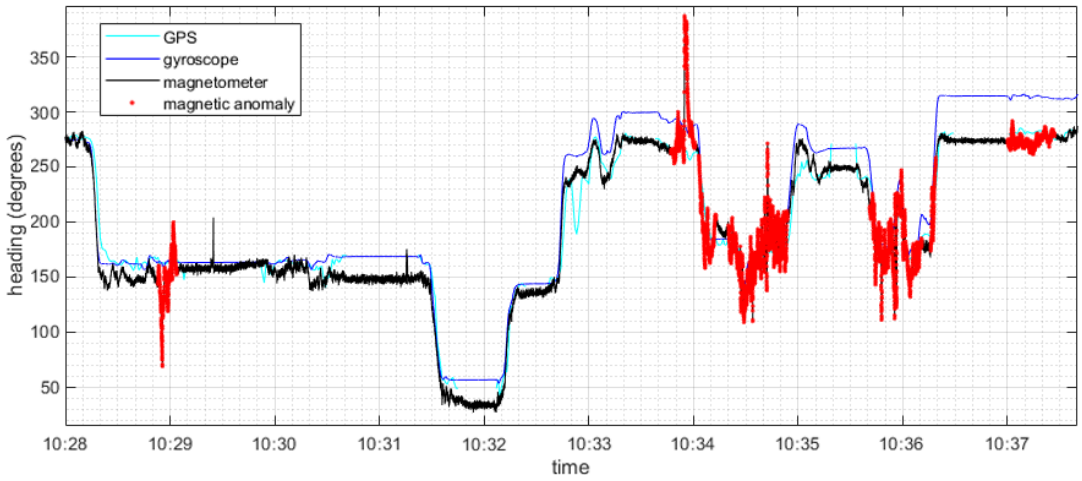


Figure 4.2: Heading data from several information sources, with highlighted magnetic anomalies.

Considering the magnetic data from those experiments, we notice thirteen of these anomalies. They occur in common areas in all four vehicles, presenting similar patterns. In Fig. 4.3, we provide one example comprising 270 seconds of the trip, where two anomalies can be perceived in the heading plot from all four vehicles. The first one is collected on a road above a subway station, and the second one is collected inside a tunnel. Looking into the locations of all found anomalies, we confirm the existence of some common types of surrounding infrastructure (see examples in Figs. 4.1 and 4.17).

We also realize that seven of the anomalies are concentrated in the downtown area, as shown in Fig. 4.4, suggesting the density of anomalies in Porto tends to be higher there. This is expected considering it is common for cities to have more infrastructures built in their urban and densely populated areas. Therefore, without loss of generality, our focus is mainly on urban scenarios since they are expected to have higher density of structures causing magnetic interference. These infrastructures vary significantly for different metropolitan areas, but from our preliminary analysis, we consider the urban density of magnetic landmarks as promising. Examples of areas where we observe them are tunnels (both inside and above), bridges, roads crossing at different heights (both under and above), roads crossing railways, and roads above underground structures such as subway lines, subway stations, or parking areas.

We performed a dedicated data collection using one vehicle with two smartphones in two locations of expected anomalies contained in the previous experiment, namely roads above a high-

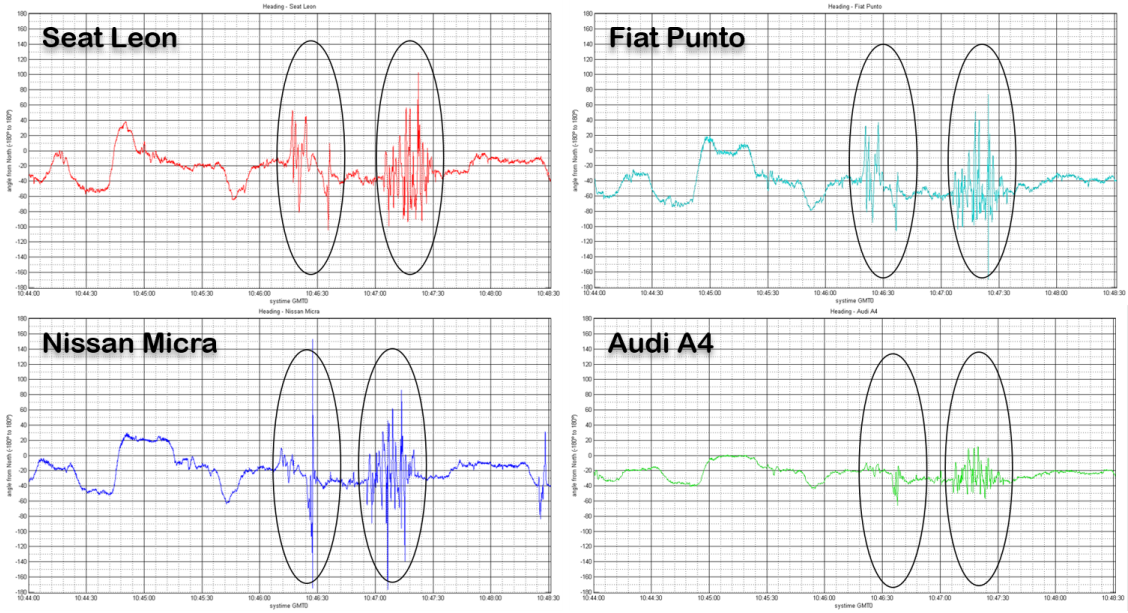


Figure 4.3: Heading estimated in each of the four vehicles for the same subset of the trip.

way and a subway station[1], passing several times with different speeds. In Fig. 4.5 we show the magnetic data for three local axes of one smartphone in the highway crossing scenario in both directions. We observe that the same path produces a particular pattern scaled by the vehicle's speed. Since anomalies correspond to a path segment, traveling in different directions results in distinct patterns. Also worthy of note is the fact that the magnetic sensor is frequently not well calibrated. Consequently, although the general patterns of the curves remain, the absolute values may vary significantly without proper calibration.

Using this highway crossing as an illustrative example, we observe that the obtained patterns are persistent in time and independent of the used vehicle and traffic conditions. In Fig. 4.6 we show the magnitude of the magnetic vector obtained on several dates, using different equipment. We confirm, as expected from our preliminary observations, that opposite road directions present different shapes, while the same path, collected in different dates and using diverse equipment, shows similar patterns. In time series these are scaled by the vehicle speed, as shown on the middle plots. When we convert to traveled distance using vehicle speed, as shown on the bottom plots, the patterns become more evident, even though they are never perfectly aligned, which makes it a challenge to compare them.

Based on these observations, we formally define anomalies and signature in the context of our approach as follows.

**Defining anomalies:** Magnetic anomalies are subsequences in a long sequence of magnetic data where the influence of local magnetic fields is noticeable. Different fields impact their surroundings in different ways and the area under their influence may vary considerably in size. Therefore, these anomalies have diverse lengths. In our dataset, they range from 10 to 870 meters.

[1]Highway crossing 2.4 and bifurcation above underground station 2.3 in Fig. 4.18

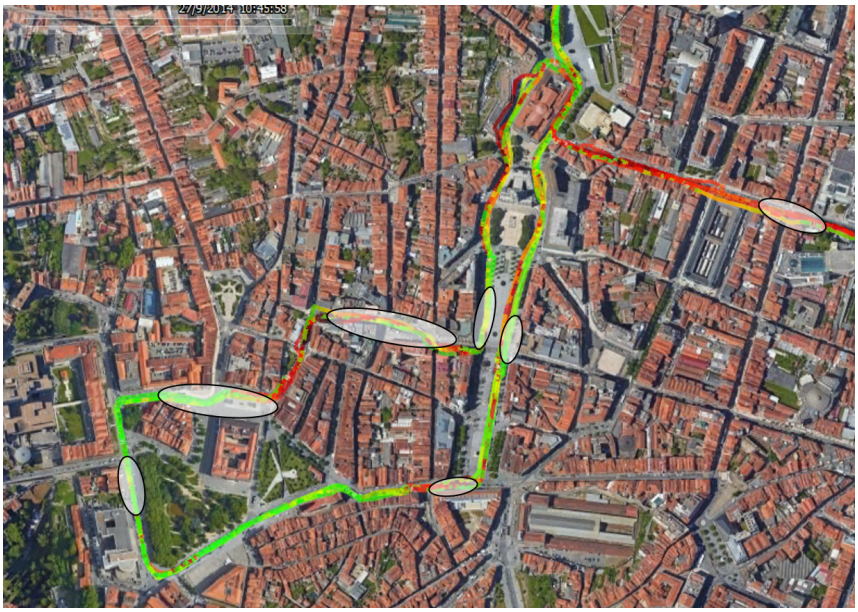

Figure 4.4: Seven locations with detected anomalies in all four vehicles in Porto's downtown area.

Because magnetic anomalies caused by permanent infrastructure are path specific, they may be viewed as magnetic landmarks.

**Defining signatures:** How to define unique signatures from magnetic anomalies is a challenge since each region of anomaly might have one or more signatures, depending on the path, direction, and lane of travel. Under the assumptions that inside regions of anomaly (1) vehicles always move forward in the allowed road directions, and (2) vehicles do not change lanes within the same road, we define magnetic signatures as follows: data collected on roads inside a region of magnetic anomaly, through a unique path and lane, creating a specific pattern. Regions comprising solely a unidirectional single-lane street have a single signature, while regions of anomaly that include alternative paths (e.g. crossroads), or lanes (both in the same direction and in opposite directions) have several, i.e. as many as the distinct paths or lanes.

The aim of this work is to design the system that leverages magnetic anomalies as landmarks, which opportunistically provide global location information for road vehicles. In the next section we provide an overview of the proposed system.

## 4.2 MagLand Overview

MagLand is based on our observations that the influence of local magnetic fields in the measured geomagnetic field caused by permanent road infrastructure (e.g. tunnel, bridge, underground area, subway or railway line) in a certain location is stable in time and not significantly impacted by notoriously changeable conditions, such as used equipment (e.g. vehicle or smartphone), traffic, or weather. The approach to leverage magnetic anomalies as landmarks for vehicle localization, involves the following three steps: detection, matching, and integration. In this work, we focus on

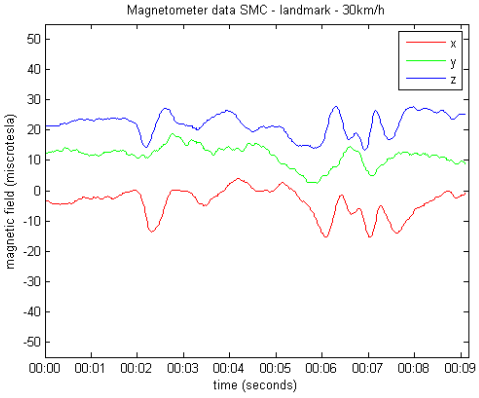


(a) South direction at 30km/h.

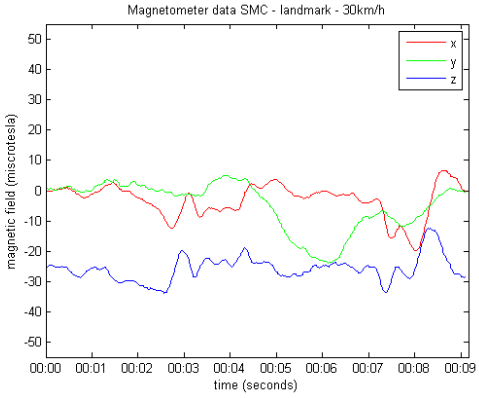


(b) North direction at 30km/h.

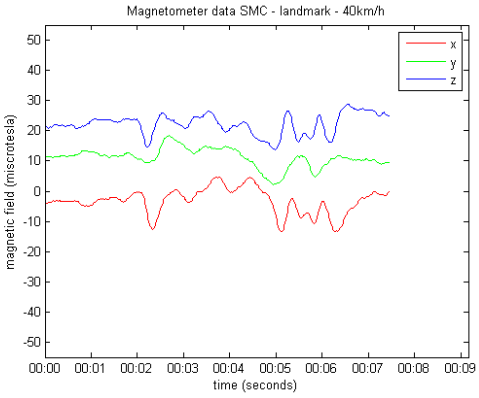


(c) South direction at 40km/h.

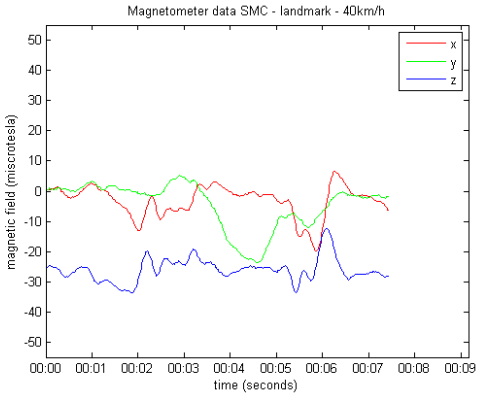


(d) North direction at 40km/h.

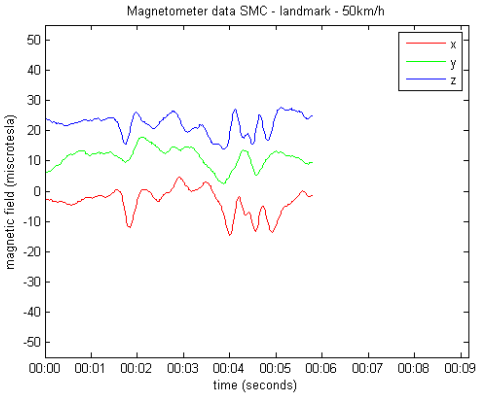


(e) South direction at 50km/h.

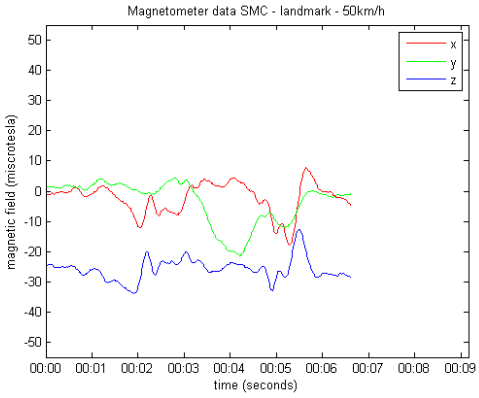


(f) North direction at 50km/h.

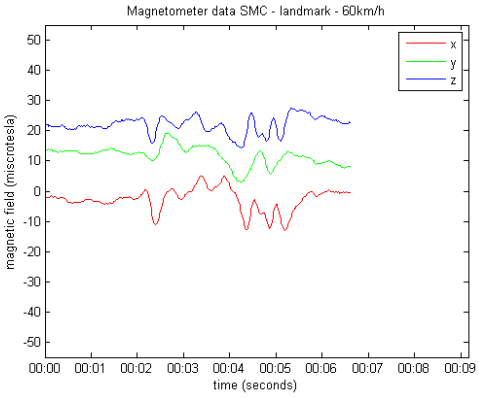


(g) South direction at 60km/h.

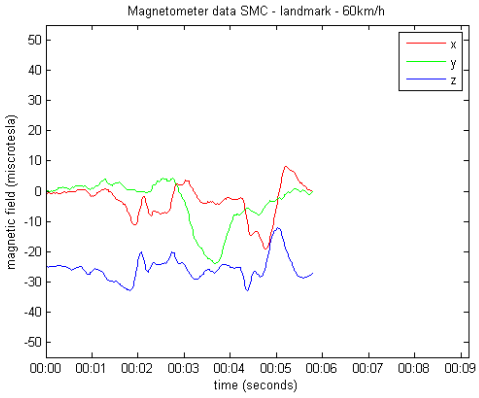


(h) North direction at 60km/h.

Figure 4.5: Magnetic data in the three local axis of the smartphone collected in a highway crossing (length 64m) with different speeds from 30 km/h to 60 km/h, in both directions of the road.

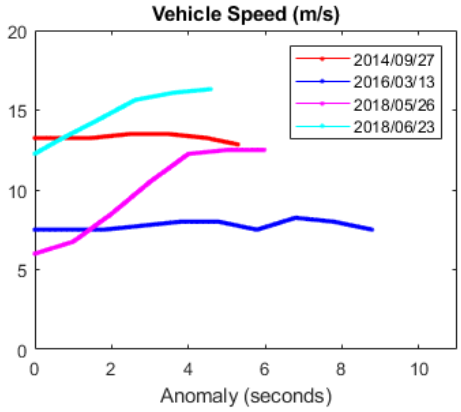


(a) Speed (South direction).

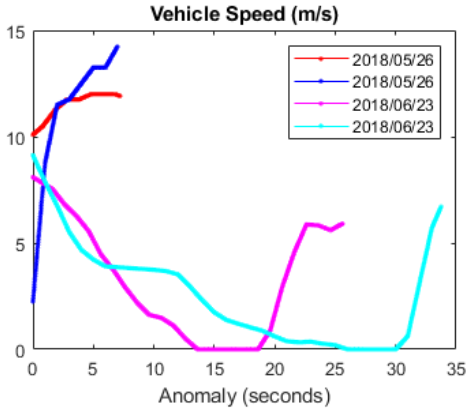


(b) Speed (North direction).

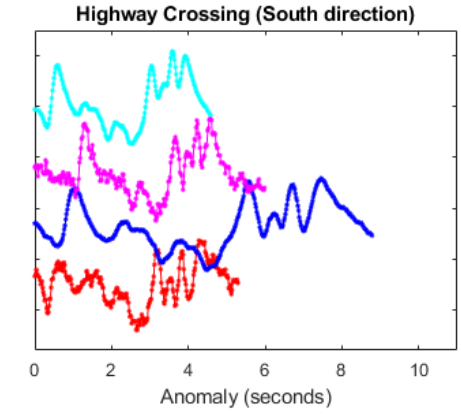


(c) Magnetometer data in time (South direction).

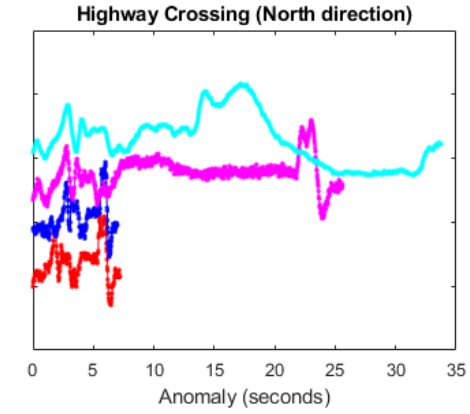


(d) Magnetometer data in time (North direction).

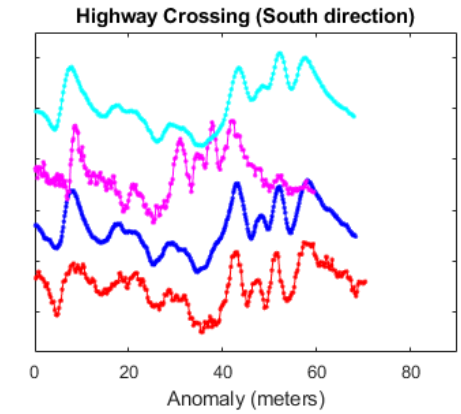


(e) Magnetometer data in space (South direction).

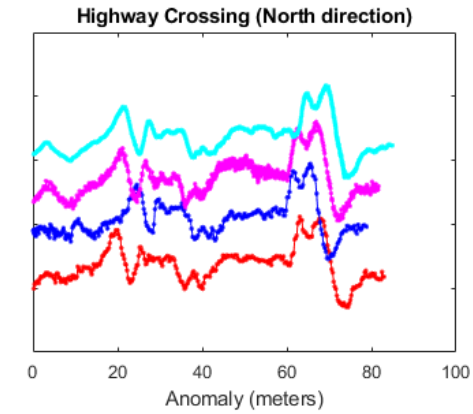


(f) Magnetometer data in space (North direction).

Figure 4.6: Data from the same highway crossing, collected on different dates, using distinct vehicles and smartphones, and with different speed patterns. The plots show the speed in m/s (top), and four magnetometer vector magnitude curves for each direction, in time (middle) and space (bottom), with offsets in $y$ axis for clarity.

the first two. The integration step would involve the integration of the previous two steps and the integration of the magnetic landmarks into a continuous location tracking algorithm.

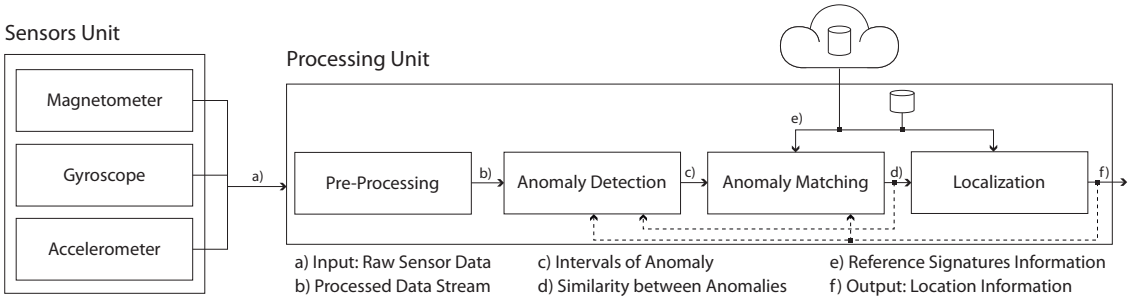


Figure 4.7: System model describing the different steps of the proposed approach.

We propose the system model represented in Fig. 4.7. Magnetic signatures are previously mapped and stored on a reference database. We propose guidelines to collect a large number of instances per signature and average them into a single reference to represent each signature. During MagLand online application, this databse might be available remotely, locally or both (cached). The first step after raw data collection is the pre-processing. It involves calibration of data from each sensor, heading calculation, and magnetic data transformation to a common reference frame. Anomaly detection, matching and localization steps are organized in a sequential manner. Anomaly detection algorithm is running online with the goal of detecting blocks of anomaly. Blocks are, in the perspective of the time series data, intervals of anomaly, which correspond to a region in space. The matching algorithm is only performed when an anomaly is detected. It outputs a similarity or dissimilarity measure between pairs of anomalies, which in this case are the detected anomaly from the data stream and each of the references. If a magnetic signature is identified, we obtain its location information from the database. In the envisioned approach the location estimation is combined with other sources of localization to provide continuous vehicle tracking. These three steps, detection, matching, and localization, and interconnected. They may share relevant information online to improve global performance of the system, e.g. a positive online matching may improve the detection step with prior knowledge concerning the anomaly size; or knowing a broad location in advance may enable the matching algorithm to considered references only within a limited area.

In order to provide a proof-of-concept for MagLand, we propose and evaluate algorithms for detection and matching of magnetic anomalies. First, we collect a dataset without any path restrictions. After pre-processing the data, we manually mark the ground truth and use supervised learning to compare ten binary classifiers for anomaly detection in time series, choosing one. Next, we perform new field trips containing a limited and known set of anomalies, including references for each. To select an algorithm for matching an anomaly to stored references, we consider two configurations with distinct goals: one uses complete versions of the anomalies for matching and evaluates the potential accuracy of the approach; the other uses incomplete versions of the anomalies to understand the impact of online matching on the performance.

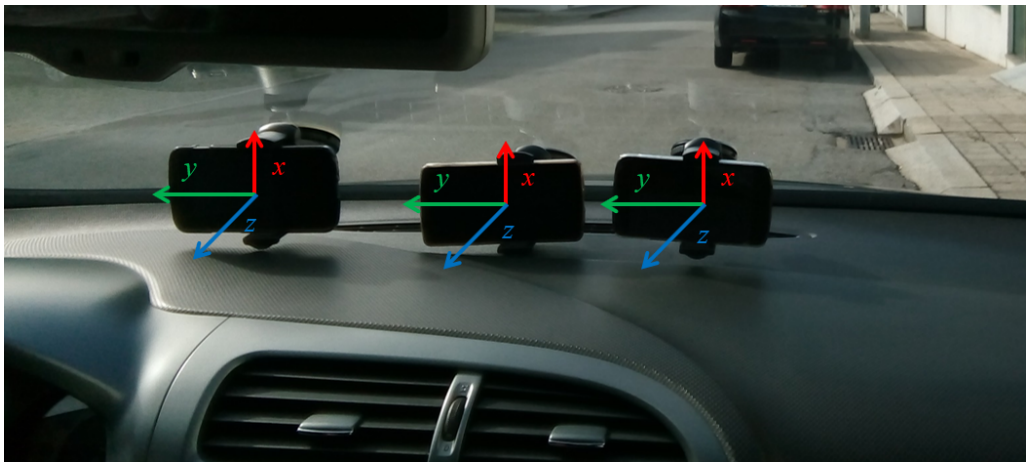


Figure 4.8: Vehicle setup for data collection in one of the trips, using three smartphones (two Nexus 4 and one Nexus 5) fixed on the windshield. Each of the smartphones includes a representation of its three local axes for illustration purposes.

## 4.3 Sensor Data and Pre-Processing

Consider a vehicle traveling on the road, with a smartphone in a fixed position gathering data. For this purpose we can use one of several available applications, e.g. SenseMyCity [138, 139]. The orientation of the smartphone relative to the vehicle is assumed to be known, otherwise it has to be estimated from the data [140]. In Fig. 4.8 we provide an illustrative example with three smartphones fixed to the windshield. This smartphone position and orientation is the one chosen for our data collection campaigns. We use the following sensors: accelerometer, gyroscope, and magnetometer. They are all collected at the maximum rates available in the device and modified, via interpolation or decimation, to the instants of the magnetometer samples at 50Hz. For training purposes we collect GPS data using the smartphone: gpstime, 3D position, speed, and heading. We assume a maximum speed of 90km/h (25m/s). Our main focus is on urban environments where speeds are typically lower.

### 4.3.1 Sensor Data

We describe in detail the data from accelerometer, gyroscope and magnetometer, collected in the three local axes of the smartphone, illustrated in Fig. 4.8.

#### 4.3.1.1 Accelerometer

The accelerometer measures the smartphone's acceleration ($m/s^2$), including the effect of gravity, in the three local axes. In our model, acceleration data is used only to estimate the Up direction in the global ENU (East, North, Up) frame, for orientation purposes. With a static object, the measured acceleration vector has the same magnitude as the gravity, pointing in the opposite direction, the Up direction (see Fig. 4.10a). With a fixed position of the smartphone inside the vehicle, we require only a small interval where the vehicle is static in a horizontal road, i.e. not particularly

steep, to estimate the Up direction vector from accelerometer data. In our experiments, we averaged the acceleration during an interval with zero speed before the driving started, confirming the result was close to the expected magnitude (the Earth's gravity, approximately 9.8 $m/s^2$).

#### 4.3.1.2 Gyroscope

The gyroscope measures the angular speed ($rad/s$) in the three local axes. Integrating these values, we can measure the orientation changes in time. However, since these errors accumulate, we should estimate this drift and compensate for it in order to reduce its effects. We can estimate the gyroscope drift as the angular speed average for a static interval. This drift usually maintains for large periods and can be valid for the whole trip, but occasionally the smartphone might recalibrate the gyroscope and in that case our estimation should be updated accordingly. In the online approach both the Up direction obtained from the accelerometer data and the gyroscope drift could be estimated and confirmed during small static (zero speed) intervals of the vehicle during the trip, for example in traffic lights.

#### 4.3.1.3 Magnetometer

The magnetometer measures the local magnetic field vector (microtesla) in the three local axes of the smartphone. Most of the time, i.e. when there are no strong magnetic fields created by nearby objects or infrastructures, the magnetometer measures the Earth's magnetic field. This points in the direction North-Up or North-Down (depending on the hemisphere)[2]. Combined with the Up direction learned from the accelerometer, this allows to estimate the orientation of the smartphone (for details about this process refer to [136]), and therefore of the vehicle, in the global ENU frame (Fig. 4.10a). In our case, this is updated at the same rate as the magnetic data. Since it uses data from both accelerometer and magnetometer and the latter is assumed to measure the geomagnetic field, whenever its measurements are affected by local magnetic fields, this orientation presents anomalies. In our road scenario, we are particularly interested in the horizontal orientation, the vehicle heading.

### 4.3.2 Data Pre-Processing

We collect raw real-world inertial data and process it in order to obtain useful features for our approach. This process involves two main challenges: magnetometer data calibration and feature engineering.

#### 4.3.2.1 Magnetometer Data Calibration

Our first challenge is to calibrate magnetic data so that we have reliable orientation and heading during normal function, without compromising the patterns that serve as signatures inside regions of anomaly.

[2]The magnetic North pole differs from the geographic North pole. It changes over time and the difference between both in the horizontal plane is an angle called magnetic declination. We do not take it into account in this work.

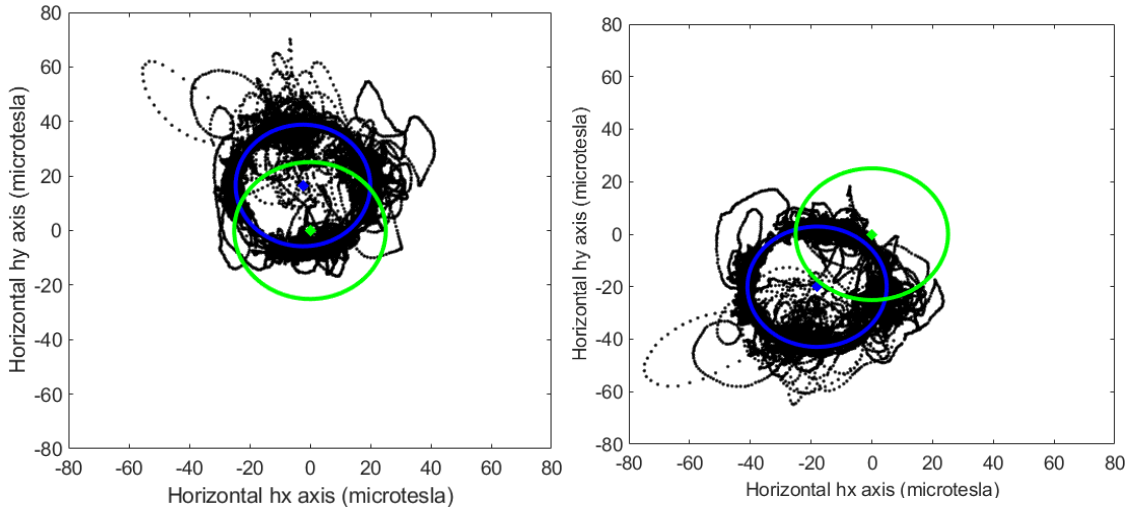


Figure 4.9: Illustrative examples of bias present in magnetometer data (trip ID 3 and trip ID 4 from Table 4.1) on the horizontal plane of the local vehicle frame (see Fig. 4.10b). The origin-centered circles (green) show the expected horizontal intensity of the geomagnetic field for the broad location (25.1$\mu$T), and the other circles (blue) fit the data.

The magnetometer data measured in the local frame is subject to different errors [141]. One of them causes the measured magnetic field to present a bias, instead of being centered in the origin of the local frame. We verified in our experiments that even small offsets in the horizontal plane can have a significant impact on the estimated heading. An illustrative example is shown in Fig. 4.9. The vehicle itself may generate a local magnetic field and calibration should be performed while the magnetometer is on-board.

Several methods address the magnetic calibration problem in the literature, presenting different conditions and limitations.Most solutions contain at least one of the following requirements: 1) movement control for calibration phase, 2) large rotation range, or 3) access to external sources of heading or orientation information. The most traditional one, compass swinging, requires user involvement in the process (rotating the compass in predefined directions), so it is not suitable for our scenario where we do not control vehicle movement. Another popular approach is ellipsoid fitting. An example of this approach is provided in [141]. It assumes a fixed device, works in 3D, and does not need an external heading source. It requires a large rotation range, which might represent a problem in case we want our online setting to work from an early stage. In [142], an automatic calibration technique is performed online with a minimum space coverage. However, it assumes knowledge not only of the horizontal magnetic field, but also of external heading source of information, allowing the device to move freely during the driving. Another example of a calibration requiring information from other sensors is given in [143]. It formulates the calibration as an orientation estimation problem and uses accelerometer and gyroscope. It attempts to compensate for the magnetic disturbances, which is not our intention in this work.

In our approach, although we have access to external sources of heading or orientation information, we prefer to maintain the fixed device limitation and keep the magnetometer data indepen-

dent from them. This enables their subsequent use to help in the detection of the type of errors we are interested in, i.e. the ones caused by local magnetic fields. Concerning the horizontal plane, we decide to apply a simpler approach to remove only the permanent offset, assuming a circle, in order to obtain suitable heading values for non-anomalous samples. This horizontal magnetic calibration allows us to use the heading as a feature, avoiding extra modifications to the collected magnetometer data.

### Circle Fitting Problem

In Fig. 4.9 we can see in green the origin centered circle relative to the theoretical values for the magnetic data for the city of Porto and in connected black dots the magnetic data for a whole trip projected on the horizontal plane. The heading of the vehicle at any moment of the trip is measured as the angle between the direction indicated by the magnetometer in the horizontal plane for that instant and the horizontal $x$ axis. The blue circle is fitting the collected data. To decrease heading errors we estimate and compensate for the offset between the center of these two circles.

The problem of finding the blue circle is known as the circle fitting problem: get the circle (both center coordinates and radius) that best fits a given set of points, usually in the least squares sense. Several approaches have been proposed [144, 145]. Solving this problem in practice is not easy, since the minimization of the least squares fitting of circles is a nonlinear problem that has no closed form solution [144]. All known algorithms are either iterative and costly or approximative by nature, and the problem becomes even more challenging when the points are sampled along solely a small arc. Getting points for the whole circle might take a very long time depending on the trajectory so, when calibrating the magnetometer data online, a good fitting is required even with a small arc. Also, these methods are based on the assumption that all points are drawn from a real circle with isotropic Gaussian noise. The presence of external magnetic fields implies that this assumption is not valid in our scenario.

### Proposed Calibration Procedure

In order to find an adequate circle fit under these particular conditions, small arc available and in the presence of strong anomalies, we assume knowledge of the radius. The radius of the circle is the horizontal intensity of the measured magnetic field and, as aforementioned, we know the expected geomagnetic field for a given broad location area. In our practical experiments, we use the theoretical horizontal intensity for the city of Porto, approximately 25.1$\mu$T, as the expected radius for the circle fitting. This presents a new problem that cannot be solved as a particular instance of the aforementioned circle fitting proposed solutions, as these estimate first the center coordinates and only then the best radius for that center.

Our problem is to find the center of the circle that minimizes the sum of the distances from all points to the circle. As we know our magnetometer data is subject, not only to measurement errors,

but also to the local magnetic fields that constitute the anomalies, we decide against the more common approach of minimizing their squares. Anomalies may have a very different behavior than the one from the points drawn from the theoretical circle that is the expected horizontal projection of the geomagnetic field, and squaring that error would give higher weights to these anomalous points. We apply a descent quasi-Newton heuristic to find a local minimum, using the origin $(0,0)$ as the starting point. Since having an unbalanced density of points in different regions can degrade the results, we round all coordinates with a precision of $0.1\mu$T and remove points with repeated values.

Regarding the vertical axis, we make an average of all available data points and apply an offset relative to the theoretical value. This might be done with the whole time series when post-processed or with a small initial interval otherwise.

#### 4.3.2.2 Feature Engineering

Smartphone inertial data is collected on the local reference frame (Fig.4.8). In order to allow comparisons between different instances, a common reference frame is required. One option is to use the World global ENU frame (Fig. 4.10a), using gravity and magnetic North for reference. We also include a second option that we believe could be more interesting in this specific scenario: a vehicle local frame. We define it as follows: the front of the vehicle (direction of movement) is the horizontal `hy` axis, `vz` is the vertical axis, and the horizontal `hx` axis is orthogonal to both `hy` and `vz`, pointing to the right of the vehicle, as depicted in Fig. 4.10b. Following our assumption of knowing the position of the smartphone inside the vehicle, we can describe the vehicle reference frame in the smartphone local coordinates. This allows us to have a common reference without relying on the magnetometer data.

Taking into account collected sensors and context, we propose to describe the calibrated data as follows (50Hz, magnetometer instants):

- **Magnetometer data** described in two distinct frames: 2 axes in the World global ENU frame (North and Up, since East is null), and 3 axes in the vehicle frame, shown in Fig. 4.10. We also use the magnetometer total magnitude and the horizontal intensity, which is the magnitude of the vector defined by the horizontal `hx` and `hy` axes.

- **Orientation** estimated from magnetometer and gravity, giving us a rotation for the global ENU frame. For simplicity, from now on we suppress the reference to the accelerometer.

- **Changes in orientation** from gyroscope integration (after gyro drift compensation).

The initial orientation is necessarily obtained from the magnetometer, since gyroscope only tracks changes in orientation. After the initial instant, we can track the orientation, and consequently the heading, from two different sources of information. Considering gyroscope data is unaffected by local magnetic fields, we expect differences to be relevant for detecting magnetic anomalies.

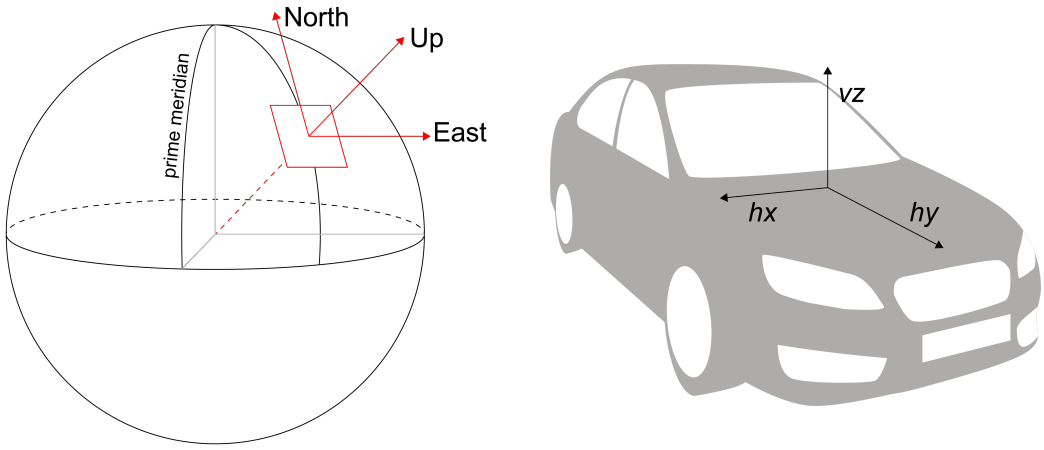


(a) Global ENU frame (b) Local vehicle frame

Figure 4.10: Reference frames for inertial data.

All magnetic data is in microtesla (μT) and angles are measured from East, positive counter-clockwise, in radians. From the above data, we define the following time series (non-periodic, 50Hz):
1) **heading** estimated from magnetometer [*hm*];
2) **magnetometer North** component in ENU frame [*mn*];
3) **magnetometer Up** component in ENU frame [*mu*];
4) **magnetometer horizontal `hx`** axis in vehicle frame [*mhx*];
5) **magnetometer horizontal `hy`** axis in vehicle frame [*mhy*];
6) **magnetometer vertical `vz`** axis in vehicle frame [*mvz*];
7) **magnetometer vector magnitude** [*mm*];
8) **magnetometer horizontal intensity** [*mh*];
9) **absolute difference** of the first derivatives (changes in consecutive values) of the **heading** estimated from magnetometer and from gyroscope [*dif1*];
10) **absolute difference** of the deviations (difference to the window mean) of the **heading** estimated from magnetometer and from gyroscope [*dif2*] (only used in detection step).

These features have significant redundancy, so we expect only a subset to be necessary for our approach. For example, features *mn* and *mu* and features *mhx*, *mhy* and *mv* describe the same magnetic vector in different frames.

## 4.4 Magnetic Anomaly Detection

The aim of this step is to detect periods of anomaly in the magnetic time series data that are associated to local magnetic fields caused by permanent road infrastructure. Successfully detecting each of these anomalous blocks, i.e. the start and end of anomalous subsequences in our multivariate non-periodic time series, is very important to their use as signatures for specific paths.

Currently, the detection of magnetic anomalies is closely related to fusion algorithms for orientation tracking. Sensor fusion using accelerometer, gyroscope and magnetometer is frequently applied to orientation estimation [35], with the most common approaches being stochastic filtering (mainly based on the Kalman Filter and its different implementations), complementary filtering, and gradient descent algorithm [146]. These fusion algorithms enable ignoring or attributing a low weight to a source that gives unexpected values during a period of time. The deviation from the expected geomagnetic field vector is generally applied as a measure of confidence in the magnetic sensor, either combined with a threshold, e.g. Harada et al. [136], or used as a weighting factor, e.g. Fan et al. [146]. Therefore, the focus is not on detecting the errors, but on minimizing their impact in the system for orientation estimation purposes.

### 4.4.1 Anomaly Detection in Time Series

Anomaly detection is a very broad topic [147]. The most interesting model for each situation depends highly on the available data and the requirements of the solution [148]. In our particular scenario the data consists of multivariate non-periodic time series with anomalous subsequences [149]. Techniques for anomaly detection in time series data may be classified in kernel-based, window-based, and predictive techniques [150]. Kernel-based techniques make use of a distance kernel to compute similarity between sequences. They are not suitable for online detection and usually present poor performance for subsequence anomalies, so we exclude these methods for our purposes. Window-based techniques analyze a short and fixed length window (or subsequence) from a test sequence at a time, assigning an anomaly score. It is usually applied combining the anomaly scores from all windows in order to find anomalous test sequences, but it can be adapted for finding subsequence anomalies in an online setting. The choice of the window size is critical. Predictive techniques learn a predictive model from the training series and compare the forecast observation with the actual observation to detect anomalies. The extensive experimenting with many different time series performed by Chandola [150], indicates that for time series data kernel and window based techniques, which are model independent, tend to give better performance that predictive techniques. Therefore, we opted for the use of a window-based technique, dividing each data sequence in small subsequences, or windows.

**Window size:** Usually windows have a fixed size corresponding to a fixed time interval, containing the same number of points for a constant sampling frequency. However, due to the spatial nature of our problem, we fix the size of the window relative to an interval in space, i.e. a fixed traveled distance. To choose the size of our window, we take into account that a very large interval may difficult the detection of small sized anomalies and reduce the space precision; on the other hand if the interval is too short there may not be enough points per window at higher speeds. Having considered a maximum speed of 90km/h, we choose a distance that guarantees at least 20 points per window with the data rate of 50Hz. The window size is fixed to 10 meters. The estimated vehicle speed is used to analyze the data in windows of 10 m. Non-overlapping windows are extracted from each sequence for both training and testing.

| Trip ID | Date | Traj. ID | Veh. ID | Duration | Trav. dist. (km) | Block anom. | Windows | Anom. Windows |
|---|---|---|---|---|---|---|---|---|
| 1 | 27-09-2014 10h06 | 1 | 1 | 45m20s | 12.889 | 19 | 1201 | 244 |
| 2* | 27-09-2014 10h06 | 1 | 1 | 45m20s | 12.899 | 15 | 1201 | 227 |
| 3 | 27-09-2014 10h06 | 1 | 2 | 45m20s | 12.785 | 13 | 1205 | 231 |
| 4 | 27-09-2014 10h06 | 1 | 2 | 45m20s | 12.785 | 13 | 1206 | 229 |
| 5 | 27-09-2014 10h06 | 1 | 4 | 45m20s | 12.874 | 18 | 1213 | 222 |
| 6 | 13-03-2016 11h06 | 2 | 1 | 14m26s | 12.285 | 6 | 1191 | 63 |
| 7* | 13-03-2016 11h52 | 3 | 1 | 55m23s | 21.848 | 32 | 2092 | 634 |
| 8 | 13-03-2016 11h52 | 3 | 1 | 55m23s | 21.848 | 32 | 2092 | 629 |
| 9 | 13-03-2016 14h56 | 4 | 1 | 30m38s | 9.775 | 10 | 927 | 254 |
| 10* | 11-11-2016 19h32 | 5 | 1 | 31m50s | 13.462 | 15 | 1298 | 213 |
| 11 | 12-11-2016 13h20 | 6 | 1 | 6m47s | 4.043 | 3 | 382 | 34 |
| 12 | 13-11-2016 12h38 | 7 | 3 | 10m32s | 5.176 | 7 | 448 | 18 |
| 13* | 15-11-2016 09h21 | 8 | 3 | 9m56s | 4.682 | 4 | 374 | 32 |
| Total | 8 | 8 | 4 | 6h26m35s | 157.351 | 187 | 14830 | 3030 |

Table 4.1: Characteristics of the anomaly detection dataset

### 4.4.2 Dataset Description

We collected a total of 13 trip datasets for analysis with Nexus 4 and 5 smartphones. Table 4.1 presents the description of each trip. The dataset has some heterogeneity, including four vehicles, eight trajectories (comprising both urban and highway sections), different dates and traffic conditions. It comprises a total traveled distance of 157 km during 6h26m, including 187 anomalies with a total of 3030 windows of anomaly (10 m each). The trips took place in the district of Porto, Portugal.

Some of the trips were collected in the same vehicle at the same time with different smartphones, namely trips 1 and 2, 3 and 4, and 7 and 8. Trips 1 to 5 were collected in the same experimental campaign with distinct vehicles driving the same route. In trips 7 and 8 the trajectory was chosen in order to repeatedly visit certain previously identified locations containing anomalies in different speeds and directions. This is the reason why these trips are the ones containing the highest ratio of anomalies, around 30%. The remaining trips were actual trips, performed in everyday life without any planning. In these, the ratio of anomalies varied between 4% and 27%.

Nine trips are used for training and the remaining four (a third of the dataset, marked with an

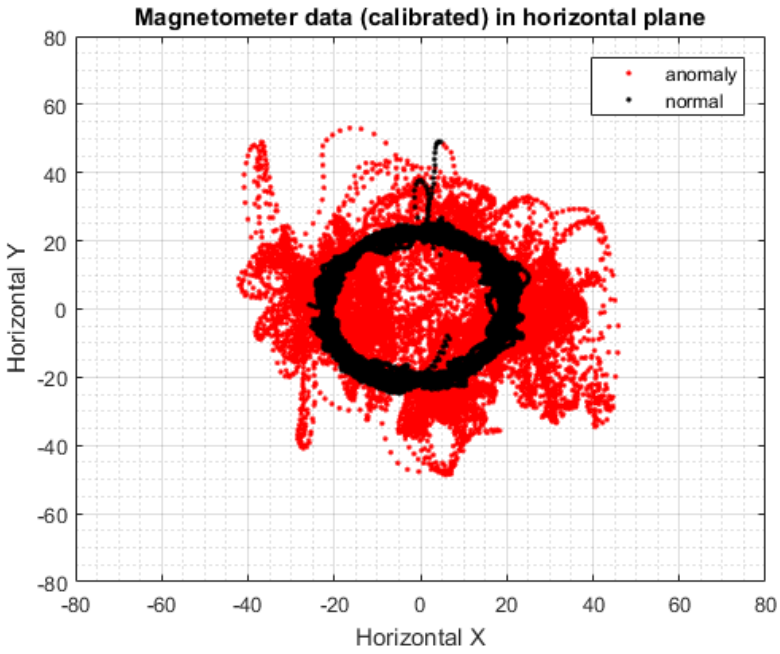


Figure 4.11: Calibrated magnetic data (microtesla) projected on the horizontal plane with highlighted anomalies.

asterisk in the trip ID) are used for testing. Two of those (trips 2 and 7) were collected in the same experiment and vehicle as others used in training. The other two (trips 10 and 13) have totally different trajectories from the ones in the training set.

**Ground Truth:** In order to apply supervised learning techniques, we manually annotate the anomalies for all trips on the dataset by visually inspecting the plots of processed time series with respect to their expected values. From gyroscope data and GPS information we learn the expected heading. See Fig. 4.2 for an illustrative example of heading data with highlighted anomalies in red. From the broad location, we consult the approximated expected geomagnetic field [151]. Fig. 4.11 shows an illustrative example of calibrated magnetic data projected on the horizontal plane with highlighted anomalies in red. Fig. 4.12 shows an illustrative example of vertical magnetic data with highlighted anomalies in red. There is an inevitable uncertainty regarding boundary points between normal instances and anomalies. The intervals of anomaly are delimited using the initial and final seconds (gpstime). Windows including any number of anomalous points are considered anomalous windows.

### 4.4.3 Data Processing

We apply 20 functions to each window from each time series. The functions, 12 from time domain and 8 from frequency domain, are described in detail in Table 4.2. We define $\mathbf{s} = \{s_i, i = 1,2,\ldots,N\}$ as the subsequence of values from one parameter contained in each window of 10 m in the time domain, having a total of $N$ points, $N$ being variable for different windows, depending on the speed of the vehicle. Applying a fast Fourier transform (FFT) to obtain the power spectral

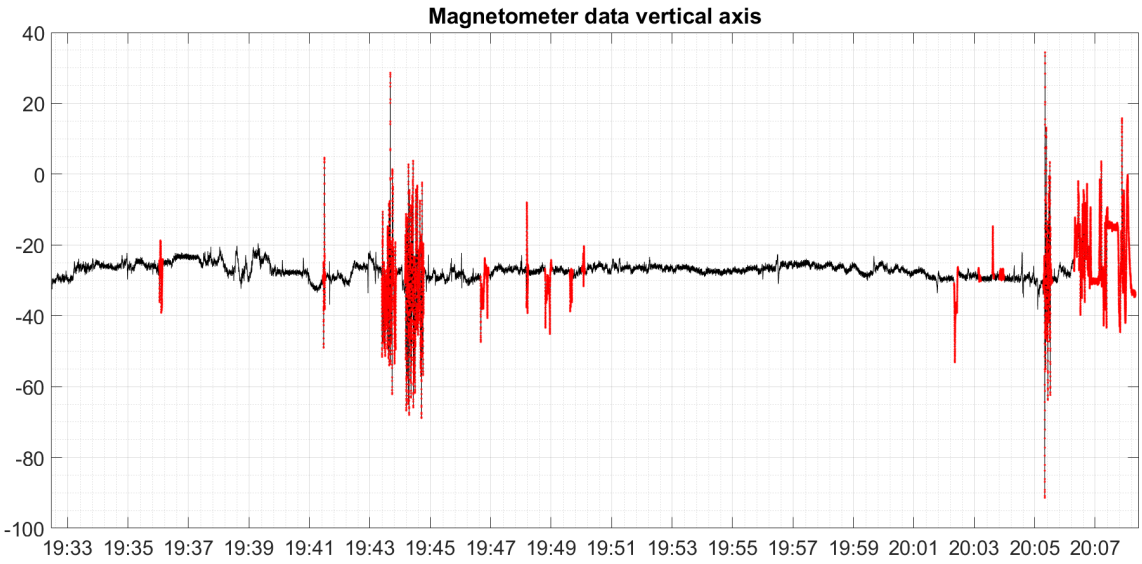


Figure 4.12: Magnetic vertical data (microtesla) with highlighted anomalies.

density of the signal for that window, $P_j$ represents the power spectrum at $f_j$, the frequency value at the frequency bin $j$ in a total of $M$.

From the resulting 200 features (20 functions applied to the windows of each of the 10 time series described in Section 4.3.2.2) there are four, namely peak frequency and median frequency for parameters *dif2* and *mm*, that result in null values for all windows, and so they are excluded from the training and testing datasets. Therefore, to consider different models for our anomaly detection task we use a dataset of 9865 windows of 10 m for training and 4965 for testing, each containing 196 features.

Using features based directly on magnetometer data requires the classifier to be specifically trained for each new area, since magnetic fields vary depending on the broad location on the globe. On the other hand, classification solely based on heading information is location agnostic. Thus, we consider two feature sets: (1) including features extracted from the magnetometer data and using all 196 features, and (2) based uniquely on the 60 features that do not depend directly on the magnetometer data, but only on the heading after processing the data.

It is very important to adequately prepare the dataset before employing the classifiers. Particular care should be taken when dealing with the presence of outliers, features of different units and scales, imbalanced data, and highly correlated features. The goal is to detect the anomalous instances, so outliers in the data are to be expected and should be taken into account. We address each of the remaining issues next.

#### 4.4.3.1 Feature Normalization

Performing feature normalization is a common pre-processing requirement. Many classifiers work under the assumption of standardization or rely on a distance measure that should not be applied to variables with different units and scales. While this step might help to balance the weights among

| | Function | Expression |
|---|---|---|
| Time Domain | 1) *min* | $\min \mathbf{s}$ |
| | 2) *max* | $\max \mathbf{s}$ |
| | 3) *mean* $\bar{s}$ | $\bar{s} = \frac{1}{N}\sum_{i=1}^{N} s_i$ |
| | 4) *mav* | $\frac{1}{N}\sum_{i=1}^{N} \lvert s_i \rvert$ |
| | 5) *ab* | $\sum_{i=1}^{N} \lvert s_i \rvert$ |
| | 6) *rms* | $\sqrt{\frac{1}{N}\sum_{i=1}^{N} \lvert s_i \rvert^2}$ |
| | 7) *md* | $\frac{1}{N}\sum_{i=2}^{N} \lvert s_i - s_{i-1} \rvert$ |
| | 8) *mad* | $\frac{1}{N}\sum_{i=1}^{N} \lvert s_i - \bar{s} \rvert$ |
| | 9) *sd* $\sigma$ | $\sigma = \left(\frac{1}{N-1}\sum_{i=1}^{N}(s_i - \bar{s})^2\right)^{\frac{1}{2}}$ |
| | 10) *ske* | $\frac{E(s-\bar{s})^3}{\sigma^3}$ |
| | 11) *kur* | $\frac{E(s-\bar{s})^4}{\sigma^4}$ |
| | 12) *atc* | $\frac{\sum_{i=2}^{N}(s_i-\bar{s})(s_{i-1}-\bar{s})}{\sum_{i=1}^{N}(s_i-\bar{s})^2}$ |
| Frequency Domain | *tsp* | $\sum_{j=1}^{M} P_j$ |
| | 13) *msp* | $\frac{1}{M}\sum_{j=1}^{M} P_j$ |
| | 14) *psp* | $P = P_j : \max P_j, j = 1, \ldots, M$ |
| | 15) *pf* | $f_p = f_j : \max P_j, j = 1, \ldots, M$ |
| | 16) *mf* | $f_m = f_j : \sum_{j=1}^{f_j} P_j = \sum_{j=f_j}^{M} P_j = \frac{1}{2}\sum_{j=1}^{M} P_j$ |
| | 17) *af* | $\frac{\sum_{j=1}^{M} P_j f_j}{\sum_{j=1}^{M} P_j}$ |
| | 18) *m1f* | $\sum_{j=1}^{M} P_j f_j$ |
| | 19) *se* | $\sum_{j=1}^{M} P_{Nj} \log_2 P_{Nj}, P_{Nj} = \frac{P_j}{\sum_{j=1}^{M} P_j}$ |

Table 4.2: Time domain and frequency domain functions applied per window to each parameter: 1) minimum, 2) maximum, 3) mean, 4) mean absolute value, 5) absolute magnitude, 6) root mean square, 7) mean absolute difference, 8) mean absolute deviation, 9) standard deviation, 10) skewness, 11) kurtosis, 12) autocorrelation, 13) total spectral power, 14) mean spectral power, 15) peak spectral power, 16) peak frequency, 17) median frequency, 18) mean frequency, 19) first moment in the frequency, 20) spectral entropy.

different features and reduce noise, in the presence of outliers it can compromise the data. Since the best choice might depend on the model, we decided to keep both options available, original features and normalized feature with z-score normalization (zero mean and unit variance), until the next step.

#### 4.4.3.2 Balancing Dataset

In our dataset the ratio of anomalies and normal instances is approximately 20% and 80%, respectively. To balance the dataset making both classes equally represented, we apply SMOTE [152], which stands for Synthetic Minority Over-sampling Technique. SMOTE artificially generates new examples of the minority class with the nearest neighbors of existing cases. We use the implementation from *DMwR* R package [153], where this is combined with under-sampling of the majority class.

#### 4.4.3.3 Feature Selection

Many of our 196 features are highly correlated. This redundancy might have a negative impact while training some models, as well as unnecessarily increase the complexity. To select a good subset of features, we use Correlation-based Feature Selection (CFS) [154], which is based on the assumption that good feature sets contain features that are highly correlated with the ground truth class, yet uncorrelated with each other. From the original features, we keep 20 selected by CFS on the training set.

The feature selection process chose the following 20 features: *min.mn*, *max.mh*, *max.mhy*, *mean.mvz*, *mav.mhy*, *mad.dif2*, *mad.mm*, *mad.mh*, *mad.mu*, *mad.mvz*, *sd.mhx*, *atc.dif1*, *pf.dif1*, *pf.mu*, *pf.mhx*, *pf.mvz*, *af.dif2*, *af.mm*, *af.mn*, and *m1f.mvz*. We observe that 12 of the features are from the time domain and 8 are from the frequency domain. None of them is directly based on the heading, although four are obtained from the differences in heading calculated from magnetometer and gyroscope data. The remaining 16 features utilize magnetometer data directly: 6 using either the local vertical or the global Up axis, 8 using some form of horizontal information, and 2 using the total magnitude.

We also applied CFS to the 60 heading-based features and obtained the following 13 features: *mad.hm*, *se.hm*, *min.dif1*, *mean.dif1*, *atc.dif1*, *pf.dif1*, *af.dif1*, *rms.dif2*, *mad.dif2*, *sd.dif2*, *af.dif2*, *m1f.dif2*, and *se.dif2*. We observe that 7 features are from the time domain and 6 are from the frequency domain. Only 2 directly use the heading from the magnetometer. The remaining 11 are based on the differences to the gyroscope heading information.

### 4.4.4 Classification Model

We search for a suitable classifier to distinguish between normal and anomalous instances among ten well known supervised models. The first five are strong and widely used algorithms for classification: **Decision Tree (DT)**, **Neural Network (NN)**, **Support Vector Machine (SVM)** with a linear kernel, **k-Nearest Neighbors (kNN)**, and **Naive Bayes (NB)**. The other five are popular

ensemble methods, combining the predictions of multiple learning algorithms in order to improve the performance compared to a single one. Three are based on decision trees: **Random Forest (RF)**, which is a bagging method, and two boosting based models, namely **Stochastic Gradient Boosting (GBM)**, and **Boosting C5.0 (C5)**. The remaining two ensembles are **Boosted Logistic Regression (BLR)** and **Model Averaged Neural Network (aNN)**. The implementation was performed in R [155] applying the train function of the *caret* package. Unless stated otherwise, default values are used.

#### 4.4.4.1 Metrics

We consider the following metrics to compare the classifiers: sensitivity, precision, specificity, accuracy, area under the ROC curve (AUC), and F2-score. While a good predictor should have a nice balance between false positives ($FP$) and false negatives ($FN$), in our case a low number of $FN$ is more important than a low number of $FP$, since missing an anomaly has a worst impact than misclassifying a normal instance. This is the reason sensitivity metric is more relevant for our application than precision or specificity. Accuracy gives an important indicator of overall performance despite its limitations on imbalanced datasets. F-scores are calculated from precision and sensitivity, using $\beta$ as the weight of sensitivity relative to precision, so we use the F2-score with $\beta = 2$. The ROC curve [156] illustrates the performance of binary classifiers by plotting the sensitivity against the specificity at various threshold settings. The AUC reduces ROC analysis to a single scalar value representing expected performance (for details, please refer to [156]). It was the selected metric to train the classifiers. We prefer classifiers with high expected values for all metrics, with particular relevance to sensitivity. A low variance is also very important in terms of consistency. Models for which the performance metrics vary significantly in the training set are expected to be unstable when applied to unseen data.

#### 4.4.4.2 Training Classifiers

We train all ten classifiers with the 20 features proposed by CFS, applying 5-fold cross-validation and repeating the procedure ten times. The box-plots for the area under the ROC curve, sensitivity and specificity are presented in Fig. 4.13a.

When comparing classifiers according to the aforementioned criteria, RF and C5 are the models which show a higher performance: high sensitivity, low variance, and a good balance between sensitivity and specificity. These results indicate that an ensemble model based on decision trees, such as RF or C5, using the selected 20 features with no normalization step is the best solution for our anomaly detection scenario. RF seems to have a slight advantage in terms of sensitivity.

We tried both normalization options and the differences were negligible, so we show solely results without normalization. Although we do not show the results from the training with all 196 features, we observed that with only 10% of the features we can reach practically the same performance for most models, and even improve in some of them. This confirms the suitability of the used feature selection model.

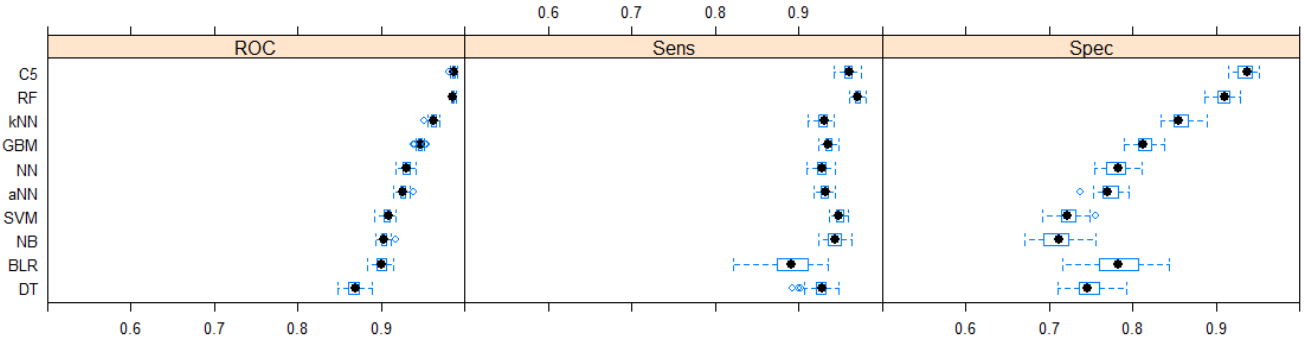


(a) Using 20 features with no normalization step after applying CFS

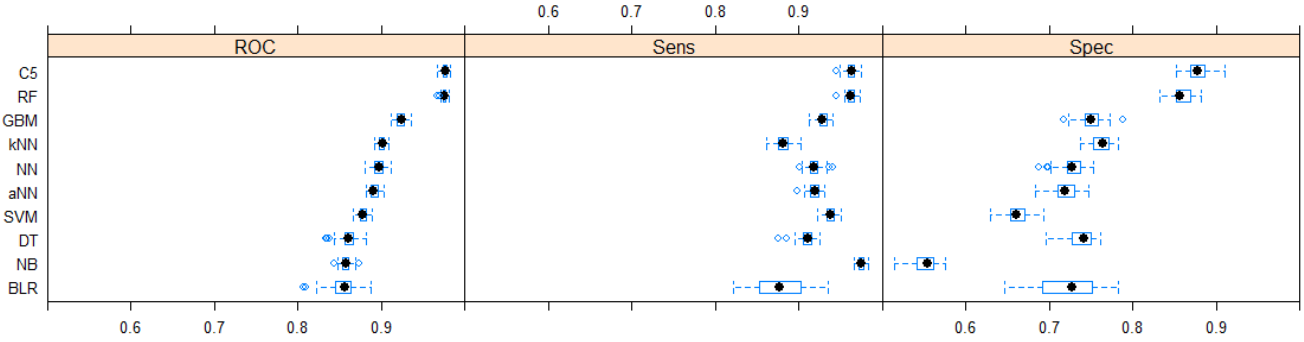


(b) Using 13 features with no normalization step after applying CFS

Figure 4.13: Boxplot for comparison of 10 classifiers using ROC, sensitivity, and specificity.

Most classifiers show a small decrease in the training performance using the 13 heading-based features compared to the 20 features, as shown in Fig. 4.13b. RF and C5 remain the classifiers with the best overall training performance, with AUC average only 1% worse, although using only 65% of the number of features.

#### 4.4.4.3 Testing Classifiers

Table 4.3 shows the performance results of trained models on the test set. Although values for specific metrics, such as AUC and sensitivity, are lower from the ones obtained with the training data, as expected, testing results support our previous observation that ensemble methods based on decision trees are a good option for our problem. We choose RF for its stability and good performance across all metrics.

The most interesting results to highlight from Table 4.3 are the sensitivity of 77% and 75%, accuracy of 91% and 88%, and F2-score of 77% and 75%, for the RF model using 20 and 13 features, respectively. We observe that although the RF classifier with 20 features offers better results, as expected, the alternative with 13 features does not decrease them significantly, providing a satisfying performance with 35% less features. These results consider each window independently.

| | | DT | NN | SVM | kNN | NB | RF | GBM | C5.0 | BLR | aNN |
|---|---|---|---|---|---|---|---|---|---|---|---|
| 20 features | Sensitivity | 69.8% | 74.3% | 75.1% | 70.1% | 71.7% | **76.5%** | 78.8% | 78.6% | 69.8% | 76.6% |
| | Specificity | 94.8% | 91.6% | 93.3% | 93.5% | 95.6% | 95.0% | 94.5% | 92.7% | 93.5% | 94.6% |
| | Precision | 79.3% | 71.8% | 76.2% | 75.6% | 82.4% | 81.4% | 80.4% | 75.6% | 77.2% | 80.4% |
| | Accuracy | 89.2% | 87.8% | 89.2% | 88.3% | 90.3% | **90.9%** | 91.0% | 89.6% | 89.9% | 90.6% |
| | AUC | 87.5% | 90.6% | 91.2% | 86.9% | 91.2% | 93.1% | 93.1% | 92.2% | 91.2% | 91.0% |
| | F2-score | 71.5% | 73.8% | 75.4% | 71.2% | 73.6% | **77.4%** | 79.1% | 78.0% | 77.3% | 77.3% |
| 13 features | Sensitivity | 75.1% | 73.9% | 70.7% | 62.8% | 59.5% | **75.1%** | 72.4% | 74.4% | 77.3% | 75.1% |
| | Specificity | 88.1% | 90.7% | 92.9% | 86.2% | 96.2% | 91.7% | 93.4% | 91.2% | 84.6% | 89.4% |
| | Precision | 64.3% | 69.5% | 74.1% | 56.6% | 81.7% | 72.2% | 75.8% | 70.9% | 59.0% | 67.1% |
| | Accuracy | 85.2% | 87.0% | 88.0% | 81.0% | 88.0% | **88.0%** | 88.7% | 87.5% | 83.0% | 86.2% |
| | AUC | 84.5% | 88.1% | 88.9% | 79.8% | 86.6% | 89.1% | 89.3% | 88.2% | 85.9% | 89.3% |
| | F2-score | 72.6% | 73.0% | 71.3% | 61.5% | 62.9% | **74.5%** | 73.1% | 73.7% | 72.8% | 73.4% |

Table 4.3: Test results for window-based anomaly detection.

#### 4.4.4.4 Random Forest Parameters

We now consider the parameters for the RF model: the total number of trees `ntree` and the number of variables randomly sampled as candidates at each split `mtry`. Until this point, all the trained RF classifiers used the default 100 trees and the parameter `mtry` was tuned during training in R with the *caret* package. The value `mtry`= 2 was chosen in most settings, but it varied from 2 to 11.

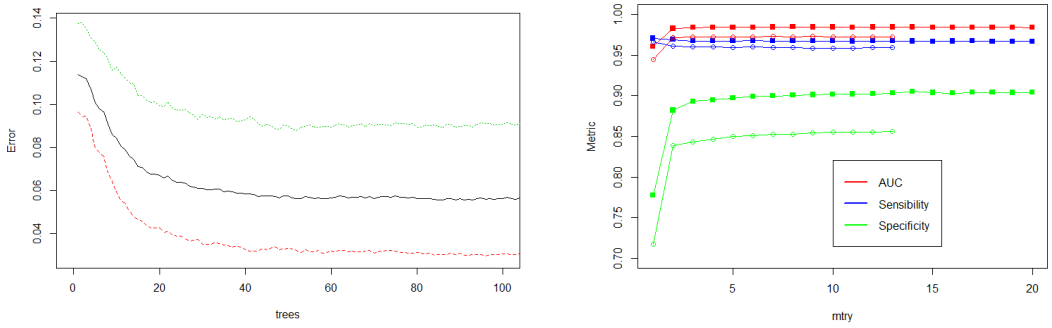


(a) Estimated OOB error as a function of `ntree`.

(b) Training metrics as a function of `mtry`.

Figure 4.14: Training random forest parameters.

Choosing the number of trees is a trade-off between performance and speed. A higher number of trees improves performance yet increases computation time, not only training the model, which in our case is not a problem, but also in classifying new instances, which is critical for an online solution. We present in Fig. 4.14a the out-of-bag (OOB) error estimation as a function of the number of trees `ntree` used in the RF model for 20 features. It also presents the error per class, which is higher in case of anomalies. We observe that the errors stabilize as `ntree` increases, the improvement becoming negligible. We choose `ntree`= 50 that has an estimated OOB error of 5.73%, with 3.30% for the normal class and 8.97% for anomalies. The curve for the model with 13 features has a similar shape but the estimated error values are slightly higher: 8.28% for the

OOB error, with 3.79% for the normal class and 14.28% for anomalies.

After fixing the number of trees, we aim to find a good balance for the parameter `mtry`. Increasing it improves the individual tree performance but lowers their overall diversity, key to the RF method. The default value used for classification is *sqrt*(`nfeat`), being `nfeat` the number of features, which would result in an `mtry` value of approximately four features for both 20 and 13 features. We vary `mtry` to find the best value for each configuration, as shown in Fig. 4.14b. The circles correspond to the configuration using 13 features, while the solid squares correspond to the configuration using 20 features. The best `mtry` values using AUC as metric were 8 and 9, for 20 and 13 features respectively, but the variation is so small that these depend highly on the used seed. Considering all three available metrics and the importance of sensitivity, we choose `mtry`= 6 for both configurations as a good balance.

### 4.4.5 Analysis per Block Anomaly

Since our goal is to detect entire blocks of anomaly, it is relevant to also analyze the detection patterns per block anomaly and per trip. Figures 4.15a and 4.15b show these in detail for the configurations with 20 and 13 features, respectively. We have a total of 61 block anomalies in our four test trips: 12 from trip 2 (A1 to A12), 31 from trip 7 (A13 to A43), 15 from trip 10 (A44 to A58), and 3 from trip 13 (A59 to A61). Some values are lower from the ones indicated in Table 4.1 because those considered all available magnetic data, and when transforming the data to distance based windows, we lost some that did not contain sufficient speed information. In our practical experiments, speed information was obtained from GPS. While the data was interpolated and short failures were overcome, this resulted in the loss of some anomalies in GPS denied environments. It is interesting to mention that although test trips 2 and 7 include trajectories equal to those used in training trips, and test trips 10 and 13 present new trajectories, we do not notice any influence on the quality of the results due to this factor.

Only one block anomaly (A42, the sole composed by a single window) was not detected. The mean of detected windows per block anomaly is 69% for 20 features and 65% for 13 features, with standard deviations of 23% and 24%, respectively. In the first case, 41% of the 61 block anomalies detected correctly at least 80% of the anomalous windows, 28% detected between 60% and 80%, and only 13% detected less than 40%. When applying the configuration with 13 features, 34% of the 61 block anomalies detected correctly at least 80% of the anomalous windows, 33% detected between 60% and 80%, and 20% detected less than 40%.

Considering Fig. 4.15a, with 20 features, we see that 90% of the detected block anomalies are classified as anomalies within the first three 10m windows: 57% in the first, 25% in the second, and 8% in the third. The remaining 10% are detected after four to eight windows. In the configuration with 13 features, in Fig. 4.15b, 90% of the detected block anomalies are classified as anomalies within the first three 10m windows as well: 52% in the first, 30% in the second, and 8% in the third. The remaining 10% are detected using between four and thirteen 10m windows. The maximum number of consecutive undetected windows is seven for the configuration with 20 features and

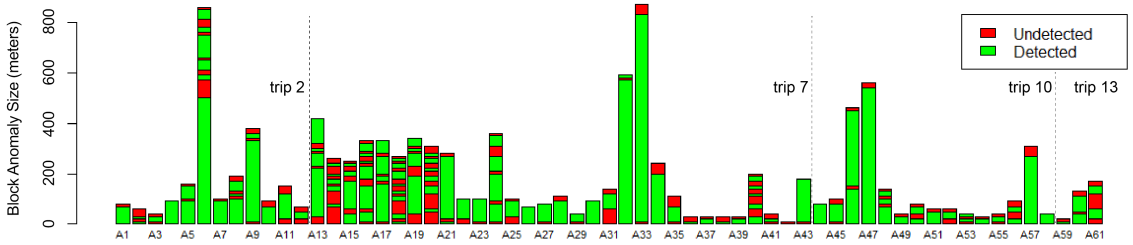


(a) Test results per block anomaly for 20 features.

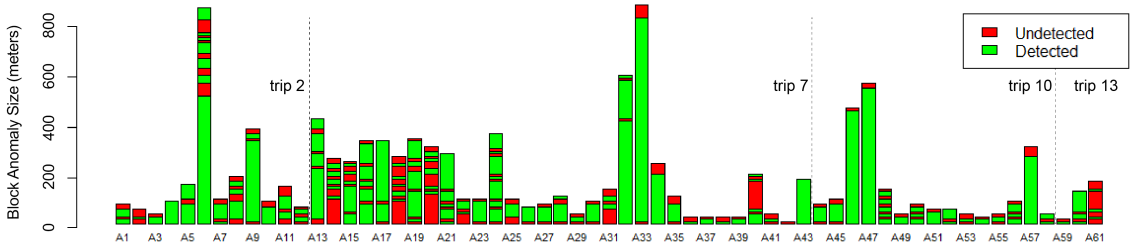


(b) Test results per block anomaly for 13 features.

Figure 4.15: Anomaly detection per block.

twelve for the configuration with 13 features. In both configurations 80% of the block anomalies have a maximum number of consecutive undetected windows of three or less.

Taking history into account would allow us to leverage the sequential property of the data and improve on these results. Even if classified as normal instances, windows before and after intervals of detected anomalies have a higher probability of being false negatives and could be processed taking this into account. Depending on the anomaly detection application, it might be beneficial to assume these as anomalies, e.g. fusion of different types of information to estimate orientation (false negatives have a strong negative impact), or include a second phase with a looser classification, e.g. using anomalies for localization purposes and including a next step that compares anomalies for identification. In the latter case, small intervals with undetected anomalous windows within a block with a high percentage of successful detection have a lower impact on the overall performance of the system than initial windows.

## 4.5 Magnetic Anomaly Matching

Our aim in this step is to identify magnetic anomalies by matching an input stream to a signature from a set of pre-recorded and stored references. We model this as a classification problem: each signature from the reference database is a class, each class is represented by a multivariate time series. The challenge is matching time series with similar patterns irrespective of their length and pace.

The main issue is to find a suitable distance measure to compare the anomalies (multivariate time series). The supervised classification algorithm k nearest neighbors with k=1, known as one nearest neighbor (1NN) is widely applied in time-series classification with Dynamic Time Warping (DTW) as a distance measure [157] (not a metric). It is commonly accepted in the

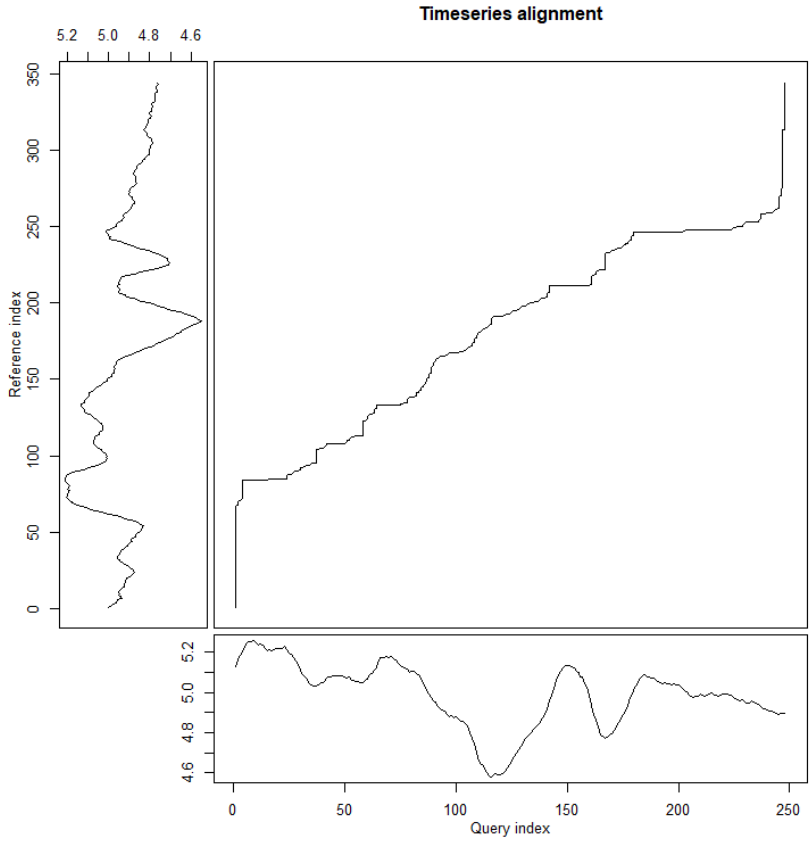


Figure 4.16: Illustrative example of a DTW alignment.

literature that this traditional 1NN-DTW classifier is hard to beat [131, 158] and it is frequently used as a benchmark [159, 160]. While experimental studies on time series classification show that no classifier outperforms all others in every domain, empirical evidence suggests 1NN-DTW gives in general very satisfactory results, often close to recently proposed more complex ensemble methods [160].

The choice of the distance to compare the time series is crucial. DTW is the oldest elastic measure and one of the earliest similarity measures proposed for time series [159]. DTW is especially adequate for matching time series containing patterns that, while having different lengths and paces, are qualitatively similar. DTW algorithm computes the stretch of the time axis which optimally maps one given timeseries (query) onto whole or part of another (reference), yielding the point-by-point correspondence (warping function) and cumulative distance after the alignment. An illustrative example of a DTW alignment for two time series is provided in Fig. 4.16. Although DTW is often assumed to be computationally expensive, there are several techniques that can be used to make it feasible for scenarios with demanding time and complexity constraints [131]. Some examples are lower bounds, early abandoning of different calculations, and using the squared distance since omitting the square root does not alter the relative rankings of nearest neighbors. For details about DTW please refer to [131, 161].

**DTW parameters:** DTW algorithm allows to define the following parameters:
1) **step pattern**: used to locally constrain the slope of the alignment function, listing the transitions allowed for local warping steps and their cost;
2) **pointwise distance function**: local distance function between matched points of query and reference. For comparison the DTW cumulative distance needs to be normalized for path length;
3) **warping window**: windowing enforces a global constraint on the envelope of the warping path, for which we can choose the window type and size;
4) **endpoints**: standard DTW algorithm matches the initial and final points from both time series. It is possible to remove one or both of these constraints for partial matches. Open-ended alignment computes the alignment which best matches the query with a leading part of the reference. Open-begin makes sense when open-end is also enabled for subsequence finding;
5) **multidimensional DTW**: having multidimensional time series, as is our case, is also important to define if DTW will be performed separately as unidimensional time series for each dimension (independent DTW) or if a single warping will be performed considering all dimensions (dependent DTW).

| | CTS classifier | PTS classifier |
|---|---|---|
| Features Normalization | Linear: Z-score;<br>Directional: scaling range | None |
| Window | Slanted band | None |
| Step pattern | Asymmetric | Asymmetric |
| Endpoints | OBE | OE |
| Pairwise distance | Linear features: Euclidean;<br>Heading: minimum angle | Linear features: Euclidean;<br>Heading: minimum angle |
| Multidimensional DTW | Dependent | Independent for linear and directional features |

Table 4.4: Alternative configurations for DTW classifiers

We present two alternative DTW configurations. The first one, designated as CTS (complete time series) classifier, is suitable for complete signatures and its purpose is to evaluate the potential accuracy of the method. The second one, named PTS (partial time series) classifier, avoids using techniques that require the complete time series to be available for matching so that we can understand the impact of online matching on the performance. The parameters selected for each configuration are summarized in Table 4.4. We explain these design choices in detail in Section 4.5.2, after we describe the datasets because the observation of the data was critical for dimensioning the algorithm.

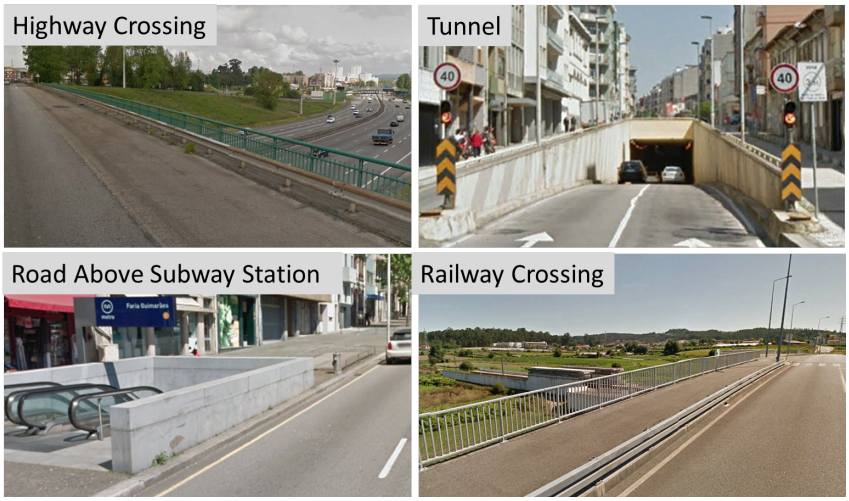


Figure 4.17: Roads where magnetic anomalies were collected: highway crossing 2.5, tunnel 2.2, road above underground station 2.1, and railway crossing 1.2. from Fig. 4.18

### 4.5.1 Dataset Description

We collect three datasets, summarized in Fig. 4.18. They have some heterogeneity, including different vehicles, smartphones, and traffic conditions. The campaigns all took place in the district of Porto, Portugal. Instances obtained for reference were collected with a constant speed of 45km/h (see section 4.5.3). For practical reasons, it was not possible to collect the same number of references for all locations, and the values in our experiments range from 3 to 25. Instances collected for training and testing include diverse speed patterns from 0 to 90km/h, combining accelerations, decelerations, short stops and constant speed sections.

**Dataset A** contains references for area 1 and queries for training the classifier. It includes four locations of anomaly (see Fig. 4.19a), each with two lanes in opposite directions, resulting in eight distinct magnetic signatures. The roads crossing the same highway have similar orientation. This is relevant to understand if a similar structure with a similar size, location (and consequently geomagnetic field) and orientation has in fact a unique pattern that might be used as a signature.

**Dataset B** contains references for area 2 and queries for testing the classifier, with a total of 13 signatures in 5 regions of anomaly (see Fig. 4.19b). These anomalies were chosen for representing particularly challenging situations. One is a bifurcation on top of an underground metro station. The beginning of the anomaly is the same and then we can either turn left or right in the crossroads. Three of these regions of anomaly have two lanes in the same road and direction, in a total of eight signatures: road above an underground metro station and a tunnel (one direction, two lanes), and road crossing a highway (two lanes in each direction), all illustrated in Fig. 4.17. We also consider the signature from the road above that tunnel, perpendicular to it.

**Dataset C** contains between 2 and 6 instances per signature for testing in all 9 regions, including a total of 66 instances. They were collected in different dates and using different vehicles and smartphones (Sony Xperia Z3 and Google Pixel) relatively to the ones used to collect the respective references.

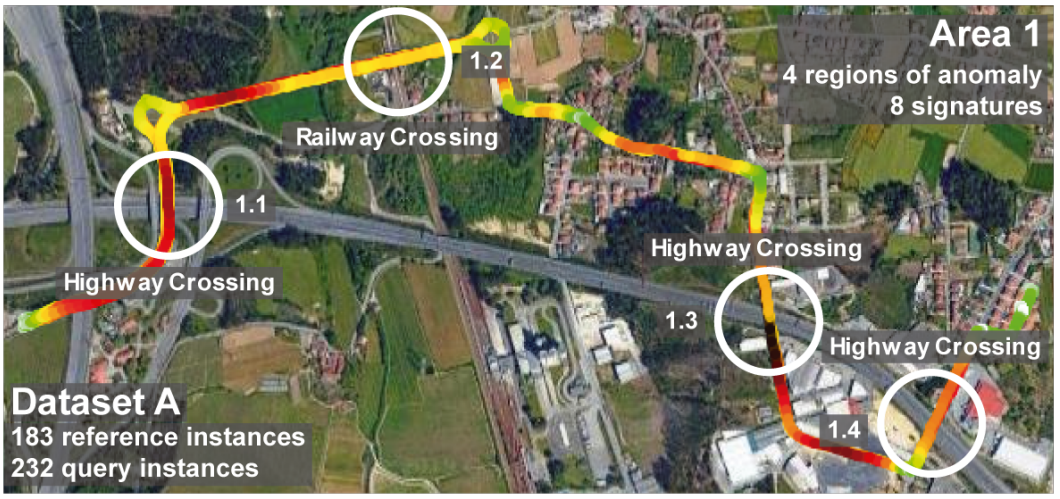


Collected 15 time series in 5 trips: 3 smartphones, 4 different vehicles, 2 days

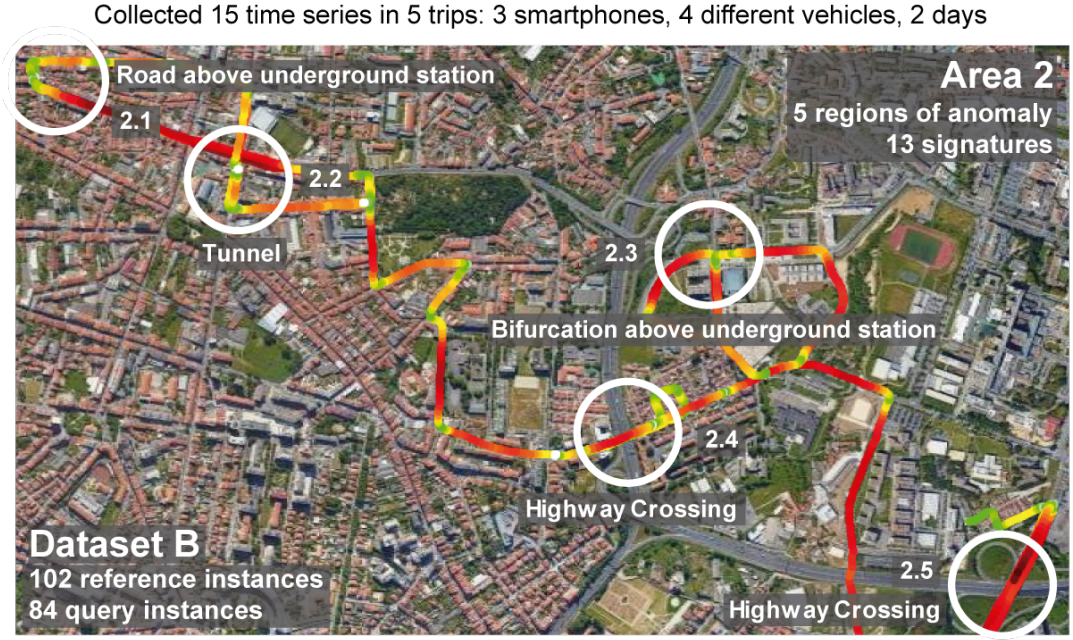


Collected 6 time series in 2 trips: 3 smartphones, 2 different vehicles, 2 days

**Dataset C (Area 1 & Area 2)** **66 query instances** **9 regions of anomaly**
Collected 3 time series in 2 trips: 2 smartphones, 2 vehicles, 2 days **21 signatures**

Figure 4.18: Datasets A, B and C maps and descriptions.

### 4.5.2 Classification Model

In this section we explain how we select the parameters for our matching classifier. Some of them are the same for both configurations, namely step pattern and pairwise distance. The others are described in subsections dedicated to each of them.

**Step pattern:** A real time open-end version of the dynamic time warping algorithm (OE-DTW) is proposed by Tormene et al. [162], in the context of a system for upper limb post-stroke rehabilitation. The problem contains two main design choices: 1) ensuring the analysis takes place in real-time, not just after the movement is finished, and 2) choosing an algorithm to quan-

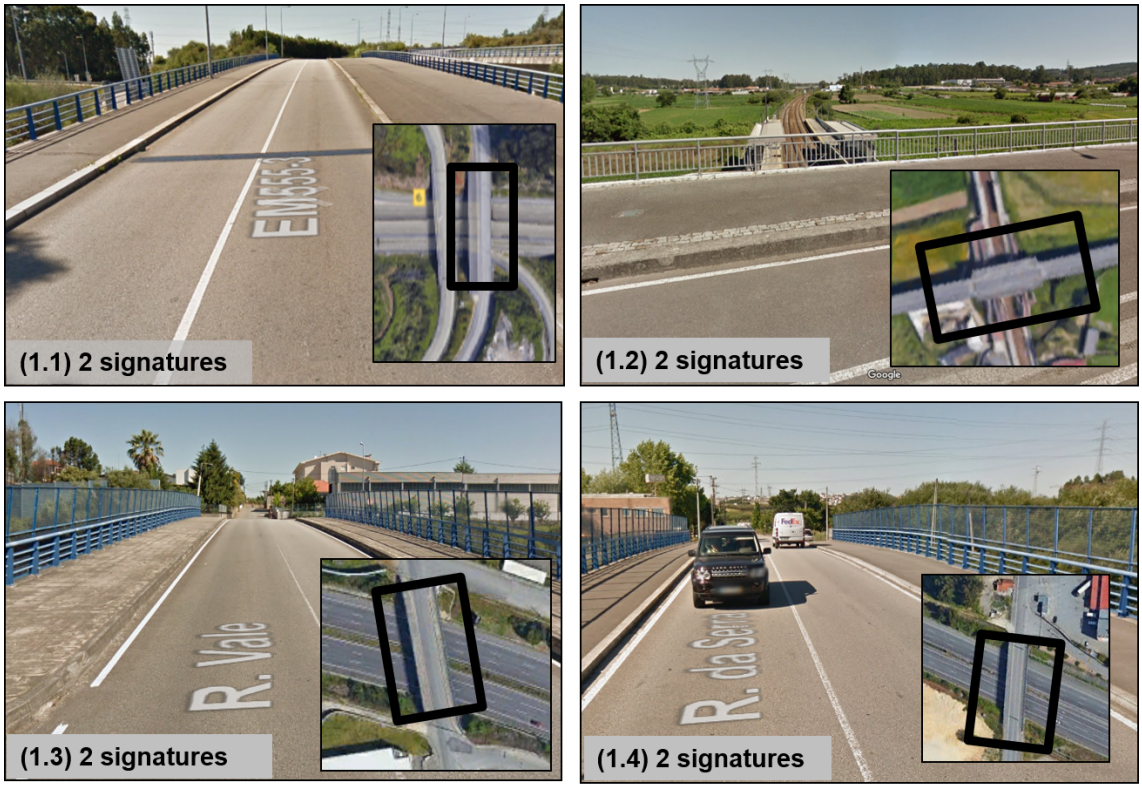


(a) Four regions of anomaly from area 1.


(b) Four of the five regions of anomaly from area 2.

Figure 4.19: Regions of anomaly obtained from Google Maps street view and Google Earth.

tify similarity between time series, irrespective of the pace of execution. We face very similar requirements. Asymmetric step pattern has useful properties for such scenarios (for details refer to Section 6.2 in [162]). At each step, the index in the query is increased by one unit with a weight of one, therefore, the warping curve length is equal to the query length. Dividing the total cumulative DTW distance by that length allows to easily normalize it for comparison among time series of different sizes. This is called DTW normalized distance and is used on the 1NN algorithm. The asymmetric step pattern determines the warping slope to vary from a minimum of zero to a maximum of two. This allows unlimited time dilatation and a query twice as fast as the reference for the maximum time compression. This results in some restrictions while collecting the references (see Section 4.5.3).

**Pairwise distance:** Euclidean distance is used as local distance function for all linear features, which are all our features except the heading that is an angle, and therefore, directional. The local distance for the heading is computed as the minimum angle difference between the two given heading angles.

#### 4.5.2.1 CTS classifier: complete time series classification

This configuration is focused on showing the feasibility of considering magnetic anomalies as signatures for a particular path, so using the complete version of each query signatures for classification.

**Endpoints:** Although in controlled examples time series have well delimited frontiers for the events they describe, in practical scenarios the exact endpoints are hard to detect [161]. An open-begin and open-end version of DTW (OBE-DTW) allows partial matchings and avoids the problem of increased DTW distance for matches whose final points are fuzzy and therefore not well aligned. However, without any further restrictions this might cause singularities, which are undesired alignments where a large subsection of a time series is matched to a single point on the other. On the other hand, very tight constraints might increase the risk of missing the correct warping path. By combining the elimination of the endpoint conditions with a global constraint in the form of a warping window, we avoid creating such singularities while allowing some flexibility concerning alignment of the endpoints, as long as the size of the warping window is well-chosen. In our particular scenario, the only legitimate case of a large portion of the query matching to a single point in the corresponding reference would be when the vehicle is static. To define a useful warping window, we assume, without loss of generality, that a vehicle can stop and immediately resume driving but it cannot stay stopped for an arbitrarily long period of time. We can easily handle this situation in practice by identifying such cases using speed information and discarding static samples or increasing the window accordingly.

**Warping window:** We use a slated band window, which imposes the warping path to lie within the band centered around the line segment that joins elements (1; 1) and ($N$; $M$), being $N$ the length of the query and $M$ the length of the reference, therefore having a slope of M/N. and not 1 like Sakoe-Chiba band [163]. It is more suitable than the latter for time series of different lengths, although it has to be applied to the complete version of both series. To determine what

is the best size, i.e. the lowest size that does not discard from the valid warping area the correct alignment, we made experiments. The most critical situations are very low speeds and traffic patterns with static moments. With our assumption that the query might have any speed plausible for a road vehicle, but cannot be static for undefined long period of time, we choose the size of the warping window as 15% of the larger time series.

**Feature normalization:** Normalization is a general requirement for most machine learning algorithms and is very relevant to obtain meaningful comparisons between time series [131]. It is especially important if they contain measurements that have different units, namely in k-nearest neighbors (kNN) algorithm using Euclidean distance, so that all features are made to contribute equally to the final solution. For linear features, the best option is using z-score normalization. However, it cannot be applied to directional features, namely the heading. These can be scaled for a range that ensures a balanced weight for different features. For this purpose, we consider the histogram of the dependent multidimensional DTW normalized distances for the linear features after z-score normalization and the unidimensional DTW normalized distance for the raw heading feature. We propose to scale the total range of the directional features to the measured range of the DTW normalized distances distribution for the linear features after z-score normalization. This way, it is possible to provide a good balance for all features when summing the squares of pairwise distances. We omit the square root calculation as it improves running time without changing nearest neighbors relative order. We observe that for the z-normalized linear features, the DTW normalized distances range from 0.1 to 2.6, as shown in Fig. 4.20a. For the heading, the distribution of the DTW normalized distances range from 0 to 2.7, as shown in Fig. 4.20b. Due to the high similarity of both ranges we concluded that a scaling of the DTW normalized distance resultant from the directional feature is not necessary in this particular case.

**Feature selection:** In Fig. 4.21a we show the classification error for each individual feature using CTS classifier, PTS classifier with complete time series and PTS classifier using only the first half. We observe that the heading is the feature that provides the lowest classification error. We apply forward selection using CTS classifier in order to choose the most promising combination of features. The results are presented in Fig. 4.21b. The classification is performed with no errors using from 2 to 6 features. However, using the complete normalized signature is the best possible scenario and we expect that in more challenging scenarios having more than 2 features will benefit the classification performance. Since the features selected in steps 2, 3 and 4 are the 3 axis of the magnetometer in the vehicle frame, we opt for a classifier with four features. The selected features are the heading *hm* and the 3 magnetometer axis in the vehicle frame *mhx*, *mhy* and *mv*.

#### 4.5.2.2 PTS classifier: partial time series classification

The second configuration for DTW is aimed at partial time series. It should be applied to successively larger subsequences of the query that contain its initial point, without requiring the complete anomaly for start the classification procedure to start. In this configuration we choose asymmetric step pattern and open-end, while enforcing the initial point constraint (matching first point of query and reference), and removing the warping window and the normalization steps. The total

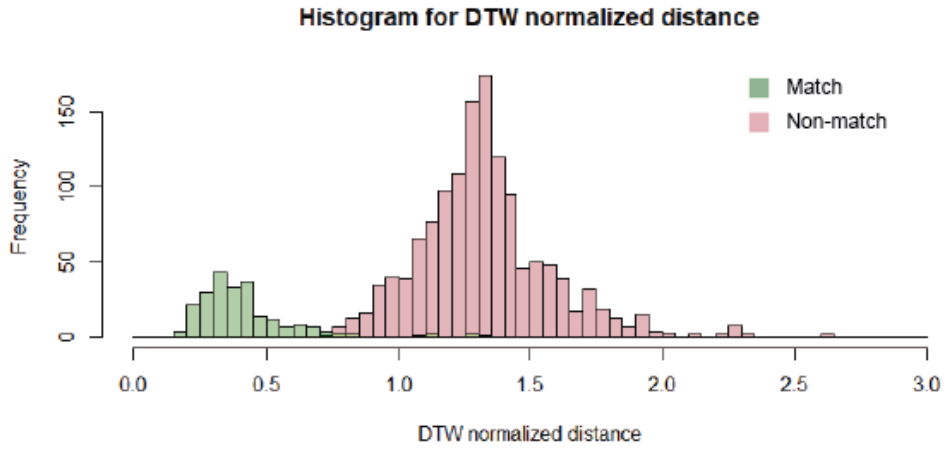


(a) DTW normalized distance histogram for linear features magnetometer axes in the vehicle frame.

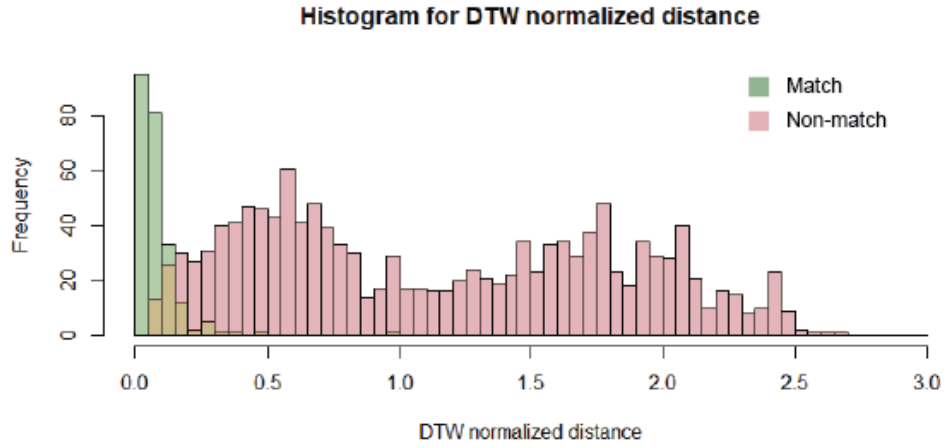


(b) DTW normalized distance histogram for directional feature heading.

Figure 4.20: DTW normalized distance histogram for CTS classifier, using dataset *A*.

length of the query anomaly, not available in PTS, would be necessary for slope calculation to apply the slanted-band window. Removing global constraints and opting for both endpoints open could result in undesirable singularities. Also, normalization needs to be applied to the same intervals of query and reference. Since our time series are non-periodic the most suitable interval is the complete subsequence that constitutes each anomaly. However, without normalization, we cannot join linear and directional features in a balanced way for dependent DTW. Non-directional features are all based on magnetic data and share the same units, so there is a lesser impact for not performing the normalization step. For directional features, the possible ranges of values are known, e.g. heading range is from 0 to $2\pi$, so they can all be scaled to share the same range. What we propose is to apply independent DTW to both types of features, obtaining separate classification results with 1NN-DTW for each. If both classifiers agree, the resultant class is assigned to the partial anomaly. Otherwise no class is selected at that moment, and the query awaits more data for

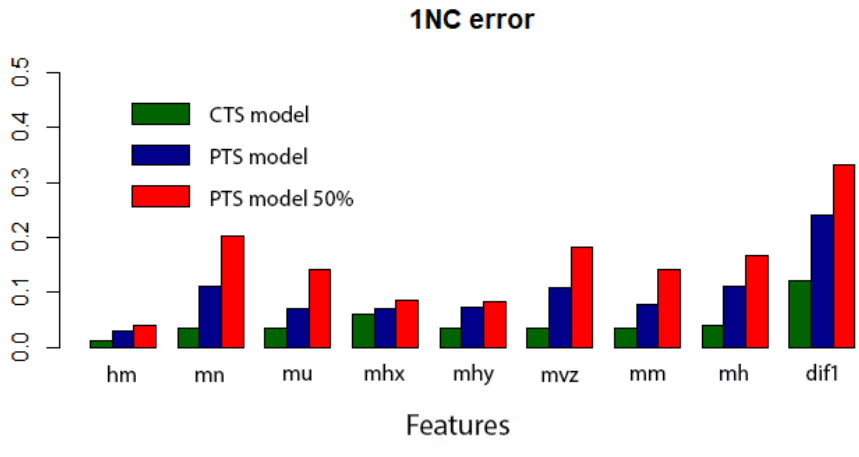


(a) 1NC-DTW classification error using each feature independently.

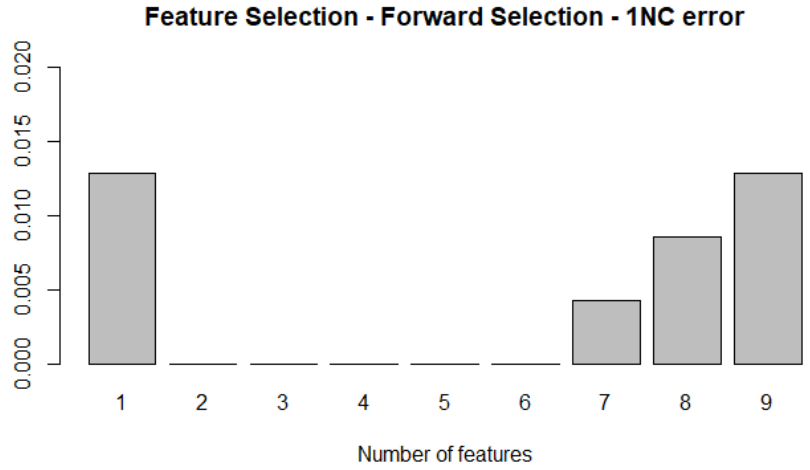


(b) Feature selection: forward selection using 1NC-DTW (CTS) classification error.

Figure 4.21: Classification errors for feature selection.

adequate classification.

### 4.5.3 Reference Signatures

Considering a data rate of 50Hz, we collect data for reference with a constant speed of 12.5 m/s (45 km/h). This is the spatial equivalent of collecting four samples per meter. Due to our choice of asymmetric step pattern, this limits the valid matchings to queries up to 25 m/s (90 km/h) at 50Hz. It is a valid assumption for urban areas. Nevertheless, queries with higher speeds or lower spatial sampling frequency can be easily supported by collecting additional references to cover those cases.

It is important to have a diverse and large reference dataset, i.e. data collected in distinct conditions and using different equipment, such as smartphones and vehicles, to make the system more robust. However, running 1NN-DTW in a large set implies substantial space and time requirements, which creates difficulties in making the classifier suitable for resource constrained devices and online use. A solution to this problem is to average the elements of each class and

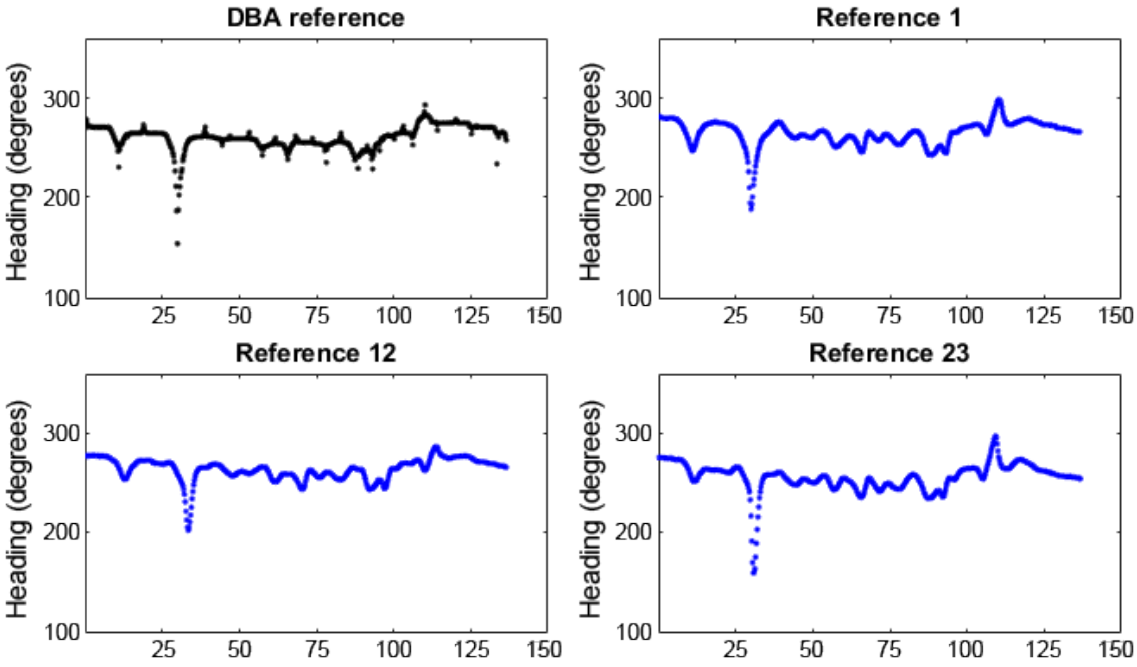


Figure 4.22: Example of heading feature averaging for highway crossing 1.1 signature in South direction, in meters. It includes three of the 24 instances collected for reference, and the resultant reference using DBA technique.

use the nearest centroid (1NC) instead of 1NN for classification [164, 165]. However, it is not trivial how to average time series data, since using the Euclidean distance typically results in a centroid that does not resemble any of the instances. Petitjean et al. [164, 165] show that a method named DTW Barycenter Averaging (DBA) [166] allows to perform a meaningful averaging of times series under DTW, and therefore use NC classifiers that are in general at least as accurate as NN, while being faster with reduced computational requirements. In some situations, it might even increase the accuracy by creating prototypes that better represent a class ideal than any of its individual instances [164]. An example of the application of DBA method is shown in Fig. 4.22 for the heading feature of a highway crossing signature from dataset A. It shows three of the 24 instances collected for reference with three different vehicles and smartphones.

### 4.5.4 Performance Analysis

For the evaluation we use the **dtw** package available for *R* statistical software [163]. The applied performance metric is 1NC-DTW classification accuracy. We consider two levels of matching: road matching that consists in correct road and direction, and lane matching that requires correct lane detection even when there are multiples lanes in the same direction.

#### 4.5.4.1 CTS Classifier

In Table 4.5 we preset the performance for CTS classifier. We start by analyzing the road matching results. This is our best scenario since we have access to the complete anomaly and ignore lane

| Dataset | Nq | Nr | Correct road and direction | | Correct road, direction and lane | |
|---|---|---|---|---|---|---|
| **A** | 232 | 8 | 232 | 100% | 232 | 100% |
| **B** | 84 | 21 | 84 | 100% | 78 | 93% |
| **C** | 66 | 21 | 61 | 92% | 54 | 82% |

Table 4.5: Classification results for CTS classifier (road and lane matching).

precision. For dataset *B*, in which the queries were collected in the same trips as the instances used to build 13 of the 21 references, we obtain perfect classification for the 84 queries. It is important to recall that it includes more challenging scenarios than the ones in dataset *A*, used to train the model. For dataset *C*, collected with a completely different equipment and on a different date relative to the whole reference dataset, we obtain a road matching accuracy of 92% for the 66 queries.

Considering lanes, we achieve correct lane matching for 93% of the queries in dataset *B* and 82% in dataset *C*. We also analyze only the 8 signatures containing another lane in the same direction. In dataset *B* they are 33 of the 84 queries. The 6 wrongly classified lanes represent 18% of these 33, resulting in a lane accuracy of 82%. In dataset *C* they are 26 of the 66 queries. From these 26, 4 had wrong location classification (15%), 7 had wrong lane classification (27%) and 15 were correctly classified (58%). These results are promising and indicate that it is feasible to use magnetic anomalies as signatures for a known path, achieving up to lane precision.

#### 4.5.4.2 PTS Classifier

| Datasets | Nq | Nr | Correct road | | Incorrect road | | Non-classified road | |
|---|---|---|---|---|---|---|---|---|
| **A** | 232 | 8 | 223 | 96% | 2 | 1% | 7 | 3% |
| **B** | 84 | 21 | 70 | 83% | 3 | 4% | 11 | 13% |
| **C** | 66 | 21 | 50 | 76% | 0 | 0% | 16 | 24% |

Table 4.6: Classification results for PTS 50% classifier (road matching).

Having successfully achieved a good accuracy for the anomalies identification using the complete signatures, we evaluate the classification accuracy for incomplete versions of them. In order to guarantee partial signatures for this purpose, we decide to use only their first half, as an illustrative example. It is important to note that, after getting the partial version of the anomalies, we do not take into account any knowledge of the percentage of the signature being classified. The classification results are shown in Tables 4.6 and 4.7. We observe that for road matching, in Table 4.6, the classification accuracy decreases 16,7% for both datasets *B* and *C* compared to the CTS version.

Considering lane matching, in Table 4.7, the classification accuracy decreases 21,4% and 19,7% for datasets *B* and *C*, respectively. It is important to highlight that very few instances

| Datasets | Nq | Nr | Correct road, direction and lane | | Incorrect road, direction and lane | | Non-classified road, direction and lane | |
|---|---|---|---|---|---|---|---|---|
| **A** | 232 | 8 | 223 | 96% | 2 | 1% | 7 | 3% |
| **B** | 84 | 21 | 60 | 71% | 9 | 11% | 15 | 18% |
| **C** | 66 | 21 | 41 | 62% | 0 | 0% | 25 | 38% |

Table 4.7: Classification results for PTS 50% classifier (lane matching).

are incorrectly classified. Most of the remaining queries are not attributed to any class since the results from independent classification using linear and directional features, respectively, do not agree.

#### 4.5.4.3 Threshold-Based Alternative

It is interesting to observe the distribution of DTW normalized distances for matches and non-matches, shown in Fig. 4.23a, for the training dataset *A*. Not only it is clear that the range of the two distributions is very different, but it is also possible to easily find the threshold that better separates the elements from both: 1.1. Only 8 matches are above the threshold (3,4% of FN) and there are no non-matches below, i.e. no FPs.

This threshold enables classification with DTW normalized distance only, without the need to apply 1NC. That may be very useful, e.g. if we have a singular candidate chosen considering a different source of information or when we require the option "none of the above", in cases of false detection or non-permanent sources of anomaly.

We consider the number of FPs and FNs using this threshold for the test datasets from the DTW normalized distances obtained with CTS classifier. For dataset *B*, shown in Fig. 4.23b, we obtain 9 FNs (10,7%) and 6 FPs (0.4%), which represent in total an error of 0.85%. For dataset *C*, shown in Fig. 4.23c, we obtain 19 FNs (28,8%) and 3 FPs (0.2%), which represent an error of 1.6%. The FP rates are very good, particularly considering that dataset *A* did not include signatures of distinct lanes in the same road and direction, which we expected to be more similar than signatures from distinct locations. The FN rates, on the other hand, are much higher than the ones obtained in dataset *A*, especially in dataset *C*. It is interesting to note, however, that this threshold is nonetheless a suitable choice since modifying it does not reduce the overall percentage of incorrect classifications.

## 4.6 Concluding Remarks

The goal of this work is to design MagLand based on our observation that the influence of local magnetic fields caused by permanent road infrastructure has a particular pattern that is stable in time and so can be used as a magnetic landmark for road vehicles.

**MagLand approach:** We leverage magnetic anomalies as signatures, providing useful location information from available sensors and infrastructure in a opportunistic fashion, to support

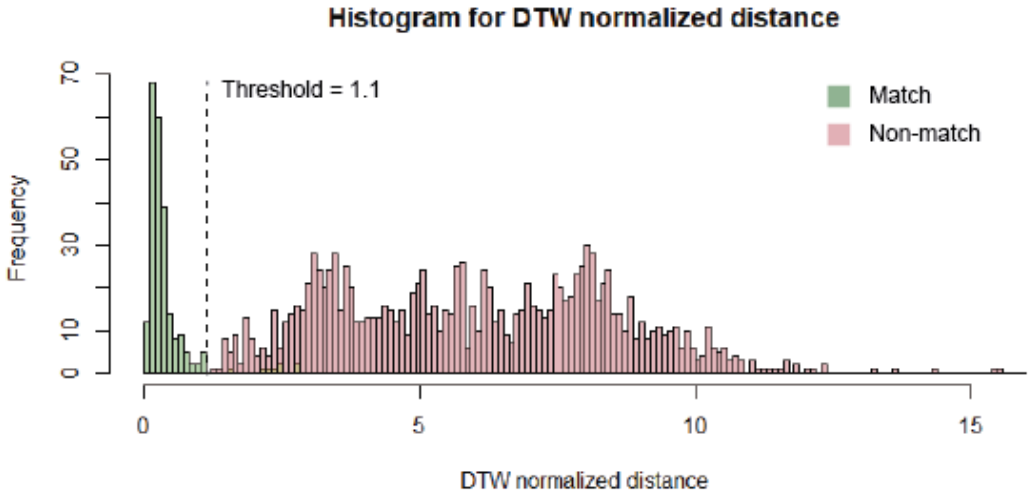


(a) Dataset *A*

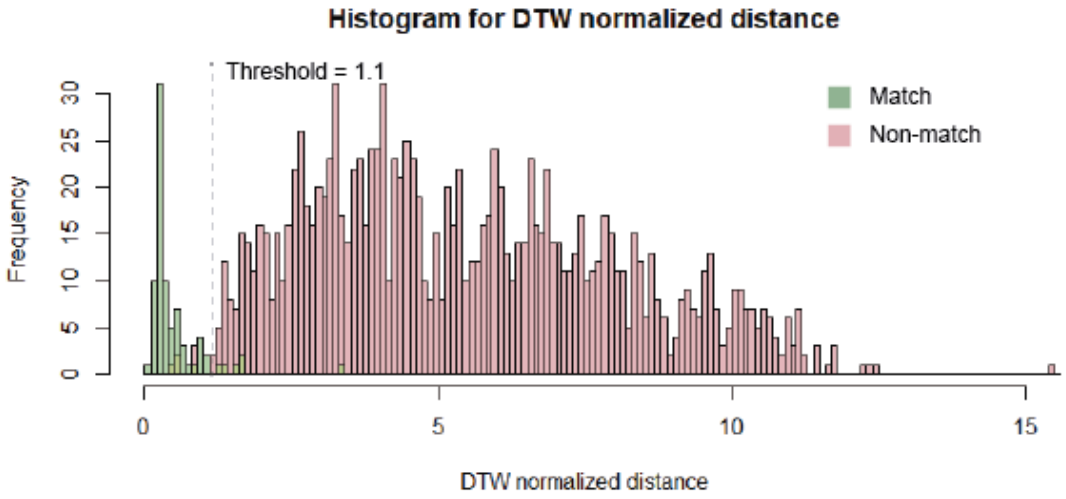


(b) Dataset *B*

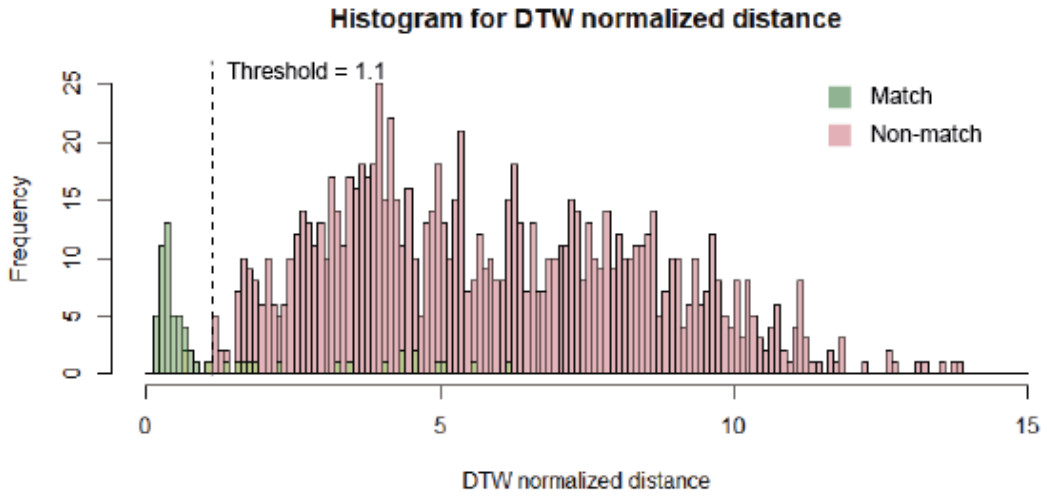


(c) Dataset *C*

Figure 4.23: DTW normalized distance histogram for CTS classifier.

existing localization systems for road vehicles. There are approaches that consider magnetic fingerprinting outdoors by mapping the whole area, e.g. Wei et al. [130], and others leveraging road landmarks that affect inertial data, e.g. Dejavu [128] and SmartLoc [129]. The first imply a high mapping effort and the second are mainly focused on finding specific driving patterns, such as a slow up and down pattern in a bridge, a fast up and down pattern in a bump, and a particular turning pattern at an intersection. MagLand is the first to consider detection with subsequent matching of magnetic anomalies, providing a good balance between current localization systems limitations and mapping effort.

**Anomaly detection:** We propose an anomaly detection algorithm that uses space-based windows of 10 m to analyze time series. It applies a random forest with 50 trees for anomaly binary classification of each window, in order to detect blocks of anomaly from the stream of magnetic data. The best results are obtained when applying the classifier to 20 features chosen with a suitable feature selection method. An alternative with 13 features based on heading information is also proposed, providing a close performance with the advantage of not requiring training the model for new locations.

**Reference database:** We provide guidelines to build a reference database that enables high classification accuracy with low complexity, by averaging time series for each signature with DBA method.

**Anomaly matching:** We propose one nearest centroid algorithm with dynamic time warping to classify magnetic anomalies relative to the reference database, which allows us to match time series irrespective of their pace. One version uses the complete signature and is concerned with showing the feasibility and full potential of this concept. The other one considers online use by matching a partial input to a complete reference.

**Evaluation with real data:** We demonstrate the feasibility of MagLand with real-world data collected in challenging scenarios. For the anomaly detection, we achieve a classification accuracy of 91% and sensitivity of 77% for 20 features. Our matching analysis shows that using magnetic anomalies as signatures is feasible. The classification accuracy for new trips with different equipment from the one used to build the database of anomalies is up to 92% for road matching and up to 82% including lanes.

These results are even more relevant for localization systems since several of the road infrastructures causing the anomalies coincide with locations where GPS has known limitations. It is the case of areas without visibility to the satellites like tunnels, urban canyons, or underground parking lots. Also roads with similar 2D positions but different heights are examples of scenarios where GPS can have a large error and make a wrong estimation of the path for some time before it is able to correct it. Our model can be valuable in such scenarios, by providing an alternative source of localization with lane precision. Magnetic landmarks can also be very useful for dead reckoning corrections, by enabling opportunistic global localization to reset cumulative errors.

# Chapter 5

# Discussion and Future Directions

We made our contributions to the broad topics of intelligent transportation systems and mobility focusing on two main aspects of road vehicles localization: cooperation and individual sources of location information. Having addressed each of these elements individually, we believe a robust solution should build on the synergy between both. In fact, the knowledge acquired from communication with neighbor nodes improves each vehicle's individual estimation. At the same time, the learning from cooperation is dependent on the quality of the information each node has to share. We are, therefore, confident that all our results, useful as individual contributions can also be conjugated harmoniously in a global approach with an even greater positive impact for the field.

In this chapter we discuss the main strengths and limitations of the proposed work, including future directions to explore.

**Cooperative localization:** From the perspective of cooperation, we propose a distributed model for nodes in a vehicular network to share their individual location information and improve it locally by relying on data collected and sent by their one-hop neighbors, which might be other vehicles with uncertain information. Our approach to this problem focuses on finding a low-cost solution in terms of equipment, infrastructure, and communication. This is the main motivation for using RSSI for ranging estimation. While it is cheaper than the alternatives, it is also more uncertain and less accurate.

We abstract individual location sent by the nodes to their neighbors in two parameters: location and confidence. This shared location is obtained solely from data collected by the vehicle itself, without including external information from other nodes. This avoids over convergence issues and limits the complexity and communication requirements of the approach, but it also prevents us from taking advantage of the full potential of cooperation. Nodes perform a single iteration in each new update step for the current location because they benefit only from information collected by their direct neighbors and not from information of all nodes propagated thought the whole network.

We believe that having presented results with real data, collected in an uncontrolled setting is of utmost importance. Nevertheless, collecting and analyzing real data always involves a high ef-

fort. Setting up the experiments with four different vehicles sharing information, gathering data in real urban traffic scenarios and processing that data presented numerous challenges. Few research works in this area present such a performance evaluation, especially those involving ranging with V2V communication devices. This not only allowed to better understand the impact of our cooperative approach, but it also enabled to propose good anchor conditions in this particular context. Due to our choice of GPS as the anchor vehicles global location source of information, anchor location quality in terms of accuracy and reliability in our experiment is frequently homogeneous, since the equipment used in all vehicles was similar and GPS presents many global errors, resulting in close positions sharing similar conditions. The experimental work comprises a single trip and is limited to three anchors, so it could be extended to study other conditions. It is important to stress that we propose one solution to this problem, with its assumptions, requirements, and goals. Different approaches have different strengths and limitations. Despite its limitations, we believe our contribution is an important step forward towards making cooperation among vehicles a reality in the future.

**Individual localization:** Concerning our contribution to individual localization, we focused on proposing an approach that would not be dependent on GPS, while being low-cost and not requiring a new infrastructure. We show that it is possible to create a database of magnetic anomalies and use them as signatures for that particular location, acting as magnetic landmarks. Using the magnetic field for localization purposes with existing infrastructure was proposed for indoor tracking inside buildings. In this context, the whole area is previously mapped and included in the fingerprinting based strategy for the online phase. In our work, with application for outdoors localization, we propose MagLand, a localization based on the magnetic field signature using only the areas where the influence of the local magnetic fields is significant and creates magnetic anomalies. We designate as magnetic anomalies the influences of local magnetic fields in the geomagnetic field perspective, which is used to obtain orientation in navigation systems. Areas near structures such as tunnels, roads above and below railways and highways, roads above underground car parks and subway stations, present these anomalies and have high density inside urban environments. Unlike the continuous magnetic fingerprinting for which the whole area needs to be previously mapped, saved and matched online, in our method the magnetic based matching to previously stored references is done solely in these opportunistic areas where the geomagnetic field presents anomalies, designated magnetic landmarks. Instead of a continuous stream matching of magnetic based data (continuous matching algorithm), we propose a stream anomaly detection and a posterior matching only in areas of anomaly (anomaly detection algorithm with a second step of matching only in case of positive detection). Therefore, the size of the required reference database is significantly reduced. This has an impact not only on storage space for the covered area, but also on the size of the search space for matching new inputs. From an online localization perspective of a mobile node, it means either the size of the local reference database stored on the node or the required amount of data for communications with the cloud is reduced.

It is important to note that MagLand, unlike magnetic fingerprinting, cannot be solely used as a continuous localization algorithm. It intends to be used jointly with other localization methods.

What is especially interesting and convenient, making it all even more useful and efficient, is that structures causing magnetic anomalies are highly coincident with locations where common widely used outdoors localization systems like dead reckoning and GPS have known limitations. Dead reckoning, which greatly suffers from the geomagnetic field anomalies created by those local magnetic fields in orientation (and consequently heading) estimation, can not only benefit from our proposed anomaly detection by ignoring magnetic data for orientation purposes, but also use the magnetic landmarks to correct the location and reset its cumulative errors. Satellite-based systems suffer from large errors and outages in areas where the receivers lack line of sight to the satellites or require good vertical accuracy, such as tunnels, highway crossings and urban canyons. Since these areas typically comprise a high density of metallic structures, resulting in magnetic anomalies, our model may provide an accurate and reliable alternative by enabling lane distinction.

There are obviously aspects that we have not addressed in detail in this work. They include particular challenges of online implementation, the combination of the detection and matching in a unique approach, the integration in a continuous localization algorithm for a joint solution with other sources, and a detailed complexity analysis of the whole system. It would be interesting to study how much the data rates of the sensors impact the performance of the approach as well as the relation between the traveled distance and the performance of the matching algorithm, i.e. how many meters are required for correct matches. Also, our experiments are limited to data gathered in the city of Porto. Despite these limitations, we have reached our goal of proposing a road vehicle localization approach which is both low-cost and independent from GPS. It can nevertheless be combined with it for improved performance. It takes advantage of ubiquitous smartphone sensors and existing road structures to provide vehicles with useful location information. We are confident that combining magnetic landmarks with (already collected) inertial data, and digital road maps would provide a continuous localization system that could serve as a low-cost alternative for road vehicles in the absence of satellite-based information.

**Information fusion:** It is worth to note that the information fusion method we used in the context of our cooperative approach allows for efficient combination of different information sources, not being dependent on the availability of any of them in particular. Another of its advantages is enabling an easy incorporation of new sources of data to the algorithm. Moreover, particle filters, unlike other less complex alternatives, do not impose any restrictions on the probability function or the dynamics of the system, which makes them more effective when dealing with complex functions and mobility patterns. This comes, however, at an increased computational cost.

We have conducted experiments with real-world data with different combinations of the following information sources: on-board sensors used for the motion model, road maps (from Open Street Maps) to restrict possible locations to the roads, GPS and RSSI ranging using V2V communications. We discuss not only accuracy but overall performance of these different combinations, namely coverage and reliability, which includes confidence values for both along the road direction and the direction orthogonal to the road. This allows us to carefully analyze the impact of each individual source on a vehicle local position estimation, and to better understand good matches such as V2V ranging and maps, since the first helps to reduce the error along the road direction, where

the closest anchors are usually distributed, while the latter limits the lateral error. Furthermore, it enables a real data analysis on the impact of the anchors location quality on the performance of the location estimation in the ego vehicle.

**Future directions:** Future work should include studying an approach to find the best selection of anchors when in range of a large number of vehicles, e.g. how many and which vehicles to choose. In order to do so, it would be useful to conduct real data experiments with more anchors in different conditions and with more heterogeneous data, enabling a practical analysis of such scenarios.

It would be interesting to extend our cooperative approach to estimate the position of the vehicles with mesh based strategies, taking into account both the collected and the learned data contained in the nodes, and exploring how to iteratively apply belief propagation theory to avoid over-convergence issues. This would include a protocol to efficiently exchange information in this setting, in order to take advantage of the collaborative potential of the network nodes in a feasible manner in such a dynamic network with high mobility patterns. Although opting for a low-cost approach, as we have done in this work, favors the choice of RSSI for V2V ranging information, the application of TOF based techniques for this purpose would be a potentially more efficient choice when relaxing this requirement, as they allow better accuracy. Future research could also include detecting and applying different models for LOS and NLOS conditions.

Concerning MagLand approach, we did not explore its third step mentioned in Section 4.2: the integration. As aforementioned, this stands for both the integration of proposed detection and matching methods into a combined approach and for its integration into a localization system. All these processes might be seen as mutually beneficial, i.e. instead of regarding them as successive steps (where results from previous step benefits the next one) we might see them as simultaneous steps with shared knowledge. It is clear that detection influences both the matching and the localization approaches, but the opposite is also possible. If a current estimation of the vehicle localization is available, it is possible to predict beforehand which are the most probable anomalies that might appear in the next moments, and that is valuable information that may be used for improved performance in the detection step. Also, during online detection and matching, a positive partial match with high confidence can positively influence the detection result. Instead of using only the binary results from previous step, this would make it possible to leverage knowledge from different steps in an integrated and probabilistic approach. On a more practical perspective, experiments allowing to extend real data analysis to new combinations of information sources, including our proposed magnetic landmarks concept, would be valuable. It would help us to understand its impact and evaluate its contribution to a joint approach with GPS, inertial data performing dead reckoning or both.

Ultimately, we envision our contributions being integrated in combined solutions for vehicular networks, each vehicle using magnetic landmarks to better estimate self location, sharing that information with its neighbors, and so improving global performance in the context of cooperation.

# Chapter 6

# Conclusion

When we started this work, our aim was to make a relevant contribution in the scientific area of localization of road vehicles, helping to devise new solutions to mobility problems. We believed the answer lied in the collaboration among nodes in a vehicular network and in fusing different types of information that complemented each other. Despite the nodes' ability to communicate with each other, which we were confident would be a common feature in future vehicles, we thought we should not impose further requirements, be it in terms of equipment or infrastructure, so that our approach could be applied in large scale. This also implied that we did not want to be dependent on a particular source of individual information, namely GPS or any other satellite based system, but allow heterogeneous nodes that could localize themselves through different sources and strategies. With this in mind, we defined as our main goal to devise a low-cost and GPS-independent reliable localization system for road vehicles, compatible with existing ones for improved performance. As stated in Chapter 1, our reseach question was to find how to acomplish this by leveraging widely available equipment and infrastructure.

We started by working in the context of road vehicle networks and proposed a cooperative approach where each vehicle receives position data with uncertainty sent by one-hop neighbors and leverages it to improve its own location information. We devised an algorithm that uses a particle filter to fuse different sources of data, including range information from signal strength measurements, inertial sensors, GPS, and road maps. Experiments with real data collected in an uncontrolled environment were performed in order to better understand and improve our algorithm. A critical analysis of the results, including different combinations of information sources, makes us confident we have attained an adequate proof-of-concept for our approach.

While considering the results of our field trials analysis, we confirmed the strong relation of the neighbors individual data quality and heterogeneity on the practical usefulness of the collaborative approach. In fact, most current localization systems are heavily dependent on GPS information, which has global sources of error that are shared by vehicles in a given area. To better benefit from the cooperative strategy, vehicles need to be close and it is therefore frequent for neighbors to simultaneously suffer similar individual localization errors or failures when relying on GPS. We felt that, in order to improve collaborative potential in practical scenarios, more research work should

be devoted to GPS-independent individual localization as well as to strategies for combining other information sources with GPS, so helping overcome its limitations. Using inertial data from on-board sensors to help navigation is the most commonly applied strategy for this purpose. The main problem with this type of approach is the cumulative nature of the errors due to the integration of accelerometer and gyroscope data. Magnetometer, widely used to measure the geomagnetic field for orientation estimation, suffers from interference from strong local magnetic fields created by road infrastructure. Considering GPS and dead reckoning (both separated and combined) as the most common and widespread localization solutions in outdoor settings, we aimed to provide an improvement or alternative to them, particularly in areas or scenarios where these solutions failed. Taking advantage of available equipment or infrastructure would be a valuable aspect for our approach for keeping it low-cost and maximizing its usefulness and large scale application.

Having noticed in our experiments the persistent pattern presented by each anomaly in the magnetic data caused by existing road infrastructure, we decided to study the possibility of leveraging these as signatures for localization purposes. We conducted new data collection campaigns that contained several locations of expected anomalies. We proposed and evaluated methods for the detection and matching of these anomalies, including data pre-processing, feature engineering, feature selection, and classification steps, as well as a procedure to gather and store signatures for reference. The good classification accuracy on the test datasets, which comprise some challenging scenarios, led us to believe that we have adequately corroborated our proposed approach. These results are even more useful when we consider that several of the road infrastructures causing the anomalies coincide with locations where GPS has known limitations, and that these landmarks can be used to reset dead reckoning cumulative errors.

Looking back to the thesis statement, we are confident that by proposing a global cooperative approach and a magnetic landmarks based individual approach, both corroborated by experiments with real data, we have successfully validated the claim of our thesis. All this brings us to the combined approach we envision for the localization of road vehicles: individual localization that fuses complementary sources of information, and a global cooperative strategy in which vehicles, as nodes in a large vehicular network, share their location data and improve it by leveraging their neighbors information. We have made contributions in both of these perspectives leading towards our goal, confident that they reinforce this larger vision of localization and mobility in the future.

# References


[1] Panos Papadimitratos, Arnaud de La Fortelle, Knut Evenssen, Roberto Brignolo, and Stefano Cosenza. Vehicular communication systems: Enabling technologies, applications, and future outlook on intelligent transportation. *IEEE Communications Magazine*, 47(11):84–95, 2009.

[2] European Parliament and Council. Directive 2010/40/EU, 7 July 2010. URL: http://eur-lex.europa.eu/eli/dir/2010/40/oj.

[3] Katrin Sjoberg, Peter Andres, Teodor Buburuzan, and Achim Brakemeier. Cooperative intelligent transport systems in Europe: Current deployment status and outlook. *IEEE Vehicular Technology Magazine*, 12(2):89–97, 2017.

[4] Georgios Karagiannis, Onur Altintas, Eylem Ekici, Geert Heijenk, Boangoat Jarupan, Kenneth Lin, and Timothy Weil. Vehicular networking: A survey and tutorial on requirements, architectures, challenges, standards and solutions. *IEEE communications surveys & tutorials*, 13(4):584–616, 2011.

[5] Pedro Santos, João Rodrigues, Susana Cruz, Tiago Lourenço, Pedro d'Orey, Yunior Luis, Cecília Rocha, Sofia Sousa, Sérgio Crisóstomo, Cristina Queirós, et al. PortoLivingLab: An IoT-based sensing platform for smart cities. *IEEE Internet of Things Journal*, 5(2):523–532, 2018.

[6] Azzedine Boukerche, Horacio Oliveira, Eduardo Nakamura, and Antonio Loureiro. Vehicular ad hoc networks: A new challenge for localization-based systems. *Computer communications*, 31(12):2838–2849, 2008.

[7] Joshua Siegel, Dylan Erb, and Sanjay Sarma. A survey of the connected vehicle landscape – Architectures, enabling technologies, applications, and development areas. *IEEE Transactions on Intelligent Transportation Systems*, 19(8):2391–2406, 2018.

[8] Felipe Cunha, Leandro Villas, Azzedine Boukerche, Guilherme Maia, Aline Viana, Raquel Mini, and Antonio Loureiro. Data communication in VANETs: Protocols, applications and challenges. *Ad Hoc Networks*, 44:90–103, 2016.

[9] Muhammad Tahir, Sayed Saad Afzal, Muhammad Saad Chughtai, and Khurram Ali. On the accuracy of inter-vehicular range measurements using GNSS observables in a cooperative framework. *IEEE Transactions on Intelligent Transportation Systems*, 20(2):682–691, 2019.

[10] Keyvan Ansari. Cooperative position prediction: Beyond vehicle-to-vehicle relative positioning. *IEEE Transactions on Intelligent Transportation Systems*, 2019.

[11] Sampo Kuutti, Saber Fallah, Konstantinos Katsaros, Mehrdad Dianati, Francis Mccullough, and Alexandros Mouzakitis. A survey of the state-of-the-art localization techniques and their potentials for autonomous vehicle applications. *IEEE Internet of Things Journal*, 5(2):829–846, 2018.

[12] Isaac Skog and Peter Händel. In-car positioning and navigation technologies – A survey. *IEEE Transactions on Intelligent Transportation Systems*, 10(1):4–21, 2009.

[13] Stefano Severi, Henk Wymeersch, Jérôme Härri, Markus Ulmschneider, Benoît Denis, and M. Bartels. Beyond GNSS: Highly accurate localization for cooperative-intelligent transport systems. In *IEEE Wireless Communications and Networking Conference (WCNC)*, pages 1–6. IEEE, 2018.

[14] Henk Wymeersch, Jaime Lien, and Moe Win. Cooperative localization in wireless networks. *Proceedings of the IEEE*, 97(2):427–450, 2009.

[15] Mate Boban, Tiago Vinhoza, Michel Ferreira, João Barros, and Ozan Tonguz. Impact of vehicles as obstacles in vehicular ad hoc networks. *IEEE Journal on Selected Areas in Communications*, 29(1):15–28, 2011.

[16] Javier Gozálvez, Miguel Sepulcre, and Ramon Bauza. IEEE 802.11 p vehicle to infrastructure communications in urban environments. *IEEE Communications Magazine*, 50(5), 2012.

[17] Moe Win, Andrea Conti, Santiago Mazuelas, Yuan Shen, Wesley Gifford, Davide Dardari, and Marco Chiani. Network localization and navigation via cooperation. *Communications Magazine*, 49(5):56–62, 2011.

[18] Yuan Shen, Santiago Mazuelas, and Moe Win. Network navigation: Theory and interpretation. *IEEE Journal on Selected Areas in Communications*, 30(9):1823–1834, 2012.

[19] Gustavo Marfiay, Giovanni Pau, and Marco Roccetti. On developing smart applications for VANETs: Where are we now? Some insights on technical issues and open problems. In *International Conference on Ultra Modern Telecommunications & Workshops, ICUMT'09*, pages 1–6. IEEE, 2009.

[20] Guoqiang Mao, Barış Fidan, and Brian Anderson. Wireless sensor network localization techniques. *Computer Networks*, 51(10):2529–2553, 2007.

[21] Hao Li and Fawzi Nashashibi. Cooperative multi-vehicle localization using split covariance intersection filter. *IEEE Intelligent Transportation Systems Magazine*, 5(2):33–44, 2013.

[22] Dhiraj Gulati, Feihu Zhang, Daniel Clarke, and Alois Knoll. Vehicle infrastructure cooperative localization using factor graphs. In *Intelligent Vehicles Symposium (IV)*, pages 1085–1090. IEEE, 2016.

[23] Ali Yassin, Youssef Nasser, Mariette Awad, Ahmed Al-Dubai, Ran Liu, Chau Yuen, Ronald Raulefs, and Elias Aboutanios. Recent advances in indoor localization: A survey on theoretical approaches and applications. *IEEE Communications Surveys & Tutorials*, 19(2):1327–1346, 2016.

[24] Pavel Davidson and Robert Piché. A survey of selected indoor positioning methods for smartphones. *IEEE Communications Surveys & Tutorials*, 19(2):1347–1370, 2017.

[25] Susana Cruz, Traian Abrudan, Zhuoling Xiao, Niki Trigoni, and João Barros. Neighbor-aided localization in vehicular networks. *IEEE Transactions on Intelligent Transportation Systems*, 18:2693–2702, 2017.

[26] GPS.gov – Official U.S. Government information about the Global Positioning System (GPS) and related topics. [Online, accessed on January 2019]. Available: http://www.gps.gov/.

[27] Information analytical centre of GLONASS and GPS controlling. [Online, accessed on January 2019]. Available: http://glonass-iac.ru/en/.

[28] European GNSS Agency (GSA). GNSS User Technology Report Issue 2. Technical report, October 2018.

[29] European Space Agency (ESA) / Navigation / Galileo. [Online, accessed on January 2019]. Available: http://www.esa.int/Our_Activities/Navigation/Galileo/What_is_Galileo.

[30] BeiDou Navigation Satellite System. [Online, accessed on January 2019]. Available: http://en.beidou.gov.cn/.

[31] European GNSS Agency (GSA). GNSS User Technology Report Issue 1. Technical report, October 2016.

[32] Fabian de Ponte Müller. Survey on ranging sensors and cooperative techniques for relative positioning of vehicles. *Sensors*, 17(2):271, 2017.

[33] EGNOS Portal. [Online, accessed on January 2019]. Available: http://www.egnos-portal.eu/.

[34] Billur Barshan and Hugh F Durrant-Whyte. Inertial navigation systems for mobile robots. *IEEE Transactions on Robotics and Automation*, 11(3):328–342, 1995.

[35] Sheng Shen, Mahanth Gowda, and Romit Roy Choudhury. Closing the gaps in inertial motion tracking. In *Proceedings of the 24th Annual International Conference on Mobile Computing and Networking*, pages 429–444. ACM, 2018.

[36] Nima Alam, Asghar Balaei, and Andrew Dempster. Range and range-rate measurements using DSRC: facts and challenges. In *IGNSS Symposium*, 2009.

[37] Neal Patwari, Joshua Ash, Spyros Kyperountas, Alfred Hero III, Randolph Moses, and Neiyer Correal. Locating the nodes: cooperative localization in wireless sensor networks. *IEEE Signal Processing Magazine*, 22(4):54–69, 2005.

[38] Neal Patwari, Alfred Hero, Matt Perkins, Neiyer Correal, and Robert O'dea. Relative location estimation in wireless sensor networks. *IEEE Transactions on signal processing*, 51(8):2137–2148, 2003.

[39] Azzedine Boukerche, Horacio Oliveira, Eduardo Nakamura, and Antonio Loureiro. Localization systems for wireless sensor networks. *IEEE wireless Communications*, 14(6):6–12, 2007.

[40] Fredrik Gustafsson and Fredrik Gunnarsson. Mobile positioning using wireless networks: possibilities and fundamental limitations based on available wireless network measurements. *IEEE Signal Processing Magazine*, 22(4):41–53, 2005.

[41] Traian Abrudan, Azadeh Haghparast, and Visa Koivunen. Time-synchronization and ranging for OFDM systems using time-reversal. *IEEE Transactions on Instrumentation and Measurement*, 62(12):3276–3290, 2013.

[42] Davide Dardari, Andrea Conti, Ulric Ferner, Andrea Giorgetti, and Moe Win. Ranging with ultrawide bandwidth signals in multipath environments. *Proceedings of the IEEE*, 97(2):404–426, 2009.

[43] Sayanan Sivaraman and Mohan Trivedi. Looking at vehicles on the road: A survey of vision-based vehicle detection, tracking, and behavior analysis. *IEEE Transactions on Intelligent Transportation Systems*, 14(4):1773–1795, 2013.

[44] Dominique Gruyer, Valentin Magnier, Karima Hamdi, Laurene Claussmann, Olivier Orfila, and Andry Rakotonirainy. Perception, information processing and modeling: Critical stages for autonomous driving applications. *Annual Reviews in Control*, 44:323–341, 2017.

[45] Nabil Drawil and Otman Basir. Emerging new trends in hybrid vehicle localization systems. *Global Navigation Satellite Systems: Signal, Theory and Applications*, 2012.

[46] Quoc Duy Vo and Pradipta De. A survey of fingerprint-based outdoor localization. *IEEE Communications Surveys & Tutorials*, 18(1):491–506, 2016.

[47] Nathan Piasco, Désiré Sidibé, Cédric Demonceaux, and Valérie Gouet-Brunet. A survey on visual-based localization: On the benefit of heterogeneous data. *Pattern Recognition*, 74:90–109, 2018.

[48] Amir Roshan Zamir and Mubarak Shah. Accurate image localization based on google maps street view. In *European Conference on Computer Vision*, pages 255–268. Springer, 2010.

[49] Torsten Sattler, Bastian Leibe, and Leif Kobbelt. Efficient & effective prioritized matching for large-scale image-based localization. *IEEE transactions on pattern analysis and machine intelligence*, 39(9):1744–1756, 2017.

[50] Christopher White, David Bernstein, and Alain Kornhauser. Some map matching algorithms for personal navigation assistants. *Transportation Research Part C: Emerging Technologies*, 8(1):91–108, 2000.

[51] Sotiris Brakatsoulas, Dieter Pfoser, Randall Salas, and Carola Wenk. On map-matching vehicle tracking data. In *Proceedings of the 31st international conference on Very large data bases*, pages 853–864. VLDB Endowment, 2005.

[52] Maan El Najjar and Philippe Bonnifait. A road-matching method for precise vehicle localization using belief theory and Kalman filtering. *Autonomous Robots*, 19(2):173–191, 2005.

[53] Nagendra Velaga, Mohammed Quddus, and Abigail Bristow. Developing an enhanced weight-based topological map-matching algorithm for intelligent transport systems. *Transportation Research Part C: Emerging Technologies*, 17(6):672–683, 2009.

[54] David Bétaille and Rafael Toledo-Moreo. Creating enhanced maps for lane-level vehicle navigation. *Intelligent Transportation Systems, IEEE Transactions on*, 11(4):786–798, 2010.

[55] Mohammed Quddus, Washington Ochieng, and Robert Noland. Current map-matching algorithms for transport applications: State-of-the art and future research directions. *Transportation Research Part C: Emerging Technologies*, 15(5):312–328, 2007.

[56] Nagendra Velaga, Mohammed Quddus, Abigail Bristow, and Yuheng Zheng. Map-aided integrity monitoring of a land vehicle navigation system. *IEEE Transactions on Intelligent Transportation Systems*, 13(2):848–858, 2012.

[57] Christopher M. Bishop. *Pattern Recognition and Machine Learning (Information Science and Statistics)*. Springer-Verlag New York, Inc., 2006.

[58] James V. Candy. *Bayesian Signal Processing: Classical, Modern and Particle Filtering Methods*. John Wiley & Sons, 2009.

[59] Robin Schubert, Eric Richter, and Gerd Wanielik. Comparison and evaluation of advanced motion models for vehicle tracking. In *11th International Conference on Information Fusion*, pages 1–6. IEEE, 2008.

[60] Fred Daum. Nonlinear filters: beyond the Kalman filter. *IEEE Aerospace and Electronic Systems Magazine*, 20(8):57–69, 2005.

[61] Simon J. Julier and Jeffrey K. Uhlmann. New extension of the Kalman filter to nonlinear systems. In *AeroSense'97*, pages 182–193. International Society for Optics and Photonics, 1997.

[62] Fred Daum and Jim Huang. Curse of dimensionality and particle filters. In *2003 IEEE Aerospace Conference Proceedings (Cat. No. 03TH8652)*, volume 4, pages 1979–1993. IEEE, 2003.

[63] Mihail Sichitiu and Maria Kihl. Inter-vehicle communication systems: A survey. *IEEE Communications Surveys & Tutorials*, 10(2):88–105, 2008.

[64] Dieter Fox, Wolfram Burgard, Hannes Kruppa, and Sebastian Thrun. A probabilistic approach to collaborative multi-robot localization. *Autonomous robots*, 8(3):325–344, 2000.

[65] Esha Nerurkar, Stergios Roumeliotis, and Agostino Martinelli. Distributed maximum a posteriori estimation for multi-robot cooperative localization. In *IEEE International Conference on Robotics and Automation (ICRA'09)*, pages 1402–1409. IEEE, 2009.

[66] Jeremy Blum, Azim Eskandarian, and Lance Hoffman. Challenges of intervehicle ad hoc networks. *IEEE Transactions on Intelligent Transportation Systems*, 5(4):347–351, 2004.

[67] Junghoon Lee, Gyung-Leen Park, Chang Oan Sung, and Hyung Do Choi. A cooperative position fix scheme based on a group management on the vehicular network. *J. Inf. Sci. Eng.*, 26(1):15–26, 2010.

[68] Norman Mattern, Marcus Obst, Robin Schubert, and Gerd Wanielik. Co-operative vehicle localization algorithm—Evaluation of the CoVeL approach. In *9th International Multi-Conference on Systems, Signals and Devices (SSD)*, pages 1–5. IEEE, 2012.

[69] Mohsen Rohani, Denis Gingras, and Dominique Gruyer. A novel approach for improved vehicular positioning using cooperative map matching and dynamic base station DGPS concept. *IEEE Transactions on Intelligent Transportation Systems*, 17(1):230–239, 2016.

[70] Macheng Shen, Jing Sun, Huei Peng, and Ding Zhao. Improving localization accuracy in connected vehicle networks using rao-blackwellized particle filters: Theory, simulations, and experiments. *IEEE Transactions on Intelligent Transportation Systems*, 2018.

[71] Thanh-Son Dao, Keith Yu Kit Leung, Christopher Michael Clark, and Jan Paul Huissoon. Markov-based lane positioning using intervehicle communication. *IEEE Transactions on Intelligent Transportation Systems*, 8(4):641–650, 2007.

[72] Macheng Shen, Jing Sun, and Ding Zhao. The impact of road configuration in V2V-based cooperative localization: Mathematical analysis and real-world evaluation. *IEEE Transactions on Intelligent Transportation Systems*, 19(10):3220–3229, 2018.

[73] Hao Li and Fawzi Nashashibi. Multi-vehicle cooperative localization using indirect vehicle-to-vehicle relative pose estimation. In *ICVES 2012-IEEE International Conference on Vehicular Electronics and Safety*, pages 267–272, 2012.

[74] Gloria Soatti, Monica Nicoli, Nil Garcia, Benoit Denis, Ronald Raulefs, and Henk Wymeersch. Implicit cooperative positioning in vehicular networks. *IEEE Transactions on Intelligent Transportation Systems*, 19(12):3964–3980, 2018.

[75] Markus Frohle, Christopher Lindberg, and Henk Wymeersch. Cooperative localization of vehicles without inter-vehicle measurements. In *Wireless Communications and Networking Conference (WCNC)*, pages 1–6. IEEE, 2018.

[76] Luis Conde Bento, Ricardo Parafita, and Urbano Nunes. Inter-vehicle sensor fusion for accurate vehicle localization supported by V2V and V2I communications. In *15th International IEEE Conference on Intelligent Transportation Systems*, pages 907–914. IEEE, 2012.

[77] Luís Conde, Rafael Chelim, and Urbano Nunes. Collaborative vehicle self-localization using multi-GNSS receivers and V2V/V2I communications. In *18th International Conference on Intelligent Transportation Systems*, pages 2525–2532. IEEE, 2015.

[78] Fabian de Ponte Müller, Diego Navarro Tapia, and Matthias Kranz. Precise relative positioning of vehicles with on-the-fly carrier phase resolution and tracking. *International Journal of Distributed Sensor Networks*, 2015:8:8–8:8, 2015.

[79] Eric Richter, Marcus Obst, Robin Schubert, and Gerd Wanielik. Cooperative relative localization using vehicle-to-vehicle communications. In *2009 12th International Conference on Information Fusion*, pages 126–131. IEEE, 2009.

[80] Daiqin Yang, Fang Zhao, Kai Liu, Hock Beng Lim, Emilio Frazzoli, and Daniela Rus. A GPS pseudorange based cooperative vehicular distance measurement technique. In *2012 IEEE 75th Vehicular Technology Conference (VTC Spring)*, pages 1–5. IEEE, 2012.

[81] Kai Liu, Hock Beng Lim, Emilio Frazzoli, Houling Ji, and Victor CS Lee. Improving positioning accuracy using GPS pseudorange measurements for cooperative vehicular localization. *IEEE Transactions on Vehicular Technology*, 63(6):2544–2556, 2014.

[82] Nima Alam, Asghar Tabatabaei Balaei, and Andrew Dempster. Relative positioning enhancement in VANETs: A tight integration approach. *IEEE Transactions on Intelligent Transportation Systems*, 14(1):47–55, 2013.

[83] Mohsen Rohani, Denis Gingras, and Dominique Gruyer. Dynamic base station DGPS for cooperative vehicle localization. In *2014 International Conference on Connected Vehicles and Expo (ICCVE)*, pages 781–785. IEEE, 2014.

[84] Fabian de Ponte Müller, Estefania Munoz Diaz, Bernhard Kloiber, and Thomas Strang. Bayesian cooperative relative vehicle positioning using pseudorange differences. In *2014 IEEE/ION Position, Location and Navigation Symposium-PLANS 2014*, pages 434–444. IEEE, 2014.

[85] Khaoula Lassoued, Philippe Bonnifait, and Isabelle Fantoni. Cooperative localization with reliable confidence domains between vehicles sharing GNSS pseudoranges errors with no base station. *IEEE Intelligent Transportation Systems Magazine*, 9(1):22–34, 2017.

[86] Mohsen Rohani, Denis Gingras, Vincent Vigneron, and Dominique Gruyer. A new decentralized bayesian approach for cooperative vehicle localization based on fusion of GPS and VANET based inter-vehicle distance measurement. *IEEE Intelligent transportation systems magazine*, 7(2):85–95, 2015.

[87] Sae Fujii, Atsushi Fujita, Takaaki Umedu, Shigeru Kaneda, Hirozumi Yamaguchi, Teruo Higashino, and Mineo Takai. Cooperative vehicle positioning via V2V communications and onboard sensors. In *2011 IEEE Vehicular Technology Conference (VTC Fall)*, pages 1–5. IEEE, 2011.

[88] Farid Bounini, Denis Gingras, Herve Pollart, and Dominique Gruyer. Real time cooperative localization for autonomous vehicles. In *2016 IEEE 19th International Conference on Intelligent Transportation Systems (ITSC)*, pages 1186–1191. IEEE, 2016.

[89] Ahmed Hamdi Sakr and Gaurav Bansal. Cooperative localization via DSRC and multi-sensor multi-target track association. In *2016 IEEE 19th International Conference on Intelligent Transportation Systems (ITSC)*, pages 66–71. IEEE, 2016.

[90] Xiaotong Shen, Scott Pendleton, and Marcelo H Ang. Scalable cooperative localization with minimal sensor configuration. In *Distributed Autonomous Robotic Systems*, pages 89–104. Springer, 2016.

[91] Han-You Jeong, Hoa-Hung Nguyen, and Adhitya Bhawiyuga. Spatiotemporal local-remote senor fusion (st-lrsf) for cooperative vehicle positioning. *Sensors*, 18(4):1092, 2018.

[92] Nabil Mohamed Drawil and Otman Basir. Intervehicle-communication-assisted localization. *IEEE Transactions on Intelligent Transportation Systems*, 11(3):678–691, 2010.

[93] Farhan Ahammed, Javid Taheri, Albert Zomaya, and Max Ott. VLOCI2: improving 2D location coordinates using distance measurements in GPS-equipped VANETs. In *Proceedings of the 14th ACM international conference on Modeling, analysis and simulation of wireless and mobile systems*, pages 317–322. ACM, 2011.

[94] Jun Yao, Asghar Tabatabaei Balaei, Mahbub Hassan, Nima Alam, and Andrew Dempster. Improving cooperative positioning for vehicular networks. *IEEE Transactions on Vehicular Technology*, 60(6):2810–2823, 2011.

[95] Venkatesan Ekambaram, Kannan Ramchandran, and Raja Sengupta. Collaborative high-accuracy localization in mobile multipath environments. *IEEE Transactions on Vehicular Technology*, 65(10):8414–8422, 2016.

[96] Dhiraj Gulati, Feihu Zhang, Daniel Clarke, and Alois Knoll. Graph based cooperative localization using symmetric measurement equations and dedicated short range communication. In *IEEE International Conference on Multisensor Fusion and Integration for Intelligent Systems (MFI)*, pages 644–649. IEEE, 2017.

[97] Nima Alam, Asghar Tabatabaei Balaei, and Andrew Dempster. A DSRC Doppler-based cooperative positioning enhancement for vehicular networks with GPS availability. *IEEE Transactions on Vehicular Technology*, 60(9):4462–4470, 2011.

[98] Keyvan Golestan, Sepideh Seifzadeh, Mohamed Kamel, Fakhri Karray, and Farook Sattar. Vehicle localization in VANETs using data fusion and V2V communication. In *Proceedings of the second ACM international symposium on Design and analysis of intelligent vehicular networks and applications*, pages 123–130. ACM, 2012.

[99] Alessio Fascista, Giovanni Ciccarese, Angelo Coluccia, and Giuseppe Ricci. Angle of arrival-based cooperative positioning for smart vehicles. *IEEE Transactions on Intelligent Transportation Systems*, (99):1–13, 2017.

[100] Peyman Hadi Mohammadabadi and Shahrokh Valaee. Cooperative node positioning in vehicular networks using inter-node distance measurements. In *2014 IEEE 25th Annual International Symposium on Personal, Indoor, and Mobile Radio Communication (PIMRC)*, pages 1448–1452. IEEE, 2014.

[101] Mariam Elazab, Aboelmagd Noureldin, and Hossam Hassanein. Integrated cooperative localization for connected vehicles in urban canyons. In *2015 IEEE Global Communications Conference (GLOBECOM)*, pages 1–6. IEEE, 2015.

[102] Weijie Yuan, Nan Wu, Bernhard Etzlinger, Hua Wang, and Jingming Kuang. Cooperative joint localization and clock synchronization based on Gaussian message passing in asynchronous wireless networks. *IEEE Transactions on Vehicular Technology*, 65(9):7258–7273, 2016.

[103] Juan Li, Xuerong Cui, Zhongwei Li, and Jianhang Liu. Method to improve the positioning accuracy of vehicular nodes using IEEE 802.11 p protocol. *IEEE Access*, 6:2834–2843, 2018.

[104] Gia Minh Hoangt, Benoît Denis, Jérôme Häirri, and Dirk Slock. Cooperative localization in VANETs: An experimental proof-of-concept combining GPS, IR-UWB ranging and V2V communications. In *15th Workshop on Positioning, Navigation and Communications (WPNC)*, pages 1–6. IEEE, 2018.

[105] Ryan Parker and Shahrokh Valaee. Vehicular node localization using received-signal-strength indicator. *IEEE Transactions on Vehicular Technology*, 56(6):3371–3380, 2007.

[106] Derek Caveney. Cooperative vehicular safety applications. *IEEE Control Systems*, 30(4):38–53, 2010.

[107] Osama Abumansoor and Azzedine Boukerche. A secure cooperative approach for nonline-of-sight location verification in VANET. *IEEE Transactions on Vehicular Technology*, 61(1):275–285, 2012.

[108] Shahram Rezaei and Raja Sengupta. Kalman filter-based integration of DGPS and vehicle sensors for localization. *IEEE Transactions on Control Systems Technology*, 15(6):1080–1088, 2007.

[109] Eun-Kyu Lee, Soon Oh, and Mario Gerla. RFID assisted vehicle positioning in VANETs. *Pervasive and Mobile Computing*, 8(2):167–179, 2012.

[110] Mariam Elazab, Aboelmagd Noureldin, and Hossam S Hassanein. Integrated cooperative localization for vehicular networks with partial GPS access in urban canyons. *Vehicular Communications*, 9:242–253, 2017.

[111] Jesse Levinson, Michael Montemerlo, and Sebastian Thrun. Map-based precision vehicle localization in urban environments. In *Robotics: Science and Systems*, volume 4, page 1. Citeseer, 2007.

[112] Maryam Alotaibi, Azzedine Boukerche, and Hussein Mouftah. Distributed relative cooperative positioning in vehicular ad-hoc networks. In *Global Information Infrastructure and Networking Symposium (GIIS)*, pages 1–8. IEEE, 2014.

[113] Chia-Ho Ou. A roadside unit-based localization scheme for vehicular ad hoc networks. *International Journal of Communication Systems*, 27(1):135–150, 2014.

[114] Sugang Ma, Fuxi Wen, Xiangmo Zhao, Zhong-min Wang, and Diange Yang. An efficient V2X based vehicle localization using single RSU and single receiver. *IEEE Access*, 7:46114–46121, 2019.

[115] Valter Pasku, Alessio De Angelis, Guido De Angelis, Darmindra Arumugam, Marco Dionigi, Paolo Carbone, Antonio Moschitta, and David Ricketts. Magnetic field-based positioning systems. *IEEE Communications Surveys & Tutorials*, 19(3):2003–2017, 2017.

[116] Ana Lopes, Fernando Moita, Urbano Nunes, and Razvan Solea. An outdoor guidepath navigation system for AMRs based on robust detection of magnetic markers. In *IEEE Conference on Emerging Technologies and Factory Automation (ETFA)*, pages 989–996. IEEE, 2007.

[117] Traian Abrudan, Zhuoling Xiao, Andrew Markham, and Niki Trigoni. Distortion rejecting magneto-inductive 3-D localization (MagLoc). *IEEE Journal on Selected Areas in Communications*, 33:2404–2417, 2015.

[118] Surachai Suksakulchai, Siripun Thongchai, Mitchell Wilkes, and Kazuhiko Kawamura. Mobile robot localization using an electronic compass for corridor environment. In *IEEE International Conference on Systems, Man, and Cybernetics*, volume 5, pages 3354–3359. IEEE, 2000.

[119] Janne Haverinen and Anssi Kemppainen. Global indoor self-localization based on the ambient magnetic field. *Robotics and Autonomous Systems*, 57(10):1028–1035, 2009.

[120] Kalyan Pathapati Subbu, Brandon Gozick, and Ram Dantu. LocateMe: Magnetic-fields-based indoor localization using smartphones. *ACM Transactions on Intelligent Systems and Technology (TIST)*, 4(4):73, 2013.

[121] Hongwei Xie, Tao Gu, Xianping Tao, Haibo Ye, and Jian Lv. MaLoc: a practical magnetic fingerprinting approach to indoor localization using smartphones. In *Proceedings of the 2014 ACM International Joint Conference on Pervasive and Ubiquitous Computing*, pages 243–253. ACM, 2014.

[122] Yuanchao Shu, Cheng Bo, Guobin Shen, Chunshui Zhao, Liqun Li, and Feng Zhao. Magicol: Indoor localization using pervasive magnetic field and opportunistic WiFi sensing. *IEEE Journal on Selected Areas in Communications*, 33(7):1443–1457, 2015.

[123] Binghao Li, Thomas Gallagher, Andrew Dempster, and Chris Rizos. How feasible is the use of magnetic field alone for indoor positioning? In *International Conference on Indoor Positioning and Indoor Navigation (IPIN)*, pages 1–9. IEEE, 2012.

[124] IndoorAtlas. [Online, accessed on January 2019]. Available: https://www.indooratlas.com/.

[125] Levent Selçuk. GPS independent outdoor positioning system. Master's thesis, Tallinn University of Technology School of Information Technologies, 2016.

[126] Moustafa Youssef, Mohamed Amir Yosef, and Mohamed El-Derini. GAC: Energy-efficient hybrid GPS-accelerometer-compass GSM localization. In *Global Telecommunications Conference (GLOBECOM 2010), 2010 IEEE*, pages 1–5. IEEE, 2010.

[127] He Wang, Zhiyang Wang, Guobin Shen, Fan Li, Song Han, and Feng Zhao. WheelLoc: Enabling continuous location service on mobile phone for outdoor scenarios. In *IEEE International Conference on Computer Communications (INFOCOM)*, pages 2733–2741. IEEE, 2013.

[128] Heba Aly and Moustafa Youssef. Dejavu: an accurate energy-efficient outdoor localization system. In *Proceedings of the 21st ACM SIGSPATIAL International Conference on Advances in Geographic Information Systems*, pages 154–163. ACM, 2013.

[129] Cheng Bo, Xiang-Yang Li, Taeho Jung, Xufei Mao, Yue Tao, and Lan Yao. SmartLoc: Push the limit of the inertial sensor based metropolitan localization using smartphone. In *Proceedings of the 19th annual international conference on Mobile computing & networking*, pages 195–198. ACM, 2013.

[130] Dongyan Wei, Xinchun Ji, Wen Li, Hong Yuan, and Ying Xu. Vehicle localization based on odometry assisted magnetic matching. In *International Conference on Indoor Positioning and Indoor Navigation (IPIN)*, pages 1–6. IEEE, 2017.

[131] Thanawin Rakthanmanon, Bilson Campana, Abdullah Mueen, Gustavo Batista, Brandon Westover, Qiang Zhu, Jesin Zakaria, and Eamonn Keogh. Searching and mining trillions of time series subsequences under dynamic time warping. In *Proceedings of the 18th ACM SIGKDD international conference on Knowledge discovery and data mining*, pages 262–270. ACM, 2012.

[132] Marko Angjelichinoski, Daniel Denkovski, Vladimir Atanasovski, and Liljana Gavrilovska. Cramér–Rao lower bounds of RSS-based localization with anchor position uncertainty. *Information Theory, IEEE Transactions on*, 61(5):2807–2834, 2015.

[133] Yuan Shen and Moe Z Win. Fundamental limits of wideband localization—Part I: A general framework. *IEEE Transactions on Information Theory*, 56(10):4956–4980, 2010.

[134] Yuan Shen, Henk Wymeersch, and Moe Z Win. Fundamental limits of wideband localization—Part II: Cooperative networks. *IEEE Transactions on Information Theory*, 56(10):4981–5000, 2010.

[135] Dieter Fox, Jeffrey Hightower, Lin Liao, Dirk Schulz, and Gaetano Borriello. Bayesian filtering for location estimation. *IEEE Pervasive Computing*, 2(3):24–33, 2003.

[136] Tatsuya Harada, Taketoshi Mori, and Tomomasa Sato. Development of a tiny orientation estimation device to operate under motion and magnetic disturbance. *The International Journal of Robotics Research*, 26(6):547–559, 2007.

[137] Abdul Alami, Khaled El-Sayed, Afif Al-Horr, Hassan Artail, and Jinhua Guo. Improving the car GPS accuracy using V2V and V2I communications. In *International Multidisciplinary Conference on Engineering Technology (IMCET)*, pages 1–6. IEEE, 2018.

[138] João Rodrigues, Ana Aguiar, and João Barros. SenseMyCity: Crowdsourcing an Urban Sensor. *arXiv preprint arXiv:1412.2070*, 2014.

[139] João Rodrigues, Ana Aguiar, and Cristina Queirós. Opportunistic mobile crowdsensing for gathering mobility information: Lessons learned. In *IEEE 19th International Conference on Intelligent Transportation Systems (ITSC)*, pages 1654–1660. IEEE, 2016.

[140] Javier Almazán, Luis Bergasa, Javier Yebes, Rafael Barea, and Roberto Arroyo. Full auto-calibration of a smartphone on board a vehicle using IMU and GPS embedded sensors. In *Intelligent Vehicles Symposium (IV)*, pages 1374–1380. IEEE, 2013.

[141] Demoz Gebre-Egziabher, Gabriel Elkaim, David Powell, and Bradford Parkinson. Calibration of strapdown magnetometers in magnetic field domain. *Journal of Aerospace Engineering*, 19(2):87–102, 2006.

[142] Ahmed Wahdan, Jacques Georgy, Walid Abdelfatah, and Aboelmagd Noureldin. Magnetometer calibration for portable navigation devices in vehicles using a fast and autonomous technique. *IEEE Transactions on Intelligent Transportation Systems*, 15(5):2347–2352, 2014.

[143] Manon Kok and Thomas Schön. Magnetometer calibration using inertial sensors. *IEEE Sensors Journal*, 16(14):5679–5689, 2016.

[144] Nikolai Chernov and Claire Lesort. Least squares fitting of circles. *Journal of Mathematical Imaging and Vision*, 23(3):239–252, 2005.

[145] Ali Al-Sharadqah and Nikolai Chernov. Error analysis for circle fitting algorithms. *Electronic Journal of Statistics*, 3:886–911, 2009.

[146] Bingfei Fan, Qingguo Li, Chao Wang, and Tao Liu. An adaptive orientation estimation method for magnetic and inertial sensors in the presence of magnetic disturbances. *Sensors*, 17(5):1161, 2017.

[147] Varun Chandola, Arindam Banerjee, and Vipin Kumar. Anomaly detection: A survey. *ACM computing surveys (CSUR)*, 41(3):15, 2009.

[148] Victoria Hodge and Jim Austin. A survey of outlier detection methodologies. *Artificial intelligence review*, 22(2):85–126, 2004.

[149] Tak-chung Fu. A review on time series data mining. *Engineering Applications of Artificial Intelligence*, 24(1):164–181, 2011.

[150] Varun Chandola. *Anomaly detection for symbolic sequences and time series data*. PhD thesis, University of Minnesota, 2009.

[151] National Centers for Environmental Information (NCEI). Compute Earth's Magnetic Field Values. https://www.ngdc.noaa.gov/geomag/magfield.shtml. Accessed: 2016-12-12.

[152] Nitesh Chawla, Kevin Bowyer, Lawrence Hall, and Philip Kegelmeyer. SMOTE: synthetic minority over-sampling technique. *Journal of artificial intelligence research*, 16:321–357, 2002.

[153] Luis Torgo. *Data mining with R: learning with case studies*. Chapman and Hall/CRC, 2016.

[154] Mark Hall. *Correlation-based feature selection for machine learning*. PhD thesis, The University of Waikato, 1999.

[155] R Core Team. *R: A language and environment for statistical computing*. R Foundation for Statistical Computing, Vienna, Austria, 2016.

[156] Tom Fawcett. An introduction to ROC analysis. *Pattern recognition letters*, 27(8):861–874, 2006.

[157] Donald Berndt and James Clifford. Using dynamic time warping to find patterns in time series. In *KDD workshop*, pages 359–370. Seattle, WA, 1994.

[158] Xiaopeng Xi, Eamonn Keogh, Christian Shelton, Li Wei, and Chotirat Ann Ratanamahatana. Fast time series classification using numerosity reduction. In *Proceedings of the 23rd international conference on Machine learning*, pages 1033–1040. ACM, 2006.

[159] Xiaoyue Wang, Abdullah Mueen, Hui Ding, Goce Trajcevski, Peter Scheuermann, and Eamonn Keogh. Experimental comparison of representation methods and distance measures for time series data. *Data Mining and Knowledge Discovery*, 26(2):275–309, 2013.

[160] Anthony Bagnall, Jason Lines, Aaron Bostrom, James Large, and Eamonn Keogh. The great time series classification bake off: a review and experimental evaluation of recent algorithmic advances. *Data Mining and Knowledge Discovery*, 31(3):606–660, 2017.

[161] Diego Silva, Gustavo Batista, and Eamonn Keogh. On the effect of endpoints on dynamic time warping. In *SIGKDD Workshop on Mining and Learning from Time Series, II*. Association for Computing Machinery-ACM, 2016.

[162] Paolo Tormene, Toni Giorgino, Silvana Quaglini, and Mario Stefanelli. Matching incomplete time series with dynamic time warping: an algorithm and an application to post-stroke rehabilitation. *Artificial intelligence in medicine*, 45(1):11–34, 2009.

[163] Toni Giorgino. Computing and visualizing dynamic time warping alignments in R: the dtw package. *Journal of statistical Software*, 31(7):1–24, 2009.

[164] François Petitjean, Germain Forestier, Geoffrey Webb, Ann Nicholson, Yanping Chen, and Eamonn Keogh. Dynamic time warping averaging of time series allows faster and more accurate classification. In *IEEE International Conference on Data Mining (ICDM)*, pages 470–479. IEEE, 2014.

[165] François Petitjean, Germain Forestier, Geoffrey Webb, Ann Nicholson, Yanping Chen, and Eamonn Keogh. Faster and more accurate classification of time series by exploiting a novel dynamic time warping averaging algorithm. *Knowledge and Information Systems*, 1(47):1–26, 2016.

[166] François Petitjean, Alain Ketterlin, and Pierre Gançarski. A global averaging method for dynamic time warping, with applications to clustering. *Pattern Recognition*, 44(3):678–693, 2011.